Identification and analysis of mechanisms that bypass the essentiality of Polo, a mitotic regulator

有糸分裂制御因子**Polo**の必須性をバイパスする機構の同定と解析

Juyoung KIM

Group of Intracellular Dynamics
Department of Biological Science
Graduate School of Science
Nagoya University

Contents

1. Abstract

Mitosis is a fundamental cellular process in which chromosomes are accurately segregated into two daughter cells. This process requires the assembly of dynamic filaments and microtubules (MTs), and is collectively regulated by various kinases and phosphatases. The processes involved in mitosis are generally well-conserved among eukaryotes. Paradoxically, the set of mitotically essential genes varies among different species. This indicates that the cellular functions of mitotically essential genes can be replaced or bypassed by alternative pathways during evolution. However, despite extensive efforts, bypass of essentiality (BOE) events for mitotic genes have rarely been reproduced in laboratory experiments. Therefore, many open questions remain regarding the BOE of mitotic regulators (BOE-M). For example, which “essential” genes can be substituted by other genes and become non-essential? What kinds of cellular functions and pathways function in the absence of mitotically essential genes? How can cells achieve BOE-M under natural conditions without artificial mutagenesis?

To uncover a novel BOE-M, extragenetic suppressor screening for mitotically essential gene disruptants was conducted using mutagenesis and subsequent evolutionary repair experiments in the fission yeast, *Schizosaccharomyces pombe*. Viable cells were isolated when the coding region of polo-like kinase (Plk) was completely removed. This was unexpected because Plk is a versatile and essential mitotic kinase in many cell types. Whole genome sequencing of viable Plk-deleted cells and subsequent experiments on genetic interactions revealed that the BOE of Plk is achieved via 16 suppressor mutations. Gene classification based on the cellular functions of suppressor mutations revealed that the BOE of Plk is enabled by specific mutations in the MT-nucleating γ-tubulin complex, which is expected to be the downstream machinery of Plk, and unexpectedly, through mutations in glucose uptake genes and the protein kinase A (PKA) pathway, which are not readily associated with mitosis. Furthermore, additional genetic screening revealed that the latter bypass was dependent on casein kinase 1 (CK1), which is involved in a delay in the septation initiation network (SIN), but is not considered a major mitotic regulator in *S. pombe*. Our genetic and phenotypic data suggest that CK1 and other suppressor mutations constitute an alternative mechanism of MT nucleation that is normally dominated by Plk. Plk and Ck1 inhibitors caused synthetically skewed bipolar spindle formation and mitotic arrest in a human colon cancer cell line. Therefore, the genetic interaction between Plk and CK1 is conserved in human cell lines.

Our study uncovered a new case of BOE-M in *Plk*, which is an essential mitotic gene to control the cell cycle, nucleate mitotic microtubules at centrosomes, and induce septation initiation. The viability of Plk-deleted cells depended on the recovery of MT nucleation via BOE-M; however, some other phenotypes were not recovered in the viable strains. Thus, BOE analysis enabled the separation of the essential and non-essential cellular functions of Plk in *S. pombe*. From a broad

perspective, this study found that BOE-M can be achieved by simple genetic or environmental changes, such as lowering glucose concentration, which can be made even in a natural environment. In addition, unusual aspects of BOE-M, such as the reinforcement of downstream machinery and changes in nutrient pathways, have been revealed that are functionally unrelated. This suggests that BOE-M constitutes a powerful means to uncover a hitherto under-studied mechanism driving mitosis and to understand various aspects of genetic interactions.

2. Introduction

2.1 Process of bipolar spindle formation during mitosis in *Schizosaccharomyces pombe*

2.1.1. Centrosome/spindle pole body (SPB): A major microtubule (MT) generation center in mitosis

Bipolar spindle formation during mitosis is important for accurate chromosomal segregation. Since abnormal segregation of chromosomes can induce cell death or eventually result in cancer by increasing the chromosomal instability (Silk et al., 2013; Thompson & Compton, 2011), each process of bipolar spindle formation is highly regulated by various factors (Nigg, 2001).

The centrosome is a multifunctional organelle consisting of many components, including cell cycle regulators, checkpoint factors, and the γ-tubulin ring complex (γ-TuRC). During mitosis, the centrosome acts as a major microtubule-organizing center (MTOC)(Vasquez-Limeta & Loncarek, 2021). SPB is a yeast organelle that is functionally equivalent to the centrosome. SPBs mature by recruiting and activating the components required for bipolar spindle formation. For example, SPB components associated with MT nucleation and control of the cell cycle significantly change upon entry into mitosis (Hagan & Yanagida, 1992; Mulvihill et al., 1999; West et al., 1998). Several dynamic processes, including SPB duplication, SPB insertion into the nucleus, MT nucleation, SPB separation, and bipolar spindle formation, are sequentially observed at SPBs during spindle assembly in the fission yeast, *S. pombe* (Fig. 1).

2.1.2 SPB duplication (Fig. 1B)

SPB duplication is highly regulated following the cell cycle and has been reported to occur from late mitosis to G2 phase in fission yeast. SPB duplication occurs in the cytoplasm, and SPBs are not inserted into the nuclear envelope (NE) until mitosis (Ding et al., 1997; Uzawa et al., 2004). The best-studied process for SPB duplication is the first half-bridge assembly step. The half-bridge is a long structure assembled from the old SPB, which plays a critical role as a scaffold for assembling the new SPB by recruiting SPB components. Half bridge components, Sfi1 and Cdc31^{centrin}, are essential proteins for duplicating SPBs, and their defects cause a monopolar spindle phenotype (Lee et al., 2014; Paoletti et al., 2003). Sfi1 is composed of a long α-helix structure containing repeat sites for Cdc31^{centrin} interaction. Sfi1 also contains phosphorylation sites for cyclin-dependent kinase 1 (Cdk1) and Plo1, whereas Cdc31^{centrin} contains a Cdk1 phosphorylation site. The presence of these sites indicates that half-bridge assembly is regulated by cell cycle kinases (Bouhlel et al., 2015; Rüthnick & Schiebel, 2016).

Although the SPB duplication process is essential to form bipolar spindles, how and in which order the components are recruited during new SPB assembly remain poorly understood at the molecular level. However, a recent study using high-resolution microscopy suggested an approximate recruiting order and timing to form a new SPB (Bestul et al., 2017). During the late mitosis and G1 phase, the half-bridge is assembled. In the G1 phase, Ppc89^{CEP57}, a core SPB protein, is recruited. Other core factors are recruited during the G1 and S phases, and γ-tubulin complex components are recruited in the early G2 phase (Bestul et al., 2017).

2.1.3 SPB insertion into the nucleus (Fig. 1C)

In contrast to the open mitosis observed in most metazoan cells, closed mitosis is observed in many fungi, including fission yeast. Closed mitosis means that chromosome segregation occurs with only partial NE breakdown (NEBD). During closed mitosis, restricted NEBD occurs underneath SPBs, which are anchored at that site and nucleate MTs for chromosome attachment (Ding et al., 1997; McCully & Robinow, 1971).

The interaction of SPBs and centromeres via the linker of the nucleoskeleton and cytoskeleton (LINC) complex induces partial NEBD (Hou et al., 2012). LINC complex is composed of the KASH domain protein, Kms1, and the SUN domain protein, Sad1^{SUN} (Fernández-Álvarez et al., 2016). They assemble ring-like structures underneath SPBs and interact with other factors, such as Csi1, Lem2, Cut12, and Cut11^{NDC1}, which are important for SPB insertion (Bestul et al., 2017, 2021). Although the linkage between centromeres and SPBs is important for partial NEBD and SPB insertion, why the linkage induces partial NEBD in closed mitosis remains poorly understood. As a hypothesis, the cluster of centromeres underneath SPBs may concentrate some mitotic regulators, such as polo-like kinases (Plks), and induce NEBD (Bestul et al., 2021).

Proper NE insertion of SPBs is important for MT nucleation and inhibits nucleoplasm leakage into the cytoplasm. For example, the mutants of Cut12 and Sad1^{SUN}, which are important factors inducing NE insertion in SPBs, show severe phenotypes. In *cut12* mutants, monopolar spindles are observed because MTs are nucleated from only one side of SPBs. In addition, nucleoplasm leakage into the cytoplasm has also been observed (Bridge et al., 1998; Tallada et al., 2009). In *sad1* mutant, centromere clustering underneath SPBs and spindle formation are rarely observed, and SPBs separate from NE during mitosis (Hagan & Yanagida, 1995; Hou et al., 2012).

2.1.4 MT nucleation (Fig. 1D)

MTs are polarized filaments composed of α/β-tubulin heterodimers that form hollow cylindrical structures. The plus end of MT is highly dynamic and undergoes repeated polymerization and depolymerization (Brouhard & Rice, 2018). The high dynamicity of plus ends enables MT to rapidly perform many cellular functions

during the cell cycle, such as maintaining cell shape, trafficking of organelles or proteins, and cell division. In contrast, the minus end of the MT is anchored at the MTOCs and rarely shows any growth or shrinkage.

The γ-tubulin complex attaches to the minus ends of MTs and acts as a key template for initiating MT nucleation (Moritz et al., 2000). It is also a core component of MTOCs, such as centrosomes and SPBs. γ-TuRC is composed of γ-tubulin and five γ-tubulin complex proteins (GCP2-6). The γ-tubulin complex containing γ-tubulin and two GCPs (GCP2 and GCP3) is called the γ-tubulin small complex (γ-TuSC).

In fission yeast, γ-tubulin (Gtb1) and five GCPs, namely Alp4^{GCP2}, Alp6^{GCP3}, Gfh1^{GCP4}, Mod21^{GCP5}, and Alp16^{GCP6} are conserved. However, among the GCPs, only Alp4^{GCP2} and Alp6^{GCP3} are essential for MT nucleation, indicating that the γ-TuSC form can produce sufficient numbers of MTs in fission yeast. This situation is different from that observed in most eukaryotes, in which the γ-TuRC form is essential (Saha et al., 2021).

Because γ-TuRC is critical for MT nucleation, the components should be recruited to the SPB during SPB duplication. Pcp1^{PCNT}, the ortholog of pericentrin in fission yeast (Flory et al., 2002a; Fong et al., 2010), is an SPB component that acts as a scaffold and recruits Alp4^{GCP2} and Alp6^{GCP3} to SPB by physical interaction.

Failure in γ-TuRC recruitment to SPBs or mutations in γ-TuRC cause problems in bipolar spindle formation during mitosis. For example, in *alp4* and *pcp1* mutants, MTs emanate from only one side of the SPB and fail to form bipolar spindles (Vardy & Toda, 2000).

2.1.5 SPB separation and bipolar spindle formation (Fig. 1E)

In most animal cells, duplicated centrosomes are separated from each other to form bipolar spindles during mitosis. This separation is performed by collaborative forces mainly generated by motor proteins that move along with the MTs (Scholey et al., 2003). Other forces generated via kinetochore–MT interaction and MT polymerization dynamics have also been suggested as a power source for centrosome separation (Tanenbaum & Medema, 2010). The balance between the pulling and pushing forces acting on the centrosomes/SPBs is important for their separation. Two kinesin families, kinesin-5 and kinesin-14, move in opposite directions along the MTs and generate a counteracting force.

Kinesin-5 is a plus end-directed kinesin that is highly conserved in eukaryotes, including *Saccharomyces cerevisiae* (Kip1 and Cin8), *Xenopus laevis* (Eg5), *S. pombe* (Cut7), and *Homo sapiens* (Kinesin-5). In fission yeast, Cut7$^{Kinesin-5}$ is recruited to SPBs and spindles during mitosis. Cut7$^{Kinesin-5}$ is a homotetrameric kinesin, and this structural property makes it a crosslinker of antiparallel MTs, which emanate from each SPB. Cut7$^{Kinesin-5}$ moves along MTs toward plus ends and slides apart MTs, generating an outward pushing force for SPB separation. This outward pushing force is essential and the main force for SPB separation (Ferenz et al., 2010; Hagan & Yanagida, 1992).

There are two kinesin-14 proteins in fission yeast, Pkl1$^{kinesin\text{-}14}$ and Klp2$^{kinesin\text{-}14}$, which are minus end-directed kinesins. Pkl1$^{kinesin\text{-}14}$ and Klp2$^{kinesin\text{-}14}$ are spatially distinct. Pkl1$^{kinesin\text{-}14}$ directly interacts with γ-TuSC and downregulates MT nucleation (Olmsted et al., 2013). In addition, it delivers Msd1 and Wdr8 to mitotic SPBs and forms a ternary complex, Msd1-Wdr8-Pkl1$^{kinesin\text{-}14}$, which is important for anchoring MTs to SPBs (Yukawa et al., 2015). In contrast, Klp2$^{kinesin\text{-}14}$ mainly localizes along MTs and plays a role in generating inward forces (Yukawa et al., 2018). The counteracting interaction of Cut7$^{Kinesin\text{-}5}$ and Pkl1$^{kinesin\text{-}14}$ not only controls the force on SPBs, but is also required for proper MT nucleation (Olmsted et al., 2014).

Other factors, such as Ase1^{PRC1}, Klp9$^{Kinesin\text{-}6}$, and Peg1^{CLASP}, are required to stably maintain antiparallel MT bundles. Ase1^{PRC1} is a non-motor MT-associated protein (MAP) that serves as an antiparallel MT crosslinker and scaffold protein at the midzone in anaphase. Cells lacking Ase1^{PRC1} show unstable mitotic spindles, and some undergo spindle breakdown during anaphase (Loïodice et al., 2005). Ase1^{PRC1} becomes the main factor generating an outward pushing force in cells lacking Cut7$^{Kinesin\text{-}5}$ (Rincon et al., 2017). Klp9$^{Kinesin\text{-}6}$ forms a tetramer, is recruited by Ase1^{PRC1} to the midzone, and acts as an MT crosslinker in anaphase (Fu et al., 2009). Peg1^{CLASP} is a non-motor MAP that localizes on MTs and acts as an MT crosslinker independent of Ase1^{PRC1} in early anaphase, but dependent on Ase1^{PRC1} in late-anaphase (Al-Bassam et al., 2010).

2.2 Polo kinases

Polo-like kinase (Plk) is an important protein kinase that controls mitosis. Plk is a serine/threonine kinase whose mutants were initially characterized in budding yeast (CDC5) and *Drosophila melanogaster* (polo), which show abnormal mitosis (Hartwell et al., 1973; Sunkel & Glover, 1988). Plks are widely conserved multifunctional kinases in fungal and animal species, including *S. cerevisiae* (CDC5), *D. melanogaster* (*polo*), *S. pombe* (*plo1*), *X. laevis* (Plx-1, 2, and 3), and *H. sapiens* (Plk-1,2,3,4 and 5). Interestingly, the *Plk1* genes are completely absent in plants.

Plks have many cellular functions during mitosis in human cells; for example, Plk4 has an important role in centriole duplication (Habedanck et al., 2005). Plk gene that has the most versatile function in human mitosis is Plk1 (Fig. 2, top). Plk1 localizes to the centrosome, kinetochore, and spindle midzone, and performs different functions depending on its localization (Arnaud et al., 1998; Petronczki et al., 2008). Plk1 in the centrosome is important for mitotic spindle formation and centrosome maturation. Plk1 is required for centrosome recruitment of γ-tubulin, which is essential for bipolar spindle formation (Casenghi et al., 2003; Lane & Nigg, 1996). At the kinetochore, Plk1 phosphorylates multiple kinetochore components and suppresses kinetochore MT dynamics, which are necessary for stabilizing kinetochore–MT attachment (Elowe et al., 2007; D. Liu et al., 2012). During late mitosis, Plk1 is localized to the spindle midzone and plays a role in the recruitment of mitotic motor proteins to stabilize antiparallel MT

overlaps (X. Liu et al., 2004; Neef et al., 2003). In addition, Plk1 functions to assemble the contractile ring made of acto-myosin at the right location (Hasegawa et al., 2013). Thus, human Plk1 is critical for almost all key processes during mitotic cell division.

In the fission yeast, *S. pombe*, Plo1, the sole Plk, performs many mitotic and cell cycle functions similar to those of human Plk1 (Fig. 2, bottom). Plo1 is recruited to SPB and mitotic spindles during mitosis and is an essential gene to maintain viability. The *plo1*Δ spore failed the first division after germination (Ohkura et al., 1995), and severe phenotypes, such as failures in bipolar spindle assembly and cytokinesis, were observed in *plo1* mutants during mitosis (Ohkura et al., 1995). Subsequent analyses using temperature-sensitive mutants revealed that Plo1 is required for septum formation as an upstream factor in the septation initiation network (SIN) (Tanaka et al., 2001). Plo1 is also suggested to be required for the maturation of SPBs (Grallert et al., 2013). Plo1 plays an important role in the stress response pathway, which controls the cell cycle in an environment-dependent manner (Petersen & Hagan, 2005; Petersen & Nurse, 2007).

2.3 Casein kinase 1 (CK1)

CK1 is a serine/threonine-specific protein kinase that is conserved in humans and yeast. CK1 has been extensively studied in mammalian cells. In mammalian cells, the CK1 family includes several isoforms, namely α, β, γ1, γ2, γ3, δ, and ε and their various splice variants. CK1 members commonly have a catalytic domain, but show divergence in the non-catalytic domain at the C-terminus (Knippschild et al., 2014).

CK1 is observed at various subcellular sites, including the cell membrane, nucleus, centrosome, MT, Golgi apparatus, and endoplasmic reticulum (ER), during the cell cycle. CK1 is a multifunctional protein that is critical for embryonic development in adult cells by regulating numerous substrates (Knippschild et al., 2005). CK1α is a well-known component of the Wnt/β-catenin signaling pathway, which is important for cell proliferation and embryo development. CK1α directly phosphorylates β-catenin and eventually downregulates Wnt/β-catenin signaling by inducing β-catenin degradation (C. Liu et al., 2002).

CK1 is also associated with MTs. CK1δ phosphorylates α- and β-tubulin and MAPs (Behrend et al., 2000; G. Li et al., 2004; Wolff et al., 2005), and interacts with and phosphorylates MAP1A and tau in vitro (G. Li et al., 2004; Wolff et al., 2005). The phosphorylation of tau by CK1δ suppresses the interaction between tau and MTs (G. Li et al., 2004). CK1δ is mainly localized in the cytoplasm and Golgi apparatus during mitosis, but it can also localize to MTs and centrosomes in response to DNA damage. This suggests that CK1δ is a component of the stress-associated pathway and has the potential to influence MT dynamics or control the cell cycle at the centrosome under stressful conditions (Behrend et al., 2000). Deregulation of CK1 is associated with many diseases, such as cancer and neurodegeneration. Notably, these inhibitors have been studied as anticancer drug candidates (Roth et al., 2022).

In fission yeast, two CK1 family members, Hhp1 and Hhp2 (hereafter called Hhp1/2), are orthologous to CK1δ/ε in terms of subcellular localization (Dhillon & Hoekstra, 1994). Hhp1/2^{CK1} is distributed throughout the cell and enriched at the SPB (Elmore et al., 2018; Johnson et al., 2013). Hhp1/2^{CK1} is involved in various cellular processes, such as DNA repair, ubiquitination-dependent regulation of septation initiation, DNA recombination, and cohesion removal during meiosis (Dhillon & Hoekstra, 1994; Johnson et al., 2013; Phadnis et al., 2015; Rumpf et al., 2010). During late mitosis, Hhp1/2^{CK1} phosphorylates Sid4, which induces the recruitment of the ubiquitin ligase, Dma1, to SPBs. The recruited Dma1 at SPBs induces Sid4 ubiquitination and inhibits Plo1 recruitment to SPBs, which delays SIN signaling, thereby preventing cytokinesis (Johnson et al., 2013).

2.4 Glucose/PKA pathway

Glucose sensing and the subsequent response are essential cellular processes that allow cells to adapt to environmental conditions and maintain homeostasis. The PKA/cAMP pathway is the most conserved glucose-mediated pathway in eukaryotes. In *S. pombe*, glucose is detected by a receptor (Git3) and the G-protein complex (Gpa2, Git5, and Git11) is activated, which then activates adenylate cyclase (Cyr1) to produce cAMP (Byrne & Hoffman, 1993). Eventually, cAMP releases the inhibitor, Cgs1, from Pka1, converting Pka1 to its active form (Maeda et al., 1994). There is a link between glucose/PKA and the MT stabilizer cytoplasmic linker-associated protein (CLASP) during interphase (Kelkar & Martin, 2015). Controlling glucose uptake is also important for maintaining homeostasis and controlling cellular functions depending on the environment. In *S. pombe*, eight hexose transporters have been identified, which show different affinities to glucose. Ght5 is a major hexose transporter with the strongest affinity to glucose that plays a critical role in glucose uptake (Saitoh et al., 2015). Depending on the nutrient conditions, cells alter the transcription levels of hexose transporters and control their levels at the cell membrane. Under low glucose conditions, Ght5 is highly expressed and localizes to the cell membrane to uptake more glucose (Saitoh et al., 2015).

2.5 Bypass of essentiality (BOE)

Different organisms have different sets of essential genes for their viability and proliferation (Rancati et al., 2018; Ryan et al., 2013). This indicates that most “essential” genes are context-dependent and can become dispensable during evolution. Perhaps, a loss of essentiality is compensated for by expression of an alternative, currently “masked”, or less active mechanism to ensure a similar cellular activity. Many experimental efforts have been made to reproduce the molecular diversity found in nature (LaBar et al., 2020). Large-scale systematic experiments have been recently conducted in budding and fission yeasts, in which a number of bypass-of-essentiality (BOE) events have been identified (J. Li et al., 2019; G. Liu et al., 2015; Takeda et al., 2019; van Leeuwen et al., 2020).

In these studies, suppressors were screened for haploid strains in which an essential gene was experimentally disrupted. For 9–27% of the essential gene disruptants, a mutation or overexpression of other gene(s), or chromosomal gain makes the strain viable, indicating that essentiality depends on genetic background and that BOE could indeed occur at a certain frequency. However, in most cases, the underlying mechanism remains unexplored. It is also unclear why BOE is rarely observed in certain processes such as mitotic cell division.

Mitotic cell division is controlled by many essential genes in a given cell type (McKinley & Cheeseman, 2017; Neumann et al., 2010; Sonnichsen et al., 2005). Evolutionary evidence of BOE is clearly visible in this fundamentally critical biological process. One striking example is the centrosome, which is assembled by the action of many essential proteins in animal, fungal, and algal species, and plays a vital role in cell division and cellular motility (Conduit et al., 2015). However, the centrosome and most of its components have been lost in land plants, and yet plant cells undergo spindle assembly and chromosome segregation at high fidelity (Yamada & Goshima, 2017). Kinetochore components, such as the CCAN complex, spindle MT-associated proteins, such as TPX2, augmin, and mitotic motors, and cell cycle regulators, such as anaphase-promoting complex/cyclosome are among other examples; they are not universally conserved or essential factors (Gourguechon et al., 2013; Leong et al., 2020; Vale, 2003; Yamada & Goshima, 2017). Despite the evidence of BOE for almost all the genes involved in mitosis, only a limited number of cases can be found in experimental BOE screening. For example, two random BOE screenings in fission yeast encompassing 23 mitotic genes have identified only a single protein, Cnp20/CENP-T, despite the fact that >20% BOE has been observed for mitosis-unrelated genes (J. Li et al., 2019; Takeda et al., 2019). The BOE of *cnp20* is conceivable, as CENP-T functions in parallel with CENP-C for kinetochore assembly (Hara et al., 2018; Malvezzi et al., 2013). Another known BOE of mitosis regulators (BOE-M) in fission yeast is Cut7$^{\text{kinesin-5}}$, a plus end-directed kinesin. The viability of *cut7*Δ was restored when the opposing minus end-directed kinesin, *pkl1* was simultaneously deleted. Thus, the balance of forces applied to spindle MTs is critical (Olmsted et al., 2014; Syrovatkina & Tran, 2015; Yukawa et al., 2015). However, many other essential mitotic genes have no apparent functionally redundant or counteracting factors, and whether these relationships are general mechanisms of BOE-M is unclear. Essential mitotic genes are potential targets of cancer chemotherapy (Otto & Sicinski, 2017); it is also important to understand the BOE that underlies drug resistance.

2.6 *S. pombe* as a model organism

S. pombe (fission yeast) is a unicellular eukaryotic organism that is used as a suitable model organism for genetic analysis. Fission yeasts are rod-shaped (7–14 μm in length and approximately 4 μm in diameter) and a septum is observed in the middle of the cell following symmetric cell division (Fig. 3A).

Three different mating types of fission yeast were isolated: a homothallic strain

(968 h^{90}) and two heterothallic strains: (972 h^{-} and 975 h^{+}). In nature, fission yeast usually exists as a homothallic haploid, which can switch its mating types (Hoffman et al., 2015). Fission yeast shows a fast cell cycle and generation: In the exponential growth phase, the doubling time is 2–3 h at 32 °C. Fission yeast undergoes two types of cell cycles: mitotic and meiotic. In the mitotic cycle, fission yeast experiences a particularly long G2 phase, which occupies approximately three-quarters of the cell cycle, G1 phase, S phase (DNA replication), and M phase (mitosis). Since fission yeast completes the G1 and S phases soon after finishing the M phase, many cells remain in the G2 phase (Nasmyth et al., 1979). Under nutrient starvation conditions, a cell fuses with other cells of different mating types, resulting in a zygote, which is a cell containing a diploid genome. The zygote either undergoes meiosis and generates four spores or stays diploid and goes through the usual mitotic cycle depending on the nutrient condition (Fig. 3B). The process of mitosis and meiosis in fission yeast has been well studied, and the regulators and procedures of the cell cycle have been shown to be highly conserved in mammalian cells (Fantes, 1979; Nurse, 1975). The genome size of fission yeast is approximately 14 megabases (Mb) and contains approximately 5,000 genes on three chromosomes (*PomBase - The Schizosaccharomyces Pombe Genome Database*, n.d.; Wood et al., 2002). The chromosome size is larger than that of another yeast model organism, *S. cerevisiae* (budding yeast), which contains a 12 Mb genome on 16 chromosomes.

Yeast has many advantages as a model organism. Its cultivation and handling are easy and inexpensive in the laboratory. Live cell microscopy and protein labeling systems are well established. These genes can be easily mutated using mutagens or deleted via homologous recombination. Rapid transition between the haploid and diploid phases, depending on nutrient conditions, is also beneficial for research. In haploid cells, transgenic line isolation is simple and genetic analysis at the genome level is easier than in animal systems. In addition, the cellular phenotype of the mutants can be easily observed using fluorescence microscopy. Heterozygous diploidy, in which one allele is mutated, is sometimes useful as it offers the opportunity to study essential genes and their effects on meiosis (deletion of an essential gene in haploid cells causes immediate death). Some processes and structures, such as the RNAi pathway and the characteristic repetitive centromere and telomere sequences, that are missing in *S. cerevisiae* are preserved in fission yeast (Hayles & Nurse, 2018). Thus, genetic studies using fission yeast can be used for understanding the more complex cellular mechanisms in higher eukaryotes.

In this study, we found that the essentiality of Plk in fission yeast (Plo1) can be bypassed. Plo1, similar to human Plk1, is assumed to be essential for spindle MT formation and spindle bipolarization. However, these essential processes were restored in the absence of Plo1 via multiple independent mechanisms that increased MT nucleation and stabilization, one of which involves a remarkably simple change in glucose concentration in the culture medium and depends on CK1. Thus, this study uncovered an unexpected alternative mechanism of

spindle MT formation and further implied that more BOE-M can be reproduced by the experimental system.

3. Results

3.1 Viable yeast cells without *plo1* in several genetic backgrounds

A previous BOE screening randomly selected 93 genes on chromosome II, which included 12 mitotic genes (Takeda et al., 2019). BOE-M could not be detected in any of these genes. To further screen for BOE-M, eight other mitotic genes (*ark1*, *bir1*, *fta2*, *fta3*, *mis6*, *mis14*, *pic1*, and *plo1*) were selected and applied by the same screening method. Seven days after plating and UV mutagenesis of spores of each disruptant, growing haploid colonies for *plo1*Δ, the sole Polo-like kinase (Plk) in *Schizosaccharomyces pombe* were found (this experiment was conducted by Prof. Gohta Goshima) (Fig. 4A, first step). Plks play versatile roles in animal cell division, including centriole duplication (by Plk4), centrosome maturation, spindle assembly checkpoint satisfaction, and cytokinesis (by Plk1). It is also a possible target for cancer chemotherapy (Archambault & Glover, 2009; Cunningham et al., 2020; Otto & Sicinski, 2017). The responsible suppressor mutations through whole genome sequencing followed by genetic crossing were hexose transporter (*ght5*), a Spt–Ada–Gcn5 acetyltransferase (SAGA) complex component (*ngg1*), and PKA pathway components (*cyr1*) (Fig. 4B, left, fourth and sixth lines; Fig. 6B, C). In *S. pombe*, eight hexose transporters have been identified, which show different affinities to glucose; Ght5 is a major hexose transporter with the strongest affinity to glucose and plays a critical role in glucose uptake (Saitoh et al., 2015). This prompted me to test and found that the *plo1*Δ strain grows, albeit slower than the wild-type when the glucose concentration of the medium was lower than 0.3% (Fig. 4B, left, third line, Fig. 6A). Simultaneously, an “experimental evolution” (EVO) (also called “evolutionary repair” (LaBar et al., 2020)) experiment was conducted for the *plo1*Δ strain in a low-glucose medium (0.08%), in which serial dilution and saturation enrich the cells that have acquired beneficial mutations for proliferation (this experiment was conducted by Mr. Aoi Takeda) (Fig. 4A, “1st EVO”). The faster-growing strains obtained through this step were subjected to further evolutionary repair experiments in a high-glucose medium (“2nd EVO”) and at a different temperature (“3rd EVO”).

I determined the whole genome sequences of several viable *plo1*Δ strains and confirmed the suppressor mutations by independently generating a double mutant with *plo1*Δ. In total, 16 genes were found to assist in the growth of the otherwise inviable *plo1*Δ strain (Fig. 4B; 5; 6B, C). An example of the evolutionary repair process is shown in Fig. 7A. This strain acquired mutations in *alp6* and *aps1* during the 1st EVO but still possessed the benefit of *plo1+* gene for strain fitness (Fig. 7A). However, additional mutations in *mip1* and *ahk1* during the 2nd EVO bypassed the requirement of Plo1, since adding back the *plo1+* gene to the original locus did not further promote colony growth (Fig. 7B). Most of the

responsible genes were categorized into three classes: SAGA complex, glucose/PKA pathway, and MT regulators (Fig. 5). The SAGA complex is a general regulator of transcription, possessing histone acetyltransferase activity, and affects the expression of many genes (Grant et al., 2021). I did not analyze this in the present study. The cAMP-PKA pathway is linked to glucose homeostasis in fission yeast. Glucose is detected by a receptor (Git3), and the G-protein complex (Gpa2, Git5, and Git11) is activated, which then activates adenylate cyclase (Cyr1) to produce cAMP (Byrne & Hoffman, 1993). Eventually, cAMP releases the inhibitor Cgs1 from Pka1, converting Pka1 to its active form (Maeda et al., 1994). Furthermore, yeast cells regulate glucose uptake by changing the localization and transcriptional level of hexose transporters, including Ght5, depending on environmental conditions (Klip et al., 1994; Saitoh et al., 2015; Shashkova et al., 2015). There is a link between glucose/PKA and MT stabilizer CLASP (cytoplasmic linker-associated protein) during interphase (Kelkar & Martin, 2015). In my case, mutations in MT regulators (*alp4*, *alp6*, and *asp1*) and glucose/PKA-pathway genes additively supported the growth of *plo1*Δ (Fig. 4B).

3.2 Monopolar spindles predominate during mitosis in the absence of *plo1*

The major MT nucleator at the centrosome is the γ-tubulin ring complex (γ-TuRC), which consists of γ-tubulin and GCP subunits, including GCP2 (Alp4/Spc97) and GCP3 (Alp6/Spc98)(P. Liu et al., 2021). In animal cells, Plk1 is a critical regulator of mitosis, which is, in the early stage, required for γ-TuRC recruitment to the centrosome and thus centrosome maturation; inhibition of Plk1 leads to monopolar spindle formation(Archambault & Glover, 2009; Lenart et al., 2007). In fission yeast, cytokinesis/septation defects are most profoundly observed in *plo1* mutants, whereas monopolar spindle formation has also been described (Bahler et al., 1998; Grallert et al., 2013; Ohkura et al., 1995; Tanaka et al., 2001; Walde & King, 2014). However, actual spindle dynamics have not been analyzed for *plo1*Δ in live imaging. To analyze spindle dynamics in the absence of Plo1, live imaging of mCherry-tubulin and a spindle pole body (SPB) marker, Sad1^{SUN}-GFP was performed after *plo1*Δ spore germination with spinning-disc confocal microscopy (Fig. 8A–C). The control cell assembled bipolar spindles immediately after the disappearance of interphase MT networks (Fig. 8A: time 0 corresponds to the onset of mitosis), and cell division was completed in ~30 min. In contrast, 53 out of 56 *plo1*Δ cells after spore germination were arrested with a monopolar spindle for >1 h (Fig. 8B, C; a stronger laser exposure was applied in Fig. 8C to visualize the faint MT signals).

I compared the phenotype with other known mutants that show monopolar spindle formation, including Cut12, which drives SPB insertion into the nuclear envelope (NE)(Tallada et al., 2009; West et al., 1998), Cut7$^{kinesin\text{-}5}$, which is required for anti-parallel MT crosslinking and sliding (Hagan & Yanagida, 1990), and Cdc31^{centrin}, which is required for SPB duplication (Paoletti et al., 2003). In the *cut12-1* temperature-sensitive (ts) mutant, the lack of insertion of one of the

duplicated SPBs causes partial breakage of the NE and detachment of an SPB from the NE (Tallada et al., 2009; West et al., 1998). In another study, Plo1 was shown to regulate the formation of the Sad1 ring structure, which might be required for SPB insertion (Bestul et al., 2021). I investigated the integrity of the NE in *plo1*Δ. First, I tagged GFP to Pcp1^{PCNT}, a core SPB component (Flory et al., 2002b; Walde & King, 2014), in the *plo1*Δ background. In contrast to the *cut12-1* mutant, I always detected punctate Pcp-GFP signals (n = 20) at the pole of the monopolar spindle, suggesting that SPBs in the NE generate spindle MTs in the absence of Plo1 (Fig. 9A, B). Next, a nuclear localization signal-green fluorescent protein (NLS-GFP) efflux assay was performed, in which partial NE breakage due to SPB insertion error leads to nuclear GFP signal efflux into the cytoplasm (Tallada et al., 2009). I first confirmed the efflux in the *cut12-1* ts mutant; GFP leaked out from the nucleus 18 ± 10 min after interphase spindle disassembly at non-permissive temperatures in 20 out of 20 cells that assembled monopolar spindles (Fig. 10B, 20, 30, and 70 min; (Tallada et al., 2009)). In contrast, *plo1*Δ cells maintained GFP signals inside the nucleus during the early stage of mitosis, similar to the control strains (Fig. 10A). These data suggest that SPBs are properly inserted into the NE at the onset of spindle formation in the absence of Plo1. Notably, GFP efflux during mitotic arrest occurred in 16 out of 20 *plo1*Δ cells (69 ± 18 min after spindle assembly), suggesting that NE was partially dissolved during prolonged arrest (Fig. 10A, 100 and 200 min).

Next, I isolated *cut7*Δ and *cdc31*Δ spores with Alp6^{GCP3}-GFP (SPB) and mCherry-tubulin markers and germinated them in normal culture medium. As expected, monopolar spindles were prevalent in each sample, with only a single dot of Alp6^{GCP3}-GFP detectable at the end of spindle MTs (compare Fig. 11A and 11B/C/D). However, Alp6^{GCP3}-GFP signal intensity was significantly lower in the *plo1*Δ spindles than in *cut7*Δ or *cdc31*Δ (Fig. 11E). Consistent with this phenotype, spindle MTs were dimmer in *plo1*Δ (compare Fig. 11B and 11C/D) and *plo1*Δ was sensitive to thiabendazole (TBZ), an MT-destabilizing drug (Fig. 12A). Finally, I checked whether Cut7$^{kinesin\text{-}5}$ localization was defective in *plo1*Δ, which would cause spindle monopolarization. Cut7$^{kinesin\text{-}5}$-GFP accumulation at the SPB and spindle was delayed in the absence of *plo1* (Fig. 12B compare WT and *plo1*Δ, 0 min). However, the signals gradually recovered and reached a level comparable to the early prometaphase of control cells, at which spindle bipolarity was not recovered (Fig. 12C). Thus, it is unlikely that failure in Cut7$^{kinesin\text{-}5}$ recruitment is the major cause of spindle monopolization in *plo1*Δ. Rather, the data favor the model whereby decreased MT nucleation at SPB leads to spindle monopolization in *plo1*Δ. Consistent with this notion, monopolar spindles have been observed in mutants of the γ-TuRC component (Alp4^{GCP2})(Vardy & Toda, 2000).

3.3 Modulation of MT nucleation and stability bypassed *plo1* essentiality

Two BOE strains had point mutations in *alp4^{GCP2}* and *alp6^{GCP3}*. Double *alp4-D440E plo1*Δ and *alp6-V664F plo1*Δ strains recovered colony-formation ability in a normal (high-glucose) medium (Fig. 4B). Thus, the essentiality of Plo1 was

bypassed by a single specific mutation in the MT nucleating machinery. I also performed a spot test for single *alp6-V664F* and *alp4-D440E* mutants (Fig. 4C). *alp6-V664F* grew more slowly than the wild-type, whereas no difference in colony growth was observed for *alp4-D440E*.

I investigated whether the mutation in *alp4* could restore γ-TuRC recruitment to the SPB in the absence of *plo1*. To address this, I isolated a double *alp4-D440E plo1*Δ mutant with Alp6^{GCP3}-GFP and mCherry-tubulin markers (Fig. 13A). Quantification indicated that both GFP and mCherry signals were partially but significantly restored by the *alp4-D440E* mutation (Fig. 13B, C). In 50% of the cells (n = 46), spindle bipolarity was recovered after a delay, and cytokinesis was completed (Fig. 13A, left), whereas monopolar states were persistent for >60 min in 30% of the cells (Fig. 13A, right), explaining the partial rescue of the viability by this specific mutant of *alp4*. Consistent with frequent spindle bipolarization, GFP efflux in the viable *alp4-D440E plo1*Δ and *ght5*Δ *plo1*Δ strains was less frequently observed than in single *plo1*Δ (19% and 21%, n = 26 and 48) (Fig. 10C, D).

Asp1$^{PPIP5K/Vip1}$ is another MT-related factor and its mutation assisted in the growth of *plo1*Δ (Fig. 4B). Asp1$^{PPIP5K/Vip1}$ is known to have a kinase domain at the N-terminus and a phosphatase domain at the C-terminus, and the latter is required for MT destabilization (Pohlmann et al., 2014). Interestingly, two mutations acquired during experimental evolution were located at the C-terminus (Fig. 5). The mutation did not affect colony growth in the presence of Plo1 (Fig. 4C). However, time-lapse imaging showed that the *asp1-D507G plo1*Δ strain exhibited more spindle MT signals than *plo1*Δ, indicating that mutations in the C-terminal domain of Asp1$^{PPIP5K/Vip1}$ cause spindle MT stabilization (Fig. 14A–D). These data suggested that bypass of Plo1 essentiality is achieved by increasing MT stability and/or generation.

3.4 Glucose limitation bypasses *plo1* essentiality

The mechanism by which glucose limitation recovers the viability of *plo1*Δ is not readily explainable. Glucose reduction did not appear to change Plo1-GFP localization. Both in high (3%) and low (0.08%) glucose media, Plo1-GFP was localized to SPBs from prophase to metaphase and delocalized at anaphase (Fig. 15A, B). To observe the process of mitosis, I followed Alp6^{GCP3}-GFP and spindle MTs in double *ght5*Δ *plo1*Δ (Ght5 is a glucose transporter). Interestingly, Alp6^{GCP3}-GFP accumulation at the SPB and spindle MT abundance was restored in the double mutant (Fig. 16A–D). MTs appeared to be more stable in *ght5*Δ, as incomplete disassembly of interphase MTs was often observed at the onset of mitosis, which reflected more total mCherry signals in the mutant than in the wild-type (arrows in Fig. 16B). Consistent with this observation, *ght5*Δ conferred resistance to TBZ (Fig. 16E).

Next, I tested the localization of Mid1^{anillin}, which is recruited to the equatorial region during mitosis and defines the division site, depending on phosphorylation by Plo1 (Almonacid et al., 2011). I observed that Mid1^{anillin} was not properly

localized to the cortex in the viable *ght5*Δ *plo1*Δ strain, whereas the cortical localization was normal in single *ght5*Δ (Fig. 17A–C). Consistent with this observation, the septum was mislocalized in *ght5*Δ *plo1*Δ, similar to *mid1*Δ (Fig. 17D–F). The results revealed that the septation error was not directly linked to the lethality of *plo1*Δ. Cdc7^{Hippo} is another downstream factor of Plo1; the SPB localization of Cdc7^{Hippo} during metaphase, but not telophase, is impaired in the *plo1* mutant (Wachowicz et al., 2015). In the viable *ght5*Δ *plo1*Δ strain, Cdc7^{Hippo}-GFP localization at metaphase SPB was not detectable (Fig. 18A, B). These results indicated that not all Plo1 downstream events, including the phosphorylation of the direct substrate, are restored by *ght5* mutations.

3.5 Casein kinase 1 (CK1) constitutes a masked mechanism for spindle bipolarization

Since proteins in the glucose-PKA pathway are not SPB- or spindle-associated, we hypothesized that other pathways are enhanced when glucose is limited, which promotes γ-TuRC localization. To identify the effector proteins in such pathways, I performed a genetic screening, with the aim to acquire mutants that were synthetic lethal with double *ght5*Δ *plo1*Δ or *pka1*Δ *plo1*Δ. For this, I first transformed a plasmid containing the *plo1*$^{+}$ gene in the double mutants, conducted mutagenesis, and selected the strains that could not lose the plasmid (Fig. 19). A total of 13 mutants were identified that were synthetic lethal with either *ght5*Δ *plo1*Δ (seven strains) or *pka1*Δ *plo1*Δ (six strains). Possibly responsible genes were selected based on sequencing (e.g. dramatic amino acid changes, nonsense mutations, or identified in multiple strains). Synthetic lethality was confirmed for five genes (*bub1*, *hhp1*, *iml1*, *mak1*, and *wis1*) and one gene (*sin1*) by gene disruption and crossing with *ght5*Δ *plo1*Δ and *pka1*Δ *plo1*Δ, respectively. However, two mutants (*iml1* and *wis1*) and one mutant (*sin1*) resulted in poor growth when singly combined with *ght5*Δ and *pka1*Δ, respectively. These were excluded from further analysis because the major basis of synthetic lethality may not involve the lack of Plo1 kinase. *mak1* showed complex genetic interaction; while *mak1*Δ *ght5*Δ grew normally, synthetic lethality was revealed when mCherry-tubulin was introduced. In addition, the double *mak1*Δ *pka1*Δ grew poorly in the absence of mCherry-tubulin expression. Therefore, this gene was also excluded from further analyses. In contrast, triple disruption was not selected for two other genes, *bub1* and *hhp1* (Fig. 20A, B), whereas the double mutants with *ght5*Δ grew in a manner indistinguishable from the single *ght5*Δ even in the presence of mCherry-tubulin. I further confirmed the synthetic lethality of *hhp1*Δ with other PKA-pathway genes *git1*Δ *plo1*Δ and *pka1*Δ *plo1*Δ (Fig. 20C, D). Thus, *bub1* and *hhp1* were essential for *plo1*Δ viability.

To identify the lethal event caused by these mutations, we observed live cells of the triple disruptants, *bub1*Δ *ght5*Δ *plo1*Δ and *hhp1*Δ *ght5*Δ *plo1*Δ. For this, I selected each triple disruptant that possessed the Plo1-GFP multicopy plasmid. Viable cells were cultured in non-selective medium, by which cells naturally lose

the plasmid at a certain probability. Time-lapse images were then acquired. I analyzed the cells that no longer had Plo1-GFP signals, as these cells represent triple gene disruptants. As a control, I prepared double *ght5*Δ *plo1*Δ possessing the Plo1-GFP plasmid and performed the identical "plasmid loss" culture. In the control strain that had no GFP signals, monopolar spindles were converted into bipolar spindles within 30 min, followed by entry into anaphase, in >60% cells, as expected (Fig. 21A, D). In contrast, in triple *bub1*Δ *ght5*Δ *plo1*Δ, anaphase began even when spindles were still monopolar in 13 out of 43 cells (Fig. 21B). This phenotype explains the lethality of the strain and is consistent with the fact that Bub1 is an integral component of the spindle assembly checkpoint, which prevents premature anaphase entry (Bernard et al., 1998). In contrast, in *hhp1*Δ *ght5*Δ *plo1*Δ, >80% of cells were arrested in monopolar states for >30 min, and spindle bipolarization and anaphase entry were scarcely observed, and the intensity level of Cherry-tubulin decreased, similar to the *plo1*Δ strain in the normal medium (Fig. 21C–E). I concluded that the lethality of *hhp1*Δ *ght5*Δ *plo1*Δ comes from a defect in spindle bipolarization, similar to *plo1*Δ in the normal medium.

hhp1 encodes casein kinase I (CK1), which is distributed throughout the cell and is enriched at the SPB (Elmore et al., 2018; Johnson et al., 2013). Hhp1^{CK1} is involved in a variety of cellular processes, such as DNA repair, ubiquitination-dependent regulation of septation initiation, DNA recombination, and cohesin removal during meiosis (Dhillon & Hoekstra, 1994; Johnson et al., 2013; Phadnis et al., 2015, p. 11; Rumpf et al., 2010). However, to the best of our knowledge, Hhp1^{CK1} has not been directly linked to spindle function in fission yeast.

To investigate the basis of the unexpected genetic interaction, I first tested whether Hhp1^{CK1} expression/localization was altered by *ght5* disruption. To this end, I tagged GFP to Hhp1^{CK1} in the wild-type *ght5⊿* and *ght5*Δ *plo1*Δ backgrounds. Time-lapse mitosis imaging and GFP intensity quantification indicated that Hhp1^{CK1} localization was unchanged, but the overall abundance became more variable and on average slightly increased in the absence of *ght5* (100 ± 12 , 145 ± 35, and 157 ± 31 [AU], n = 30 each)(Fig. 22A, B). However, the level of *hhp1* mRNA was not elevated by a glucose reduction, suggesting that post-transcriptional regulation underlies the increased Hhp1 in the cell (Fig. 22C). Next, I tested whether the upregulation of Hhp1^{CK1} is necessary for the bypass of Plo1. I selected the *hhp1*Δ *ght5*Δ *plo1*Δ triple disruptunt that possesses the Hhp1^{CK1}-GFP multicopy plasmid, and conducted a plasmid-loss experiment. In this experiment, GFP signal intensity served as an indicator of intracellular levels of the Hhp1 protein. Time-lapse imaging and subsequent image analysis showed that the level of the Hhp1^{CK1} protein was overall correlated with the efficiency of spindle bipolarization (Fig. 23A). However, the impact of the slight increase in Hhp1^{CK1} observed in *ght5*Δ was marginal, and when I compared the time required for monopolar-to-bipolar conversion in the cells with endogenous Hhp1-GFP levels, I saw a slight and statistically nonsignificant decrease (Fig. 23B). Thus, a moderate increase in Hhp1 helps cell division, but is likely not essential for BOE by glucose reduction.

Next, I investigated whether ectopic expression of Hhp1^{CK1} was sufficient for the recovery of *plo1*Δ viability. I tested the expression of Hhp1^{CK1} by two different promoters on the multicopy plasmid, but I could not obtain data that reproducibly showed that Hhp1^{CK1} expression restored *plo1*Δ colonies (Fig. 24). In addition, Hhp1^{CK1} expression from the plasmid did not enhance the growth of *alp6-V664F plo1*Δ or *alp4-D440E plo1*Δ, which was viable on its own but had slower growth than the wild-type (Fig. 24). Thus, an increase in Hhp1^{CK1} levels alone did not increase the fitness of *plo1*Δ. Collectively, I concluded that the increase of Hhp1^{CK1}is not sufficient or prerequisite for the bypass of Plo1 essentiality.

Finally, I observed spindle dynamics in the *hhp1* single disruptant. Most of the cells (99%) assembled bipolar spindles, and mitosis proceeded comparably to the wild-type. However, among the 272 cells monitored, I found that 3 cells (1%) formed monopolar spindles; this was not observed in my imaging of control Hhp1^{CK1}+ cells (N >336) (Fig. 25A, B). Furthermore, *hhp1*Δ *ght5*Δ was more sensitive to TBZ than *ght5*Δ (Fig. 16E). Thus, Hhp1^{CK1} has a very mild, almost negligible level of contribution to MT stability and bipolar spindle assembly in the presence of Plo1, but becomes essential in the absence of Plo1. In *S. pombe*, *hhp2*$^{+}$ also encodes CK1 (Dhillon & Hoekstra, 1994). Therefore, I selected the *hhp1*Δ *hhp2*Δ double disruptant expressing mCherry-tubulin and Alp6^{GCP3}-GFP, and performed time-lapse microscopy. Interestingly, monopolar spindles appeared at a much higher frequency than single *hhp1*Δ (29%, n = 79)(Fig. 25A). Other phenotypes, such as undeveloped spindle MTs, were also observed in the double disruptant (Fig. 25B, right). I further determined if *hhp2*Δ would be synthetically lethal with three viable *plo1*Δ strains (*ght5*Δ *plo1*Δ, *git1*Δ *plo1*Δ, and *pka1*Δ *plo1*Δ). Unlike *hhp1*Δ, no strains showed synthetic lethality with *hhp2*Δ. Thus, Hhp1^{CK1} and Hhp2^{CK1} were not completely redundant for bypass-related functions, which corroborates the previous report that they are different in subcellular localization and abundance (Elmore et al., 2018).

3.6 Masked contribution of CK1 to spindle formation in a human colon cancer cell line

Among the four Plks in mammals, Plk1 is required for centrosome maturation and bipolar spindle formation in many cell types and is thus most analogous to *S. pombe* Plo1. There are also several CK1 family members in mammals. As CK1δ is localized at the centrosome(Greer et al., 2014; Greer & Rubin, 2011), I tested whether CK1δ constitutes the masked mechanism behind Plk1 in human cells (Fig. 26). The treatment of a human colon cancer line (HCT116) with a low concentration (3 nM) of Plk1 inhibitor BI2536 resulted in a slightly higher frequency of monopolar spindle appearance in early prometaphase (Fig. 26A, B). PF670462, an inhibitor of CK1δ/ε (Aquino Perez et al., 2021; Meng et al., 2010), did not increase the number of monopolar spindles. However, when both inhibitors were simultaneously treated, 36% of the cells first assembled monopolar spindles (Fig. 26A, B). The monopolar spindles were eventually converted to bipolar spindles; however, this process required >30 min in ~20% of

the cells when two compounds were simultaneously added (Fig. 26C). These results highlight the importance of CK1, perhaps CK1δ, in spindle bipolarization in human colon cancer cells, when Plk1 function is partially impaired.

4. Discussion

This study represents a rare example of the experimental BOE of genes required for mitosis. The BOE occurrence in Plo1 was unexpected, as it has been recognized as a versatile, essential kinase in mitosis not only in animal cells but also in fission yeast. However, there is evolutionary evidence supporting that this gene can be deletable; for example, plants have lost Plks, whereas the ancestral algae possess Plks (Okamura et al., 2017).

4.1 Property of bypass pathway of *plo1* and characteristics of mutations obtained from different screening

Plo1 loss can be rendered non-lethal by mutations in several genes, some of which were unrelated to each other and not associated with spindle functions at first glance. However, this is in accordance with many previous examples of BOE or evolutionary repair in the laboratory, where compensatory mutations are often found in genes outside of the perturbed functional module (LaBar et al., 2020).

In initial BOE screening using *plo1*Δ spores, only one viable strain was recovered, in which the gene encoding the glucose transporter Ght5 was lost through a deletion event. Subsequent evolutionary repair (experimental evolution) experiments led to the identification of more mutations, many of which restored viability of *plo1*Δ without the *ght5* mutation. The mutated genes identified in EVO strains were also divergent as they rarely overlapped among different EVO strains. Thus, EVO strains can increase fitness using different combinations of genes, which might constitute different functional modules. In contrast, the initial mutagenesis-based screen, namely UV mutagenesis, led to the identification of *ght5* mutations in five out of the eight strains. Thus, the fitness-increasing mutations were quite different depending on the method used, and our UV mutagenesis screen was not sensitive enough to capture all possible BOE events. More BOE events, including BOE-M, may be observed in yeasts by applying more sensitive methods or simply by increasing the screen scale.

4.2 Glucose reduction as a bypass pathway of *plo1*

The bypass of Plo1 essentiality by glucose reduction in the medium is intriguing from multiple perspectives. First, it illustrates the non-absolute nature of gene essentiality (Rancati et al., 2018). If the low-glucose medium was used as the standard yeast culture medium, then Plo1 would have been assigned as a non-essential gene in *S. pombe*. Second, a change in available nutrients occurs, perhaps frequently, in the natural yeast habitat. The decrease in available glucose allows the yeast to lose a critical mitotic kinase and develop an alternative mechanism. The data support the theory that environmental change combined with gene mutations drives molecular diversity, namely, variation in genes required for an essential process (LaBar et al., 2020). Third, the change in

fundamental metabolism alters the expression of many genes (Saitoh & Yanagida, 2014), offering a unique “genetic background” that is not achieved by mutations in a few mitotic genes. In the case of *plo1*Δ, a critical factor for survival was Hhp1^{CK1}. Because Hhp1^{CK1} is SPB-associated, it is possible that critical Plo1 substrates (such as γ-TuRC or its associated factor) are phosphorylated by Hhp1^{CK1}. However, CK1 is unlikely the sole element of BOE based on glucose repression and other factors should be also involved, as Hhp1^{CK1} overexpression alone was not sufficient to restore the viability of *plo1*Δ (Fig. 27). Interestingly, *S. cerevisiae* Hrr25^{CK1} can phosphorylate and activate the γ-tubulin complex *in vitro* and this phosphorylation is required for *in vivo* γ-tubulin functions (Peng et al., 2015). Whether Hrr25^{CK1} constitutes a masked mechanism of Cdc5^{Plk1} in *S. cerevisiae* is an intriguing question for future investigation.

4.3 Essential and non-essential functions of essential genes

A series of analysis suggested that bypass mutations converge into a common outcome: the increase in spindle MTs. This was achieved by multiple direct and indirect mechanisms, such as mutations in an MT destabilizer and MT nucleator, or through glucose starvation. In contrast, the septum phenotype was not rescued in the viable strain. Thus, although multiple defects have been identified in the *plo1* mutants, MT formation is directly linked to viability.

This illustrates that an essential gene has both essential and non-essential functions for cell survival, which can be distinguished by BOE analysis. Furthermore, it indicates the importance of the use of complete knockout strains in BOE analysis despite the labor involved; otherwise, critical functions of an essential gene and many bypass pathways may be overlooked. In fission yeast, partial mutants, such as temperature-sensitive (ts), cold-sensitive (cs), and analogue-sensitive (as) mutants, have been generally used to study essential genes. They are easy to handle, but many of them do not fully lose their viability, even under non-permissive conditions. For example, many of *plo1*.ts mutants were viable at 36 °C (Fig. 28A), while a *plo1*.as mutant completely lost its viability only at extremely high concentrations of 3-BrB-pp1 (50 μM) (Fig. 28B). In these mutants, the partial functions of essential genes are still intact, and these functions are likely to be the core functions for cell survival. Indeed, the monopolar spindle phenotype, which is frequently observed in *plo1*Δ, makes up only a small proportion of the defective phenotypes of *plo1*.ts mutants. Therefore, use of non-knockout mutants can decrease the sensitivity of BOE screening, resulting in failure to identify many BOE cases in which the core functions of the essential genes are substituted.

4.4 BOE research for cancer chemotherapy

BOE, or synthetic viability, is a critical challenge in cancer chemotherapy because of the emergence of resistance (Ashworth et al., 2011). Plk inhibitors have been recognized as promising antitumor drugs (Cunningham et al., 2020;

Otto & Sicinski, 2017). However, our study suggests that there may be resistant cells involving CK1 and that double inhibition of Plk1 and CK1δ may be more suitable for mitotic cell perturbation.

Various cancer cells show different systems of glucose uptake and metabolism compared to normal cells (Lin et al., 2020). In the tumor microenvironment, there are different preferences for nutrient consumption depending on the cell type (Reinfeld et al., 2021). Hence, BOE through nutrient changes, as in the case of *plo1*, is also intriguing from this perspective.

4.5 Cause of the monopolar spindle phenotype observed in *plo1*Δ

Although the monopolar spindle phenotype was observed in *plo1*Δ (Fig. 8B, C; 9 B), the cause and underlying mechanism remain unclear. A few studies have reported that the monopolar spindle phenotype in *plo1*Δ is caused by the failure of SPB insertion into the nucleus (Bestul et al., 2021; Fong et al., 2010). However, there are several differences between *plo1*Δ and other SPB insertion mutants. In *plo1*Δ, (1) spindles were observed (Fig. 8C), (2) SPBs were attached to the NE (Fig. 9A), (3) SPBs were not separated from each other (compare Fig. 9A and B), and (4) NLS-GFP leakage was not observed immediately after entering mitosis (compare Fig. 10A and B). Therefore, I suggest that monopolar spindle formation in *plo1*Δ is caused by defective MT assembly rather than SPB insertion. In support of this notion, (1) many *plo1*Δ suppressor mutations were associated with MTs rather than SPB insertion (*alp4*, *alp6*, and *asp1*; Fig. 5), (2) *plo1*Δ phenotype, which decreased alp6-GFP intensity at SPBs after mitosis entry (Fig. 11E, 13B, 16C), is similar to the *pcp1-15* mutant, which cannot recruit a γ-TuSC component to the SPB (Fong et al., 2010), and (3) Plo1 is implicated in the maintenance of $Pcp1^{PCNT}$ at SPB (Walde & King, 2014). Based on these results, I speculate that the most critical cause of monopolar spindle formation in *plo1*Δ is a problem in MT nucleation, which is mediated by $Pcp1^{PCNT}$ in mitotic SPB.

4.6 Interpretation of suppressor mutations of *plo1*

There are suppressor mutations that were determined by our BOE screening but not seriously analyzed in this study (Fig. 5, categorized in others). $Mip1^{RAPTOR}$ is an essential gene and homologous to the regulatory-associated protein of mTOR (Raptor) in mammals. Raptor interacts with the target of rapamycin complex (TOR) kinase and makes. TOR pathway is stimulated by nutrients (glucose, amino acid) or growth factors, and controls cell growth and cell proliferation (Saxton & Sabatini, 2017). The location of the $Mip1^{RAPTOR}$ mutation, as determined by our whole genome sequencing, was in Trp-Asp (WD) 40 repeat domain, which is usually associated with protein-protein interaction.

Ahk1 is a mitogen-activated protein kinase (MAPK) pathway scaffold protein. The function of Ahk1 is little known in fission yeast. However, in budding yeast, Ahk1 is a scaffold protein for the high-osmolarity glycerol (HOG) MAPK pathway. Because multiple MAPK pathways share their components, the function of Ahk1

to recruit components in one place ensures that only HOG MAPKs are active when stimulated (Nishimura et al., 2016). Since both the TOR and MAPK pathways are regulated by nutritional status, mutations in those pathway components may offer a special genetic background to restore *plo1*Δ lethality, as in the case of recovery of *plo1*Δ lethality by the Glucose/PKA pathway.

Nudix hydrolase Aps1^{DDP1} is a phosphatase involved in inositol pyrophosphate (IPP) metabolism (York et al., 2005). The metabolism of intracellular IPP has been reported to be related to MT stabilization and destabilization (Pohlmann et al., 2014). One of the suppressor mutations I determined, Asp1$^{PPIP5K/Vip1}$, also regulates intracellular inositol hexakisphosphate (IP^7) concentration and is implicated in MT destabilization (Pohlmann et al., 2014). Similarly, the mutation in Aps1^{DDP1} has been reported to increase intracellular IP^7 concentrations (Steidle et al., 2016). Thus, the mutation of Aps1 ^{DDP1} may restore *plo1*Δ lethality by altering the intracellular IPP metabolism and enhancing MT stabilization, similar to the restoration of *plo1*Δ lethality by *asp1* mutations.

5. Materials and methods

Yeast strains and media

I followed Takeda et al. (2019) for the yeast culture and gene disruption. Complete medium YE5S contained 1% yeast extract and 3% (w/v) glucose, supplemented with adenine, leucine, histidine, uracil, and lysine, whereas glucose was reduced to 0.02% in the low-glucose medium. Synthetic PMG and EMM media were used when selection was based on adenine, leucine or uracil. Cells were cultured at 32°C (plate) or 30°C (liquid), unless other temperatures are indicated. Sporulation was induced in an SPA plate. Gene disruption, site-directed mutagenesis, and GFP/mCherry tagging were performed using the standard one-step replacement method (i.e. homologous recombination). Transformation was performed using the conventional LiAc/PEG method (Moreno et al., 1991), and targeted integration was confirmed by PCR. Selection of the strain after random spore or transformation was based on leucine, uracil, G418 (100 μg/mL), hygromycin (50 μg/mL), clonNAT (100 μg/mL), or blasticidin S deaminase (37.5 μg/mL). The strains, plasmids, and primers used in this study are listed in Tables 1, 2, and 3, respectively.

Human cell culture

The human colon cancer-derived HCT116 line, in which the endogenous TubG1 gene (γ-tubulin) was tagged with mClover, was cultured in McCoy's 5A medium (Gibco) supplemented with 10% serum and 1% antibiotics (Tsuchiya & Goshima, 2021). Plk1 inhibitor BI2536 (3 nM) and CK1 inhibitor PF670462 (2 μM) were treated for 24–30 h prior to imaging, whereas 30 nM BI2536 was added at the beginning of imaging. MTs were stained with 50 nM SiR-tubulin for 2 h prior to imaging; this concentration of SiR-tubulin did not significantly affect MT growth and nucleation in this cell line (Tsuchiya & Goshima, 2021).

BOE screening and confirmation

A preliminary experiment done by Prof. Gohta Goshima followed the method described by Takeda et al. (2019). The UV mutagenesis for *plo1* screening was performed with a larger scale (9×10^7 spores). 12 viable colonies were isolated from this screening. Mutations were detected by PCR and whole genome sequencing performed on 8 among 12 viable colonies. Analysis of the genome sequence of the strain identified a unique ~7 kb deletion on chromosome III, in which three genes, *SPCC1235.17*, *SPCC1235.18*, and *ght5,* were included. Sequencing of the three strains verified that all had mutations or deletions in the *ght5* locus; one showed a mutation from TGG to TAG that introduced a premature stop codon in *ght5* and another showed Gln^{152} to Pro substitution of *ght5*. To confirm this suppression, the *ght5* gene was independently deleted by homologous recombination, and the growth of *ght5*Δ *plo1*Δ cells was investigated using a spot test. Whole genome sequences of the other three *plo1*Δ revertants identified other suppressor candidates. One strain had TT instead of AC in the

ngg1 coding region, which introduces a premature stop codon. Ngg1 (also called Ada3) is a component of the SAGA complex (Ringel et al., 2015). To investigate whether the mutations in *ngg1* rescue *plo1*Δ lethality, a genetic linkage test was conducted with the *rec6* gene, which is located close to *ngg1*. The other two revertants had mutations in the *cyr1* gene (encoding adenylate cyclase, a component of the PKA pathway). Nucleotide insertion in *cyr1* of one strain caused a frameshift that induced a premature stop codon, whereas the other strain had an amino acid change from Asn to Lys. Therefore, the *plo1*Δ rescue ability by *pka1* or *cyr1* deletion was tested. The strains lacking both *pka1* and *plo1* or *cyr1* and *plo1* grew on 3% glucose medium, albeit slower than the wild-type.

Whole genome sequencing

Approximately 2 × 10^8 cells were harvested, and their genomic DNA was extracted using Dr. GenTLE (Takara). The genomic DNA was sequenced by BGI, Novogene, or the gene sequencing facility at Nagoya University, where the read length of the sequence was 150 bp or 81 bp. The FASTQ file was modified and mapped using CLC genomic workbench software. The ends (5 bp from the 5′ end and 1 bp from the 3′ end) of each fragment were trimmed, and these fragments were then filtered for a minimum sequencing quality of 30 datasets to reduce the error ratio. The fragments were aligned to the *S. pombe* genome reference and formatted as BAM files. IGV was used to visualize the BAM file and check the mutation site. Insertion, deletion, single nucleotide variation (SNV), and large indels were investigated. All the WGS data are available at Sequence Read Archive (SRA) at NCBI (accession number: PRJNA768628).

Experimental evolution

Experimental evolution was conducted with serial dilution and saturation (Laan et al., 2015). Saturated culture after passage (10 mL) was 1,000-fold diluted for the next passage. After culturing for 150–200 generations, cell cultures were spread onto agar plates, and the fastest growing colonies were selected for each culture. In the first round, six *plo1*Δ colonies were inoculated into 0.08% glucose liquid medium with G418 (10 μg/mL; in order to avoid microbial contamination) and cultured at 30°C. Eventually, six independent colonies were picked up (hereafter called "1st EVO" strains). They showed faster colony growth on 0.08% glucose agar plate than the original *plo1*Δ strain. Three of them also formed small colonies on the normal 3% glucose medium. These strains were further subjected to experimental evolution using 3% glucose medium with G418 (10 μg/mL) at 30°C (two or three independent cultures). In the end, eight "evolved" strains (i.e. the fastest growing strains) were obtained as *plo1*Δ second-round evolution strains (hereafter called 2nd EVO). Another round of experimental evolution (3rd EVO) was carried out for *git1*Δ *plo1*Δ and *pka1*Δ *plo1*Δ strains at 36°C (two and six independent cultures, respectively), as these formed tiny colonies at 36°C, whereas the *plo1*Δ strain did not grow even in the low-glucose medium at this high temperature. I determined the genome sequences and identified the specific mutations in five out of six strains from 1st EVO, including three strains for which

2nd EVO selection was carried out, and six out of eight strains from 2nd EVO. On average, I found 2.2 mutations introduced in the open reading frame. Three out of the five 1st EVO strains had a point mutation in SAGA complex genes (*spt20*, *sgf73*, and *spt7*). Mutations in glucose transporters or PKA-pathway genes (*ght5*, *ght8*, *git1*, and *ght8*) were found in four of the six 2nd EVO strains. From the 3rd EVO, I sequenced the three fastest growing clones and found *asp1* mutations in two strains and *tra1* (SAGA) in the third strain.

Synthetic lethality screening

Double disruptants *ght5*Δ *plo1*Δ and *pka1*Δ *plo1*Δ were transformed with the Plo1 plasmid (*ura4+*). Cells ($5 \times 10^4 - 1 \times 10^6$ cells) were mutagenized with UV (150 or 200 × 100 $\mu J/CM^2$; UVP Crosslinker CL-1000) and plated onto a PMG (*ura4–*) plate. After 6 d, the colonies were replica plated onto YE5S plates. After 2 d, the colonies were replica plated onto 5-FOA and PMG (*ura4–*) plates. Cells that could not survive in the absence of the plasmid were isolated (inviable colonies after replica plating onto 2 mg/mL 5-FOA-containing plates). For one of the obtained strains, the genomic DNA library (pTN-L1, NBRP) was transformed into the strain, and the colonies found on 5-FOA plates were isolated. The plasmid extracted from the colonies was sequenced and found to encode *hhp1+*. However, this method did not work well for other strains. Therefore, for the other 12 strains, whole genome sequences were determined and candidate mutations (nonsynonymous and frameshift) were inspected by independent deletion and crossing.

Microscopy

Exponentially growing yeast cells or spores were attached to a 1 μg/mL lectin-coated glass plate for >10 min at 32°C (Ashraf et al., 2021). Live imaging was performed with a spinning-disc confocal microscope (Nikon Ti; 100× 1.45 NA) with a perfect focus system. The cells were maintained at 32°C in a stage-top heater. Images were taken using an ImagEM CCD camera (Hamamatsu) every 1 –3 min for exponentially growing cells or every 1 or 2 min for germinating spores (z-stacks: 1 μm × 5 sections). Spores were pre-incubated for 10–12 h in 3% YE5S medium before imaging. For imaging that involved plasmid loss, cells were pre-incubated overnight in PMG without uracil or leucine and exponentially growing cells were transferred to 3% YE5S medium for ~24 h prior to microscopy. Human cell live imaging was performed with a spinning-disc confocal microscope (Nikon Ti; 40× 1.45 NA) with a perfect focus system. Images were captured using an ImagEM CCD camera (Hamamatsu). The cells were maintained at 37°C in a stage-top heater, where CO_2 was supplied. Z-stack images (3 μm × 5 sections) were taken every 3 min. Images were analyzed using FIJI, and the data were plotted using GraphPad Prism software. The signal intensity of mCherry-tubulin on the spindle and Hhp1-GFP in late G2 was measured after maximum projection, whereas a single focal plane was selected for Alp6-GFP and Cut7-GFP measurements. Two Alp6-GFP signals on the bipolar spindles were summed to obtain the total intensity. The maximum projection images are presented in the

figures.

Real time PCR

Exponentially growing yeast cells were lysed with zymolyase (50 U per 1×10^7 cells), and total RNA samples were prepared using the RNeasy Plant Mini kit (Qiagen), using the yeast protocol described in the manufacturer's instructions of RNeasy Mini Kit (Qiagen). To eliminate genomic DNA contamination, an additional DNase treatment was performed using an RNase-free DNase Set (Qiagen). PrimeScript II (Takara) was used for the reverse transcription. Real-time PCR was performed and analyzed using Step One Plus (Applied Biosystems) with SYBR Green Master Mix (Applied Biosystems). The primer set designed at the C-terminus of *act1* was used as the control (Saitoh et al., 2015). The copy number of *hhp1* mRNA relative to *act1* was calculated from a standard curve drawn using serial dilutions of cDNA as the templates.

Statics

All statistical analyses were performed using the GraphPad Prism software. Two-way ANOVAs were applied between the two groups in Fig. 13B, 13C, 14D, 16C, 16D, and 21E, and a two-way ANOVA with multiple comparisons using Tukey's test to compare multiple groups in Fig. 11E and Fig 22B and a one-way ANOVA with multiple comparisons using Tukey's test to compare the three groups (Fig. 23B), and a simple linear regression in Fig. 23A. The data distribution was assumed to be normal, but this was not formally tested. Established P values were denoted as follows: $P > 0.05$ (ns), $P < 0.05$ (*), $P < 0.01$ (**), $P < 0.001$ (***), and $P < 0.0001$ (****). Error bars in the graph represent the SEM or SD of each group. Experiments were performed twice or more, and the data from one experimental set were presented after quantitative analysis, except for Fig. 16C, 16D, 22B, 23A, 23B, 26B and 26C, where the data from multiple experiments were combined because of insufficient sample numbers in a single experiment.

6. Figures

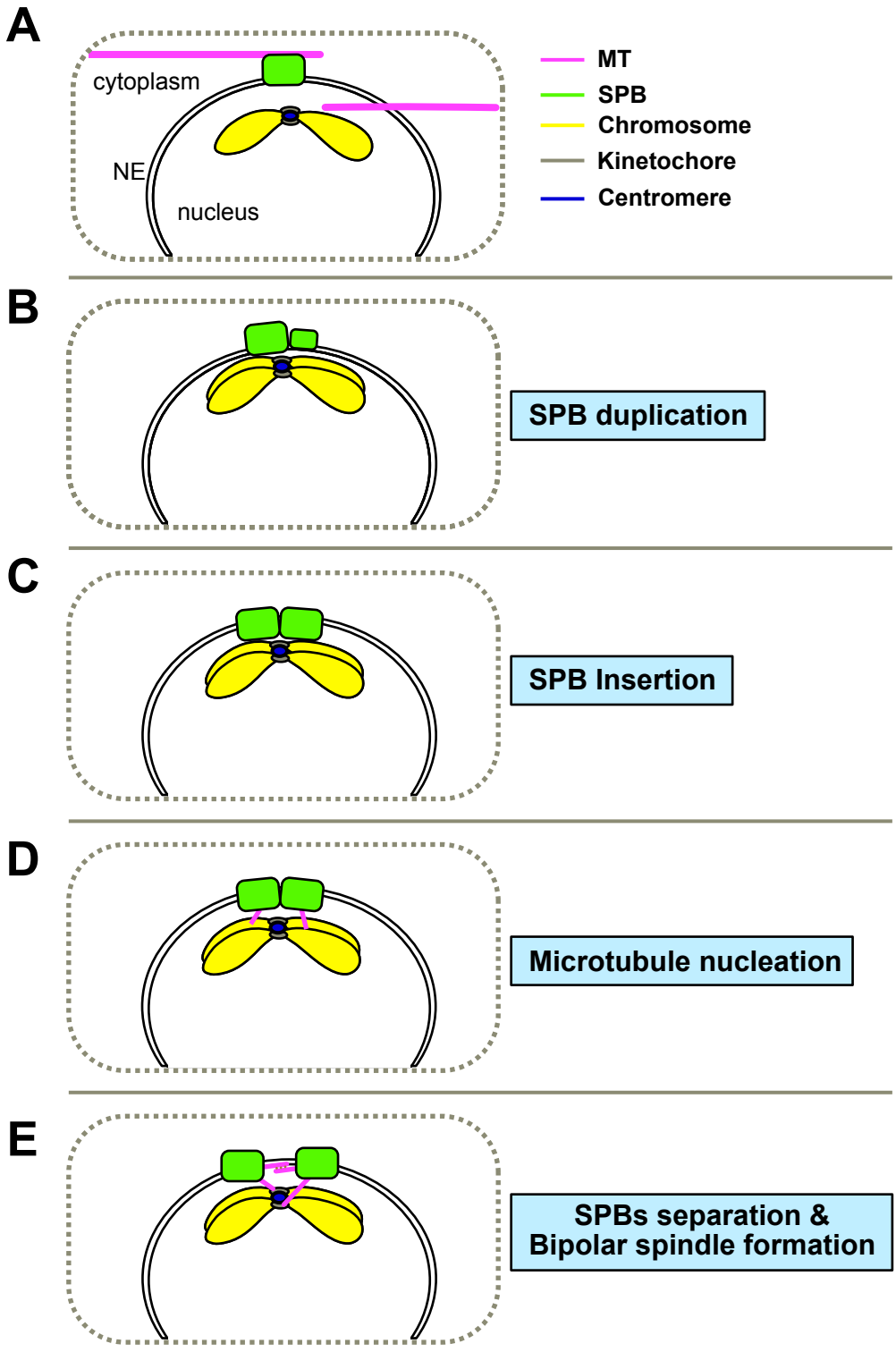
A
cytoplasm
NE
nucleus
MT
SPB
Chromosome
Kinetochore
Centromere
B
SPB duplication
C
SPB Insertion
D
Microtubule nucleation
E
SPBs separation &
Bipolar spindle formation

Figure 1. Process of bipolar spindle formation during mitosis in S*chizosaccharomyces pombe*

Schematic presentation of the nucleus and cytoplasm from SPB duplication to bipolar spindle formation. Spindle pole body (SPB), microtubules (MTs), nuclear envelope (NE) (A) Explanation for schematic presentation. MT (magenta), SPB (green), chromosome (yellow), kinetochore (grey), centromere (blue). Two black lines indicate NE. (B) SPB duplication. A smaller SPB (left side) indicates the newly formed SPB. (C) SPB insertion process. Duplicated SPBs enter NE. (D) MT nucleation. MTs are nucleated from SPBs (E) SPB separation and bipolar spindle formation. MTs nucleated from each SPBs are aligned. Some of MTs attach to kinetochores.

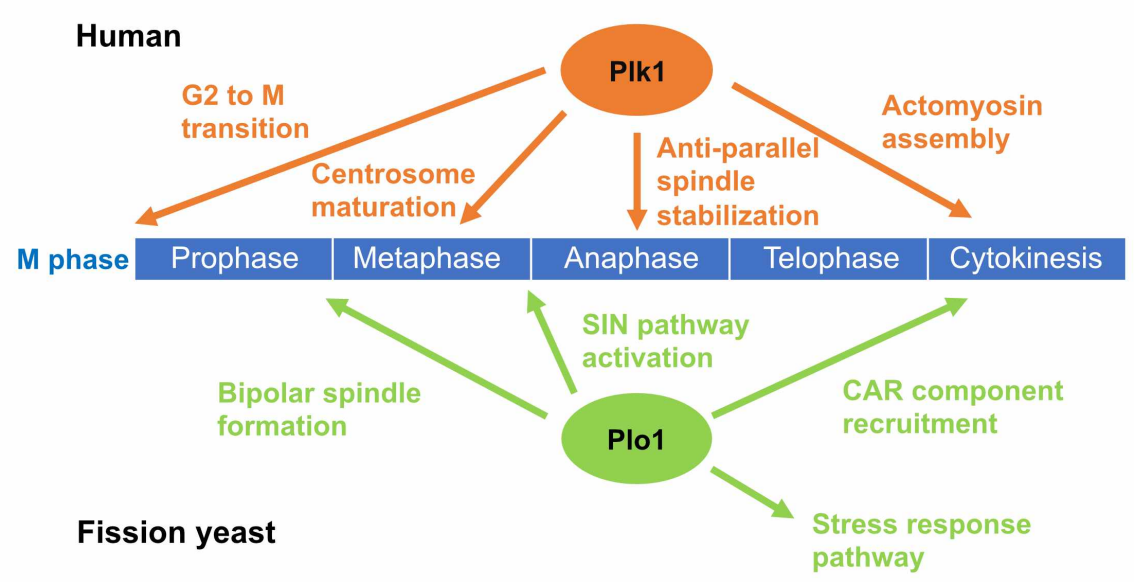

Figure 2. Roles of polo-like kinases during mitosis
This figure illustrates the roles of polo-like kinase during mitosis in human (Plk1) and fission yeast (Plo1).
Plk1 (top): activation of G2 to M transition, centrosome maturation at metaphase, stabilization of anti-parallel MTs at anaphase, and actomyosin assembly for cytokinesis.
Plo1 (bottom): bipolar spindle assembly, activation of septum initiating network (SIN) pathway, assembly of cytokinetic actomyosin ring (CAR) for cytokinesis, and regulation of stress response pathway.

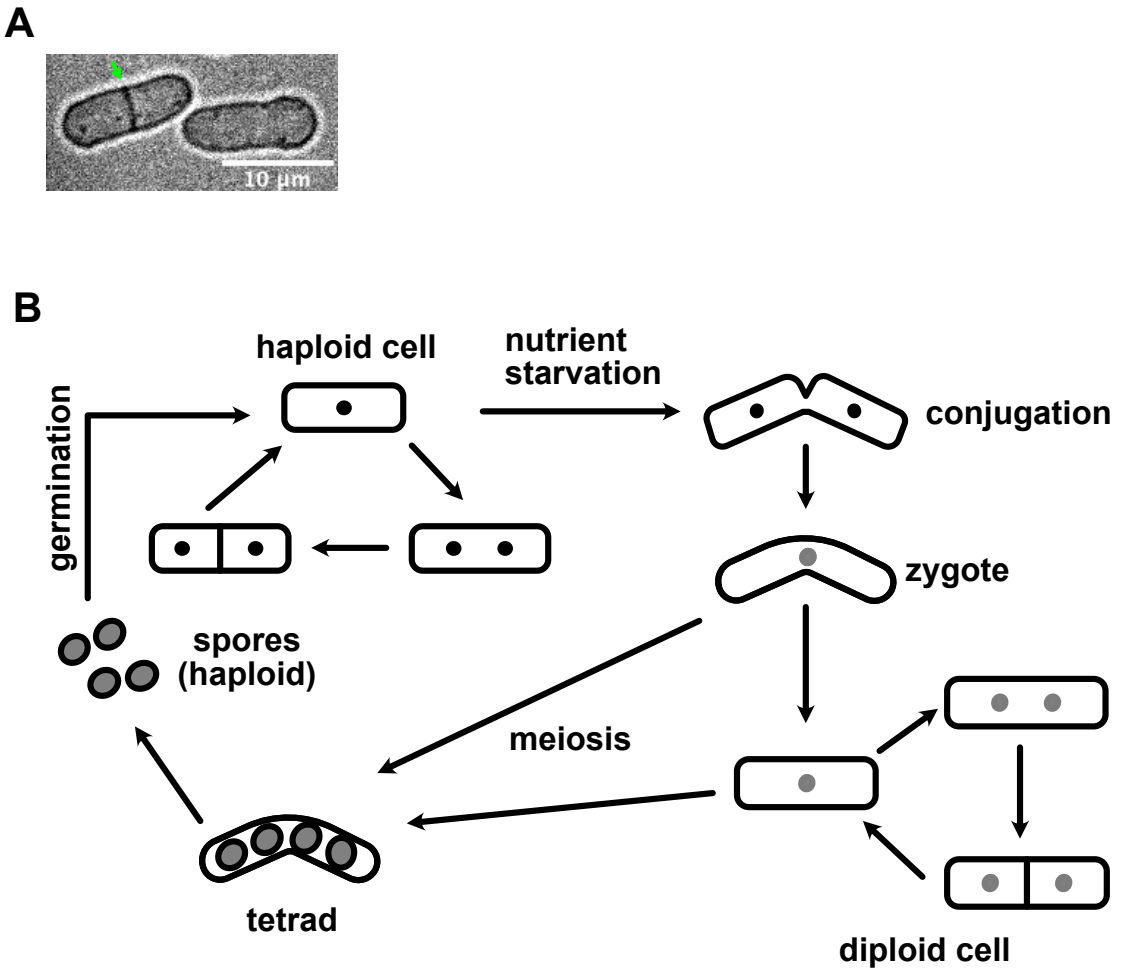

Figure 3. *Schizosaccharomyces pombe* as a model organism
(A) Bright field images of wild-type haploid cells. A green arrow indicates a fission plate (B) Life cycle of *Schizosaccharomyces pombe.*

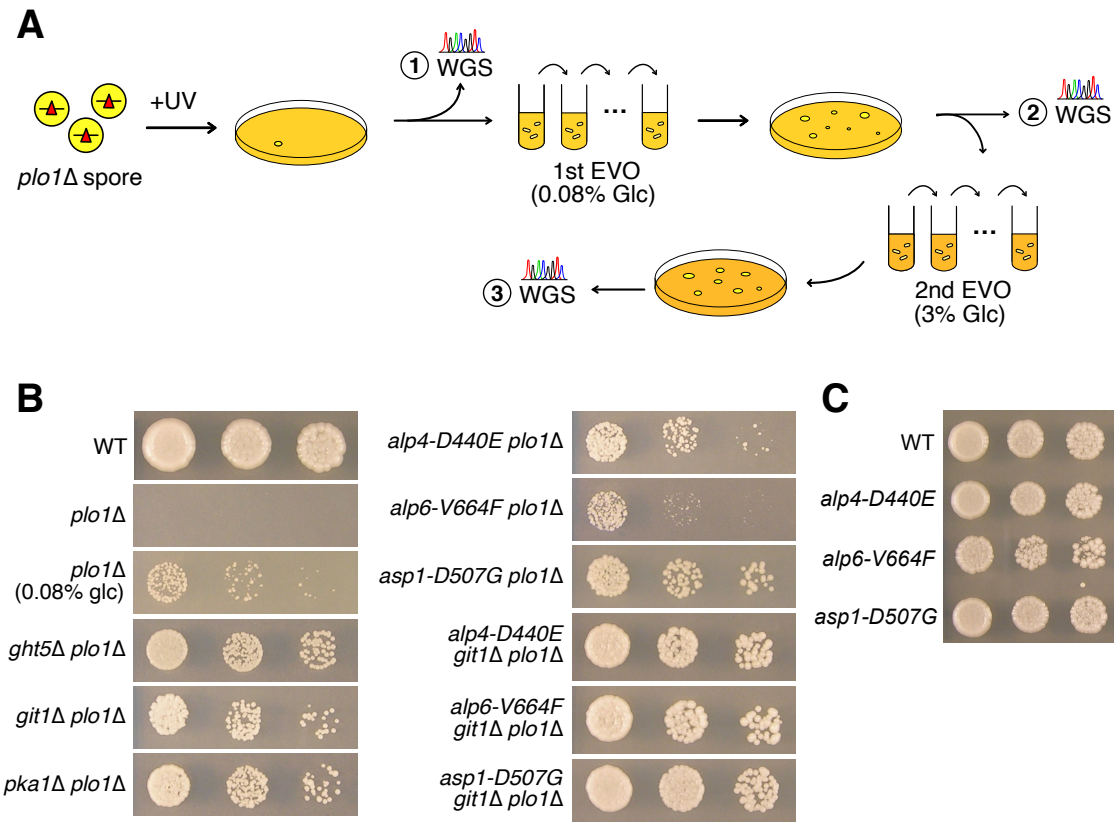

Figure 4. Isolation of viable *plo1*Δ strains

(A) Experimental procedure to isolate *plo1Δ* strains. The yeast spores in which *plo1* gene was replaced by a drug-resistant cassette were mutagenized by UV and plated onto the selective medium. The haploid colonies that appeared after several days represent the *plo1Δ* strains. The whole genome sequencing ("WGS") was determined to map the responsible suppressor mutations, while a few strains were subjected to experimental evolution (EVO), where serial dilution and saturation accumulated fitness-increasing mutations. EVO was repeated three times in different conditions, and suppressor mutations were determined by WGS. (B) Viable *plo1Δ* strains obtained by indicated suppressor mutations. Cells (5,000, 1,000, and 200) were spotted onto normal YE5S plates, except for the third row, where glucose (glc) concentration in the medium was reduced to 0.08% (YE5S, 4 d, 32°C). (C) Single mutants of *alp4-D440E*, *alp6-V664F*, and *asp1-D507G*. Cells (5,000, 1,000, and 200) were spotted onto normal YE5S plates and incubated for 3 d at 32°C.

Classification	Gene	Function and/or Orthologue	WGS	Mutation type	Rescue
Glucose /PKA	*ght5*	Glucose transporter	1 & 3	Deletion, Frame shift	+
	ght8	Glucose transporter	3	Partial deletion	N.D.
	git1		3	Frame shift	+
	git5	G protein beta	3	H105Y	N.D.
	cyr1	Adenylate cyclase	1	N691K, Frame shift	+
	pka1	PKA	–		+
Microtubule regulator	*alp4*	GCP2(γ-TuRC)	3	D440E	+
	alp6	GCP3(γ-TuRC)	2	V664F	+
	asp1	PPIP5K/Vip1	*	D507G, T575I	+
SAGA	*spt7*	SUPT7L	2	775-1G>T	N.D.
	spt20	SUPT20H	2	Frame shift	–+
	sgf73	ATXN7	2	C87F	N.D.
	ngg1		1	E4D/Q5stop	+
Others	*mip1*	RAPTOR (TOR pathway)	3	A1233S	+
	ahk1	MAP pathway scaffold protein	3	Frame shift	+
	aps1	Nudix hydrolase/DDP1	2	Frame shift	+

* 36°C experimental evolution

Figure 5. List of suppressor mutations for *plo1*Δ

(A) The "WGS" column indicates at which step in Fig. 4A the mutation was identified. The "Rescue" column indicates whether the indicated mutation alone bypassed the essentiality of Plo1. The colony grew extremely poorly for the *spt20*Δ *plo1*Δ (marked with –+).

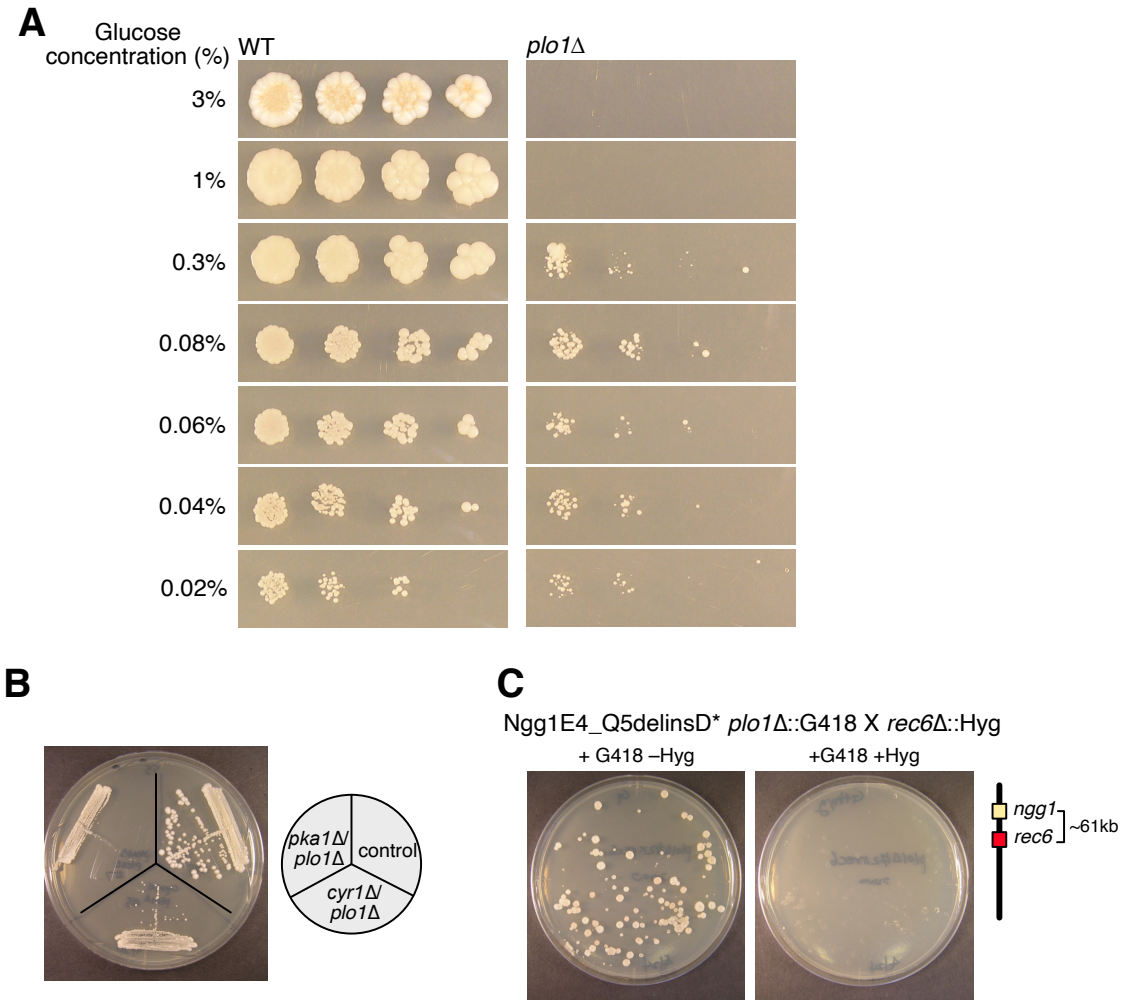

Figure 6. The bypass of essentiality (BOE) of Plo1
(A) Colony spotting on YE5S (+ G418, CHX) plates with various glucose concentrations. Spores (7,500, 1,500, 300, or 60) were spotted and incubated for 5 d at 32°C (expected drug-resistant cell numbers: 1,875, 375, 75, and 15, respectively). (B) Disruptant of PKA (*pka1*) or adenylate cyclase (*cyr1*) bypassed Plo1 essentiality. Colonies were grown on YE5S plates for 4 d at 32°C. (C) An example of suppressor mutation confirmation based on linkage test. *ngg1* and *rec6* genes are closely located on chromosome II. Double *plo1*Δ *rec6*Δ was never obtained after crossing *rec6*Δ (marked with hygromycin resistance) with a surviving *plo1*Δ strain (G418 resistant) in which a mutation was identified in *ngg1*.

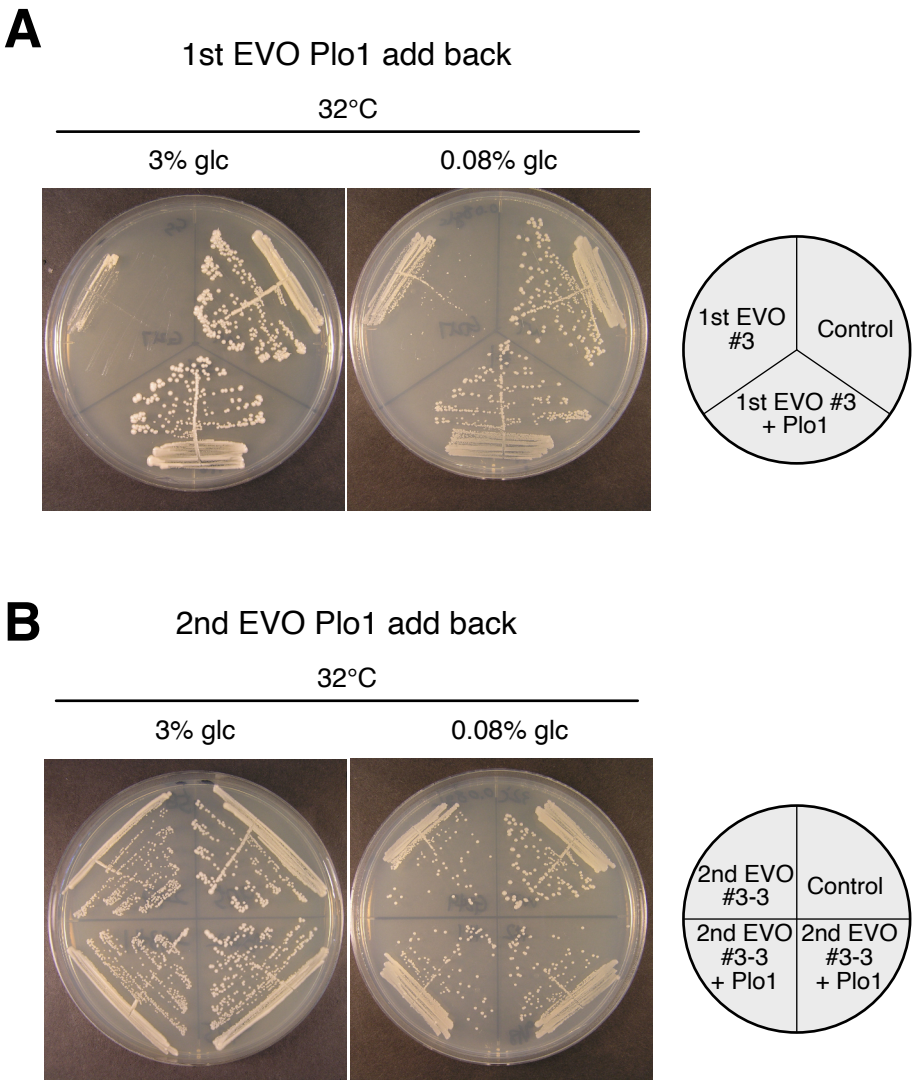

Figure 7. Experimental evolution (EVO) of *plo1*Δ strain
Experimental evolution (EVO) of *plo1*Δ strain was performed sequentially, as described in Fig. 4A. After each round, I isolated a few of the fastest growing colonies. I converted *plo1*Δ to *plo1*+ and tested if this enhanced the colony growth.
(A) Return of Plo1 helped colony growth of a strain obtained after the 1st round of evolution (1st EVO #3).
(B) A further evolved strain was insensitive to Plo1 (2nd EVO strain #3-3). Two glucose concentrations were tested (3% and 0.08%). Wild-type was used as the control.

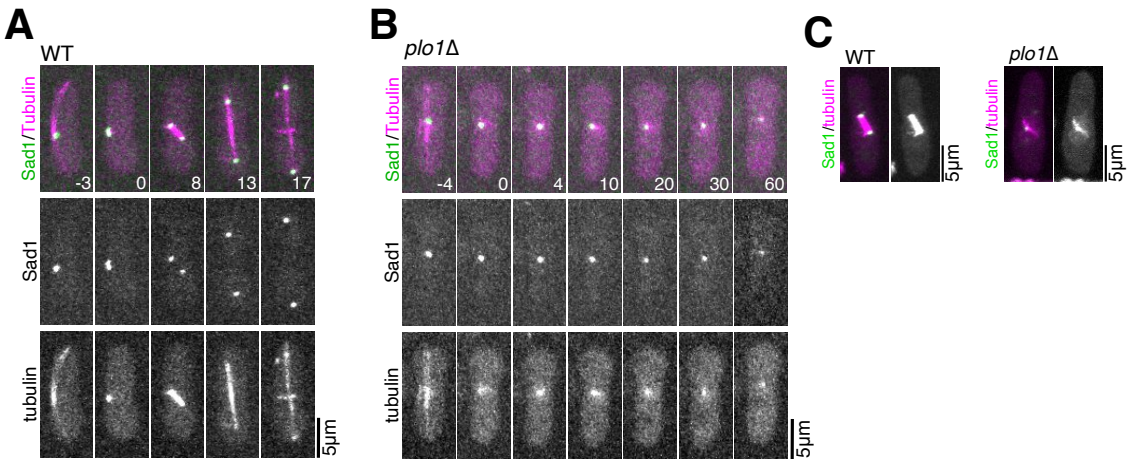

Figure 8. Monopolar spindle formation in *plo1*Δ

(A, B) Live imaging of the control and *plo1*Δ strains expressing Sad1^{SUN}-GFP and mCherry-tubulin. The first mitotic phase after spore germination was imaged. (C) Mitotic spindles of control and *plo1*Δ strains expressing Sad1^{SUN} -GFP and mCherry-tubulin with longer exposure time. Time 0 (min) was set at the onset of spindle formation.

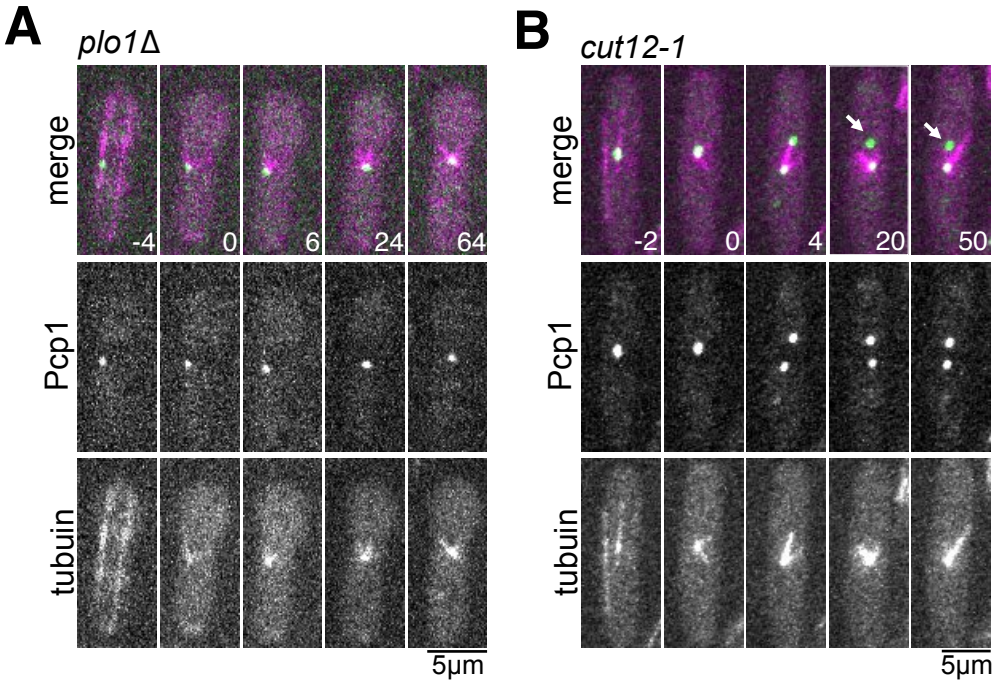

Figure 9. Nuclear envelope appears to be intact in *plo1*Δ
(A, B) Live imaging of *plo1*Δ and *cut12-1* strains expressing Pcp1^{PCNT}-GFP and mCherry-tubulin. *cut12-1* cells were incubated at 36°C for 3 h before imaging. Arrows indicate an SPB in which spindles were not nucleated. Time 0 (min) was set at the onset of spindle formation.

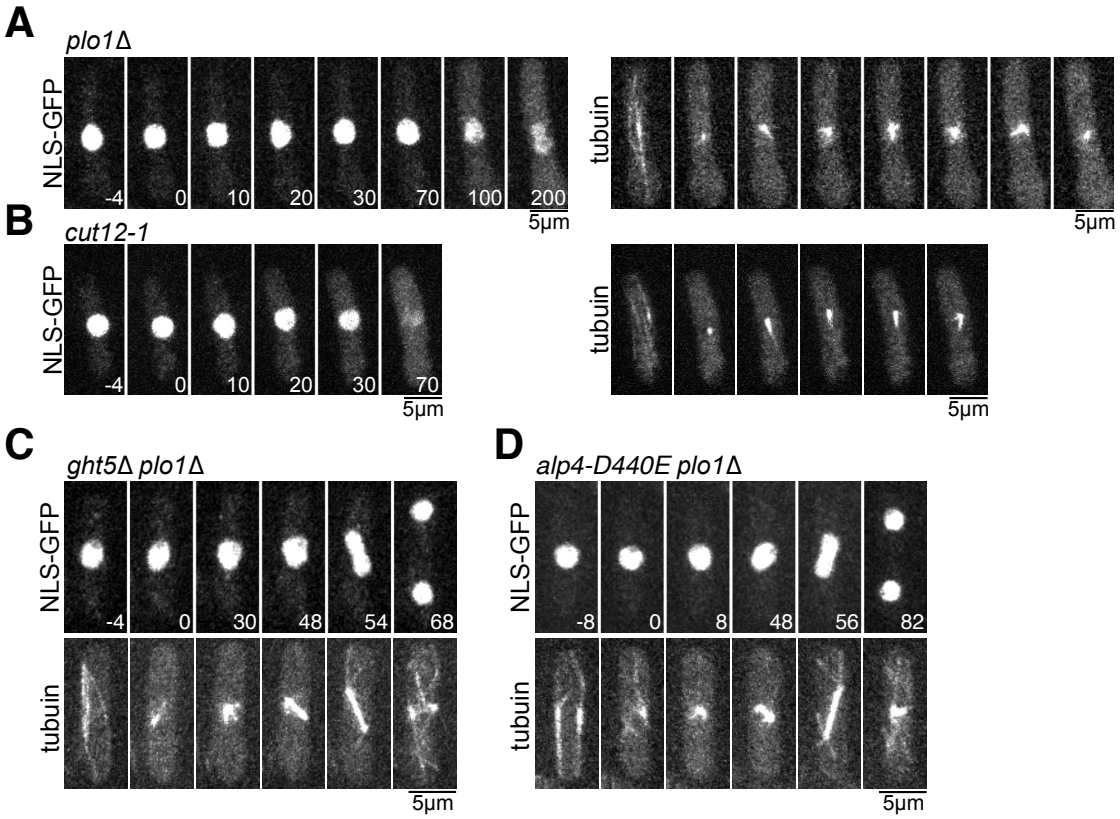

Figure 10. Nuclear efflux assay in *plo1*Δ and viable *plo1*Δ strains
(C–F) Live imaging of *plo1*Δ*, cut12-1, ght5Δ plo1*Δ, and *alp4-D440E plo1*Δ strains expressing NLS-GFP-β-Gal and mCherry-tubulin. *cut12-1* cells were incubated at 36°C for 3 h before imaging. Time 0 (min) was set at the onset of spindle formation.

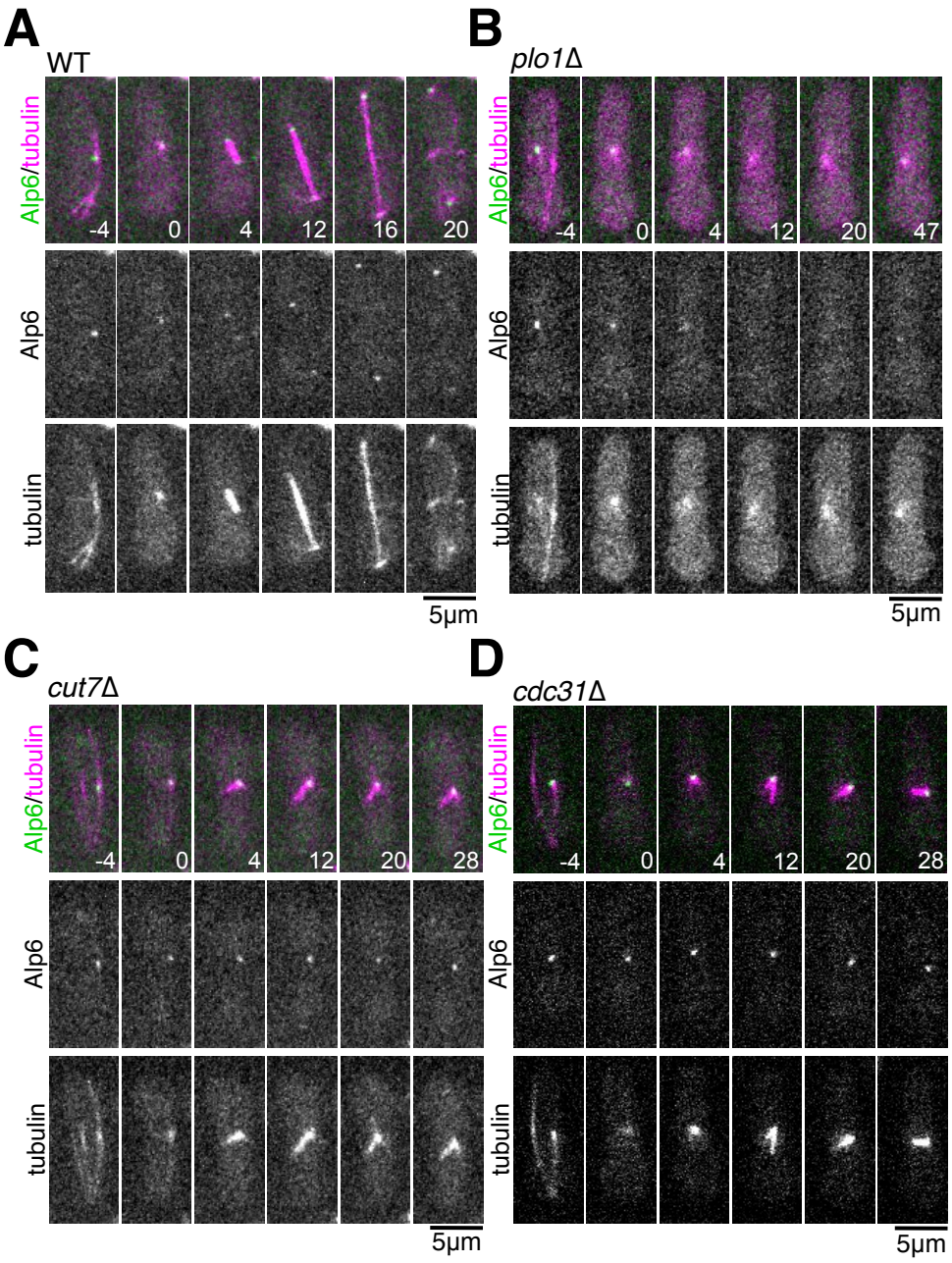
A
WT
Alp6/tubulin
Alp6
tubulin
-4
0
4
12
16
20
5μm
B
plo1Δ
Alp6/tubulin
Alp6
tubulin
-4
0
4
12
20
47
5μm
C
cut7Δ
Alp6/tubulin
Alp6
tubulin
-4
0
4
12
20
28
5μm
D
cdc31Δ
Alp6/tubulin
Alp6
tubulin
-4
0
4
12
20
28
5μm

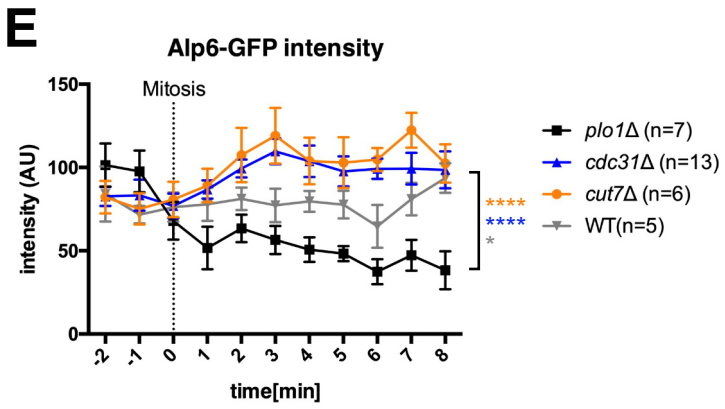
E
Alp6-GFP intensity
Mitosis
intensity (AU)
150
100
50
0
-2
-1
0
1
2
3
4
5
6
7
8
time[min]
****
****
*
plo1Δ (n=7)
cdc31Δ (n=13)
cut7Δ (n=6)
WT(n=5)

Figure 11. Reduced recruitment of a γ-TuRC subunit in *plo1*Δ compared with other monopolar spindle mutants

(A, B) Live imaging of the control and *plo1*Δ strains expressing Alp6^{GCP3}-GFP and mCherry-tubulin. (C, D) Monopolar spindles of the *cut7*Δ and *cdc31*Δ strains after germination. (E) Quantification of Alp6^{GCP3}-GFP intensity during mitosis. The signal intensities from 5 to 8 min were compared between the *plo1*Δ and wild-type (WT), *cut7*Δ, or *cdc31*Δ (****, $p < 0.0001$; *, $p = 0.0226$). Error bars indicate the standard error of the mean (SEM). Time 0 (min) was set at the onset of spindle formation.

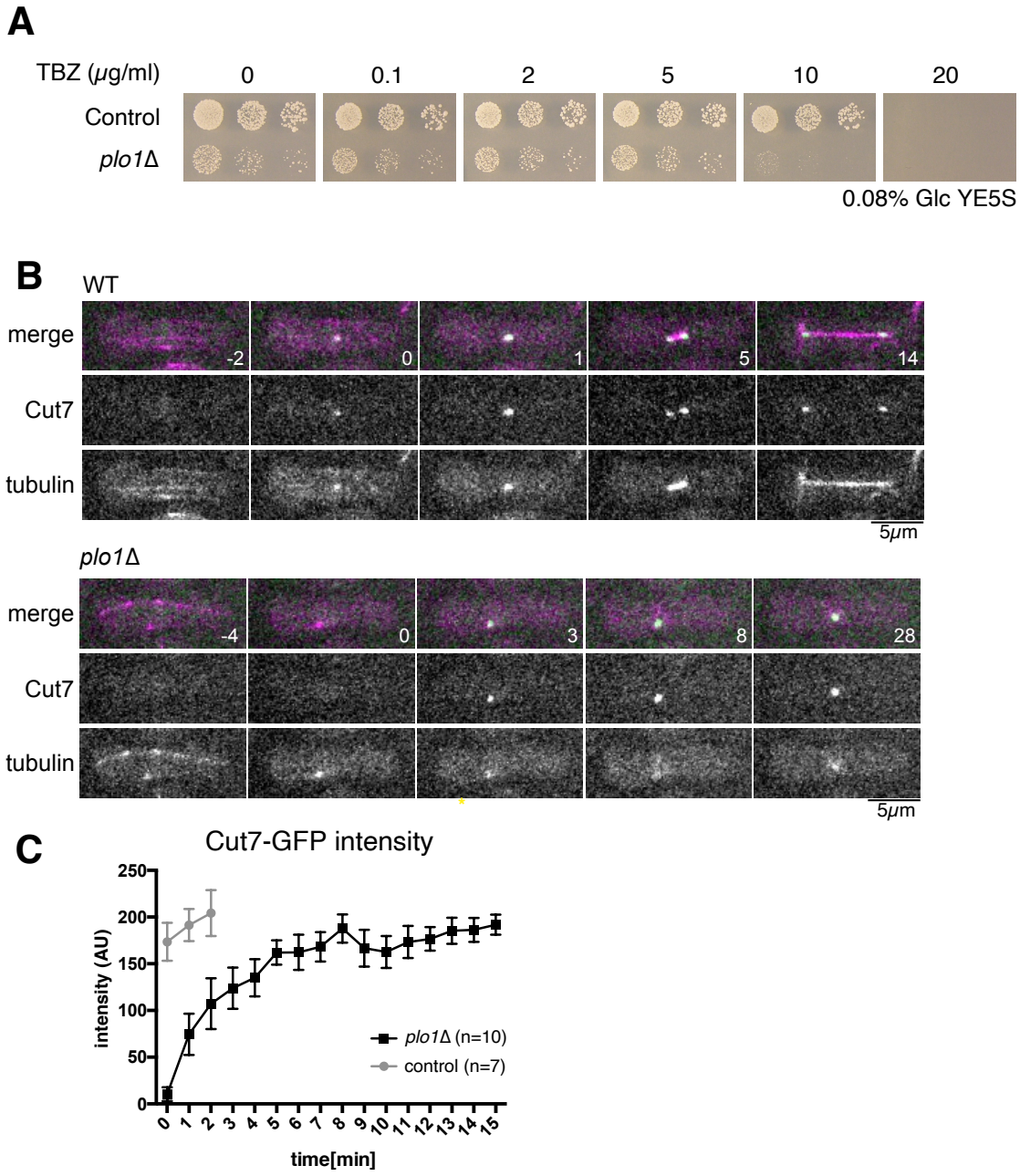

Figure 12. *plo1* deletion is sensitive to thiabendazole (TBZ) but does not critically affect Cut7$^{kinesin-5}$ localization

(A) In the presence of 10 μg/mL TBZ, *plo1*Δ failed to form colonies even in a low glucose medium. Spores (10,000, 2,000, and 400) were spotted and colonies were formed on 0.08% glucose, G418-containing plates for 5 d at 32°C (expected G418-resistant cell numbers: 5,000, 1,000, and 200 cells, respectively). (B, C) Failure in spindle bipolarization even when Cut7$^{kinesin-5}$-GFP accumulated on the SPB at a normal level after a delay in *plo1*Δ. Error bars indicate the standard error of the mean (SEM). Time 0 (min) was set at the onset of spindle formation.

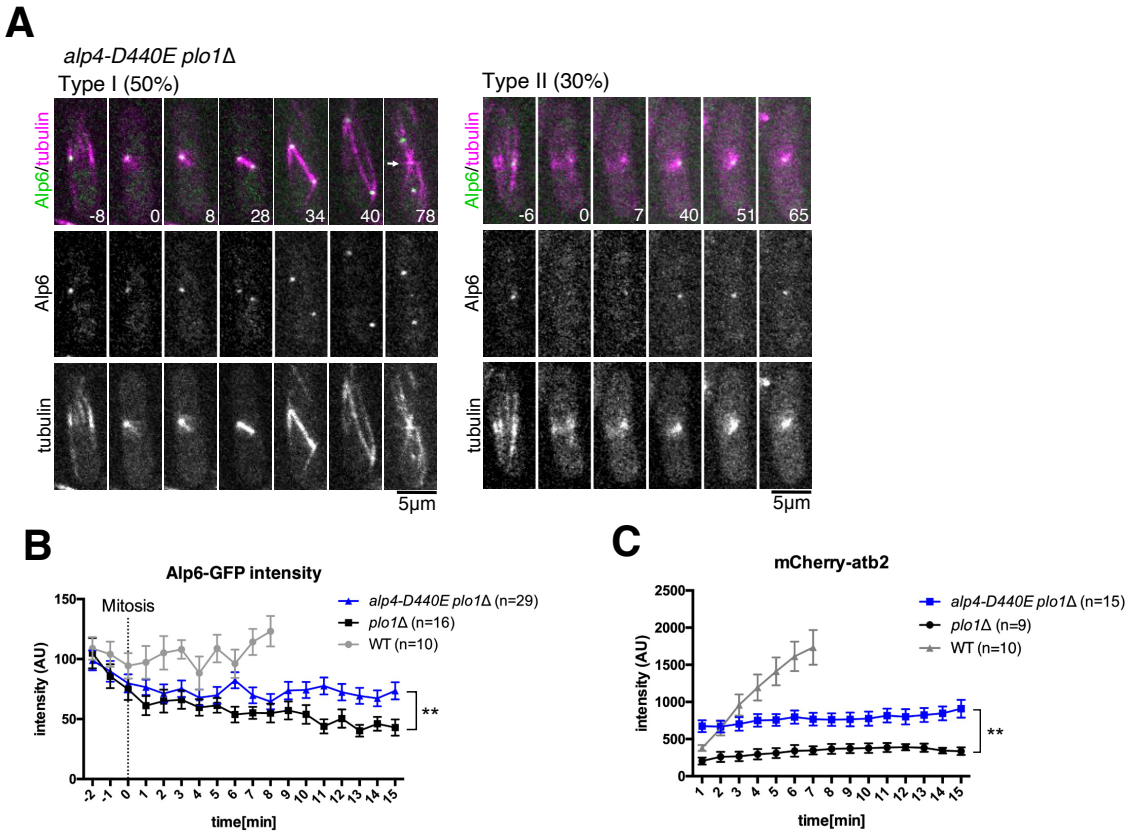

Figure 13. Microtubule (MT) nucleation and spindle bipolarization were rescued by a point mutation in a γ-TuRC subunit

(A) (Left) Spindle bipolarization after a prolonged monopolar state by a specific mutation in the *alp4*^{GCP2} gene. Equatorial MTs during telophase were also recovered (arrow at 78 min). (Right) Failure in spindle bipolarization. (B, C) Partial recovery of Alp6^{GCP3}-GFP and MT (Atb2 is tubulin alpha 2) intensities by a specific mutation in the *alp4*^{GCP2} gene. The signal intensities from 12 to 15 min were compared between *plo1*Δ and *alp4-D440E plo1*Δ; Alp6^{GCP3}-GFP intensity (**, p = 0.0049), and MT intensity (**, p = 0.0017). In the graphs, error bars indicate the standard error of the mean (SEM). Time 0 (min) was set at the onset of spindle formation.

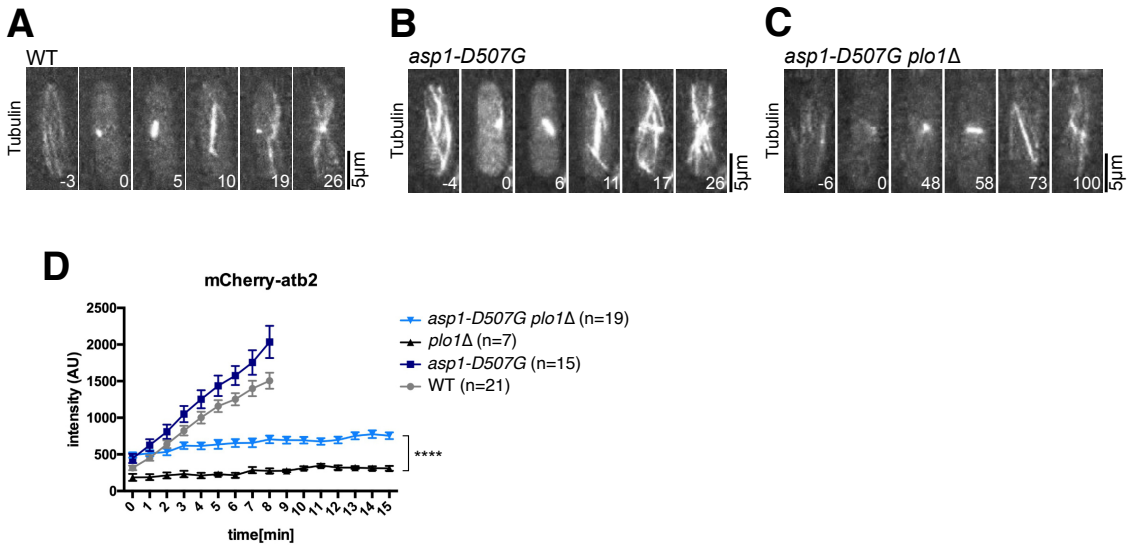

Figure 14. Microtubule (MT) nucleation and spindle bipolarization were rescued by a point mutation in an MT destabilizer

(A–D) Partial recovery of MT intensities by a mutation in the *asp1*$^{PPIP5K/Vip1}$ gene. MT intensity from 12 to 15 min was compared between *plo1*Δ with *asp1-D507G plo1*Δ (****, $p < 0.0001$). In the graph, error bars indicate the standard error of the mean (SEM). Time 0 is set at the onset of spindle formation. Time 0 (min) is set at the onset of spindle formation.

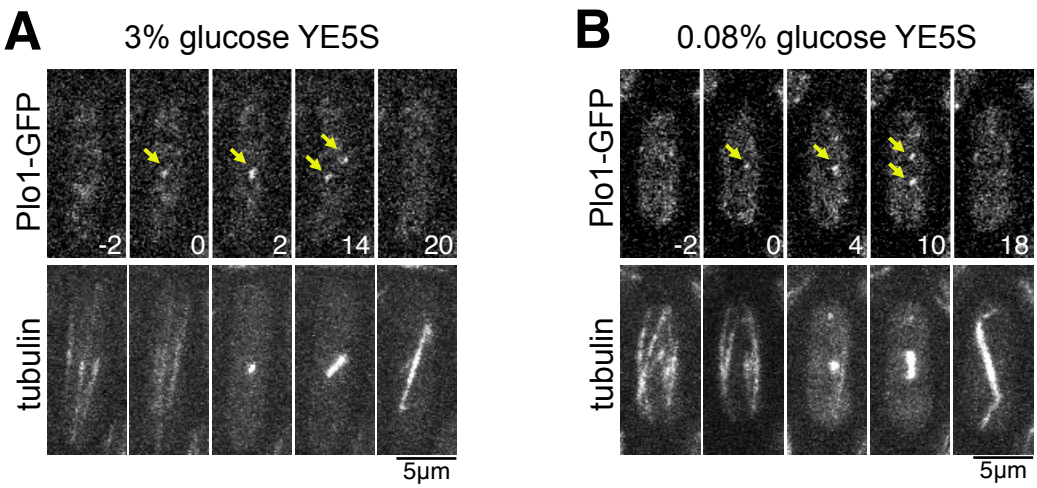

Figure 15. No difference in Plo1 localization under high (3%) and low (0.08%) glucose conditions

(A, B) Live imaging of *plo1*Δ strains expressing Plo1-GFP and mCherry-tubulin. Cells were incubated in the YE5S medium containing 3% or 0.08% glucose. Arrows indicate GFP signals at SPBs. Time 0 (min) was set at the onset of spindle formation.

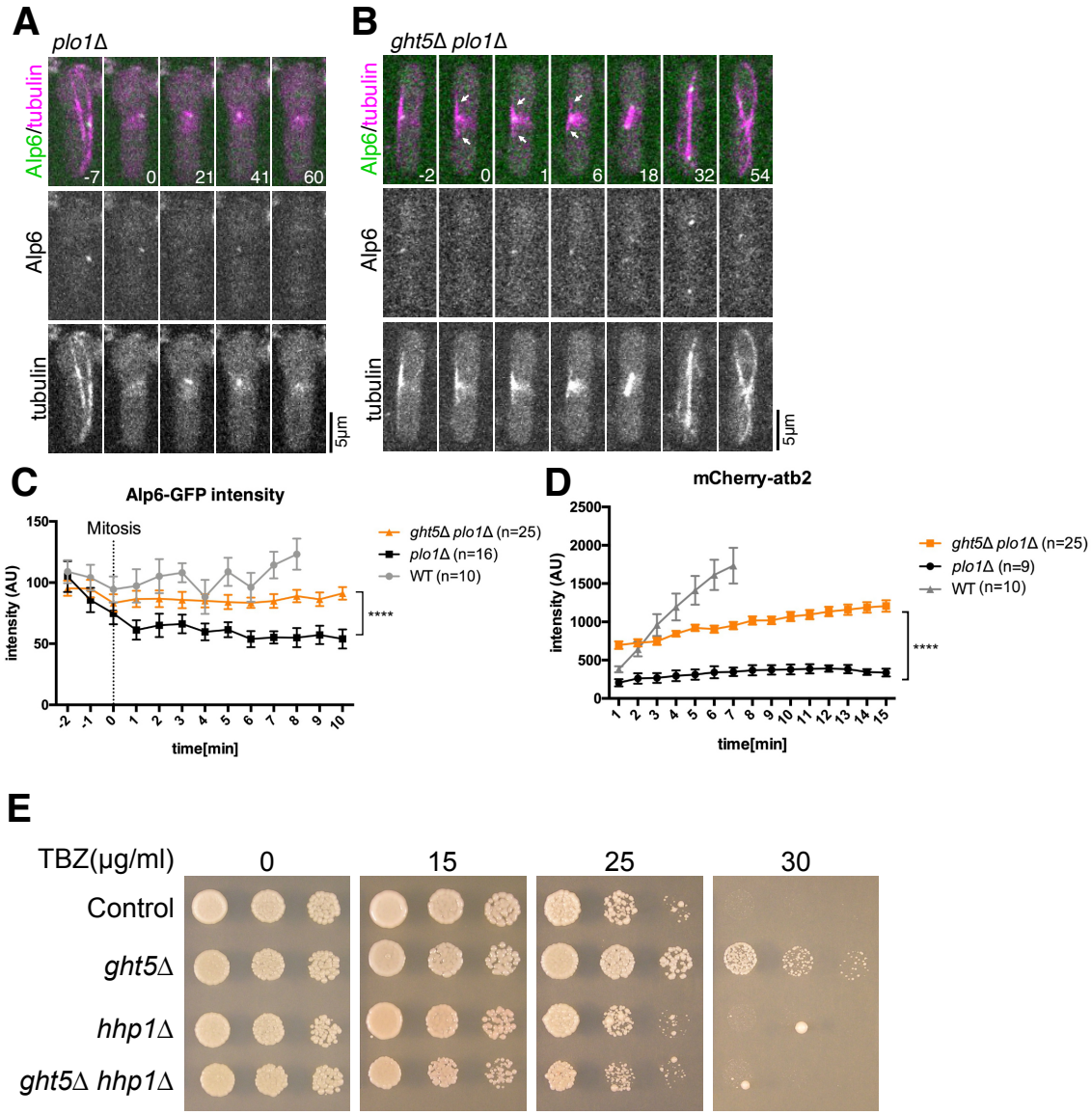

Figure 16. γ-TuRC localization was restored by mutations in a glucose transporter in the absence of Plo1

(A) Live imaging of the *plo1*Δ strain expressing Alp6^{GCP3}-GFP and mCherry-tubulin. The first mitotic phase after spore germination was imaged. (B) Live imaging of the *ght5*Δ *plo1*Δ strain expressing Alp6^{GCP3}-GFP and mCherry-tubulin. Mitosis in the exponentially growing phase was imaged. Arrows indicate interphase microtubules (MTs) that remain during spindle assembly. (C, D) Quantification of Alp6^{GCP3}-GFP and MT intensities during mitosis. The signal intensities were compared between *plo1*Δ with *ght5*Δ *plo1*Δ; Alp6^{GCP3}-GFP intensity from 7 to 10 min (****, $p < 0.0001$) and MT intensity from 12 to 15 min (****, $p < 0.0001$). Error bars indicate the standard error of the mean (SEM). Time 0 is set at the onset of spindle formation. Control data is identical to that in Fig. 13B and C. The increase in MT intensity during the early mitotic stage in *ght5*Δ *plo1*Δ is due to the incomplete disassembly of interphase MTs (see arrows in B).

(E) *ght5*Δ confers resistance to TBZ, whereas *hhp1*Δ suppresses the effect. Cells (5,000, 1,000, and 200 cells) spotted and cultured in YE5S medium for 3 d (0 and 15 μg/mL TBZ plates) or 6 d (25 and 30 μg/mL TBZ plates) at 32°C.

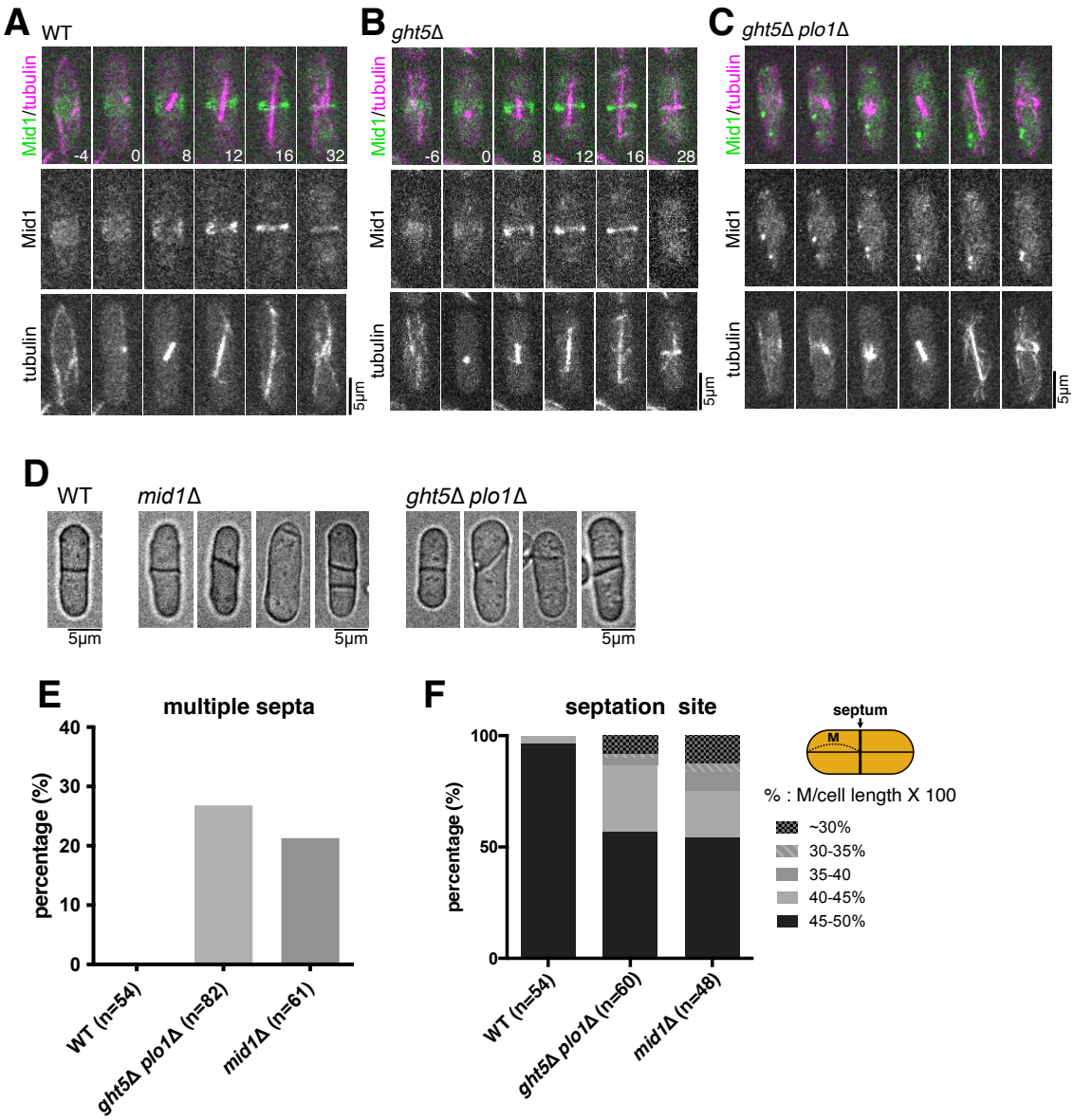

Figure 17. Septation defect of *plo1*Δ is not rescued by *ght5* deletion
(A–C) Equatorial accumulation of Mid1^{annilin}-GFP is not restored in the viable *ght5*Δ *plo1*Δ strain. Time 0 (min) is set at the onset of spindle formation. (D) Bright-field images of wild-type (WT), *mid1*Δ, and *ght5*Δ *plo1*Δ. (E) Quantification of multiseptated cells. A total of 21% of *mid1Δ* cells and 26% of *ght5*Δ *plo1*Δ cells had multiple septations, whereas this was never observed in control cells. (F) Quantification of the septation site. The relative position of the septum along the long axis of the cell was determined.

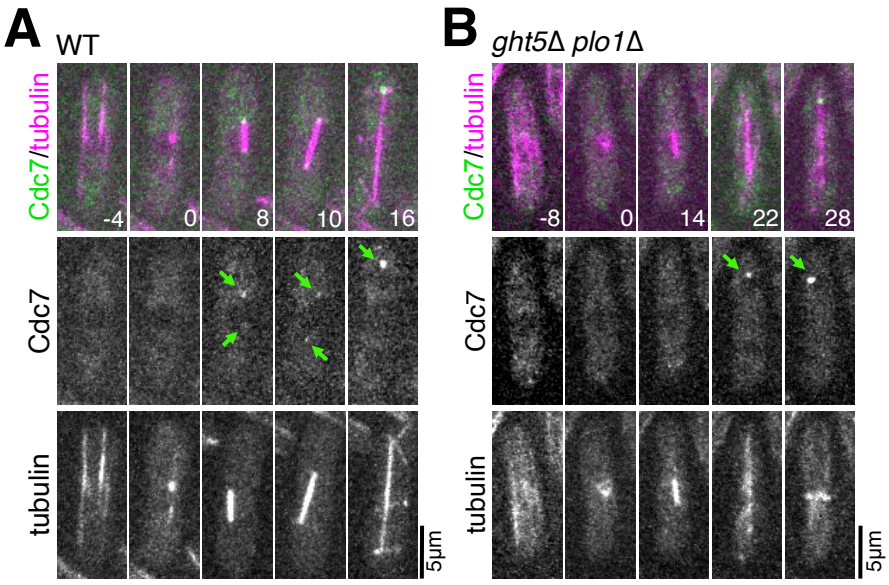

Figure 18. Cdc7 localization defect of *plo1*Δ is not rescued by *ght5* deletion
(A, B) Spindle pole body (SPB) localization of Cdc7^{Hippo}-GFP at metaphase is not restored in the viable *ght5*Δ *plo1*Δ strain. Arrows indicated GFP signals at SPBs. Time 0 (min) is set at the onset of spindle formation.

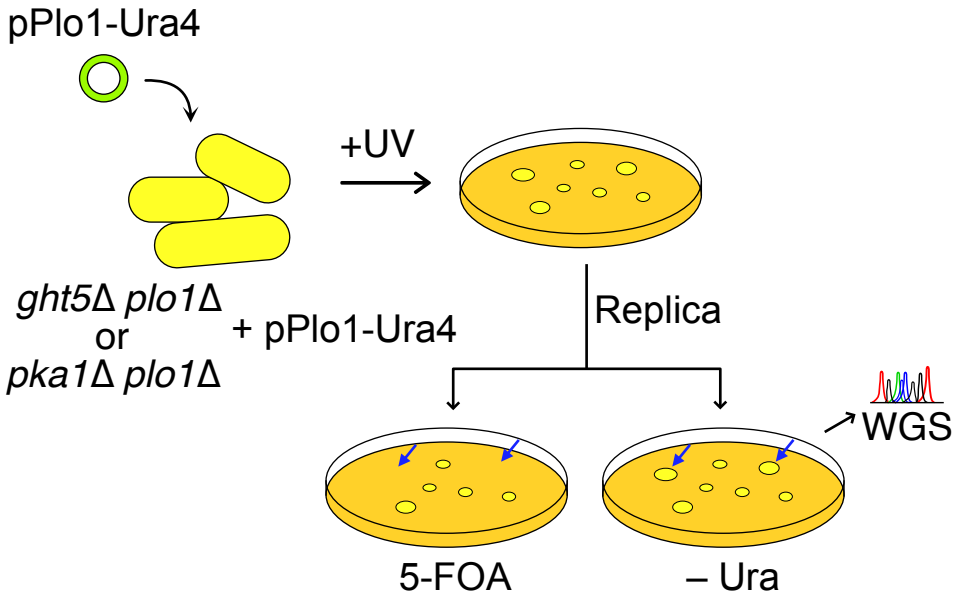

Figure 19. Schematic presentation of the synthetic lethal screening
(A) The strain possessing Plo1 plasmid (*ura4+*) is sensitive to 5-FOA and therefore, does not grow. The strain that cannot grow specifically on the 5-FOA plate should have a mutation that is synthetic lethal with *ght5*Δ *plo1*Δ or *pka1*Δ *plo1*Δ. The genome sequences of these strains were determined ("WGS").

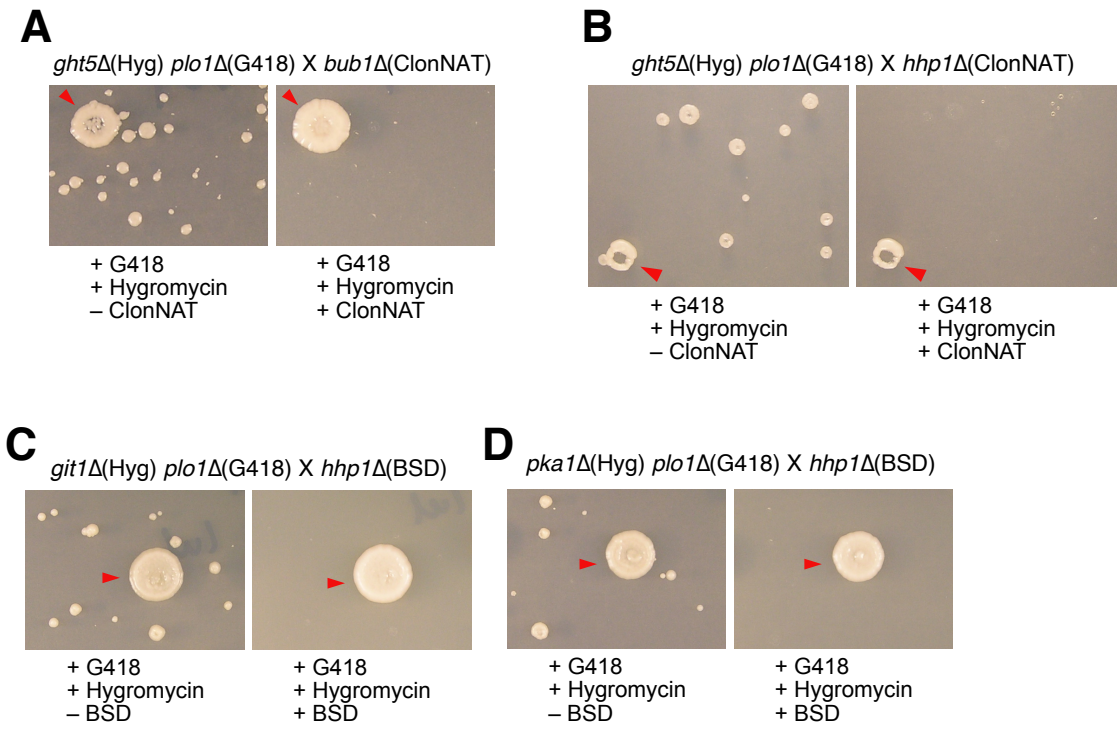

Figure 20. *ght5*Δ *plo1*Δ is synthetic lethal with *hhp1*Δ
(A–D) Confirmation of synthetic lethality between the indicated strains by random spore spreading followed by replica-plating onto selective plates. The *bub1* and *hhp1* ORFs were replaced with ClonNAT-resistant or BSD-resistant cassettes. The *plo1* ORF was replaced with a G418-resistant cassette. *ght5*, *git1*, and *pka1* ORFs were replaced with a hygromycin-resistant cassette. Colony formation of heterozygous diploids (red arrowheads) indicates the functionality of the plate.

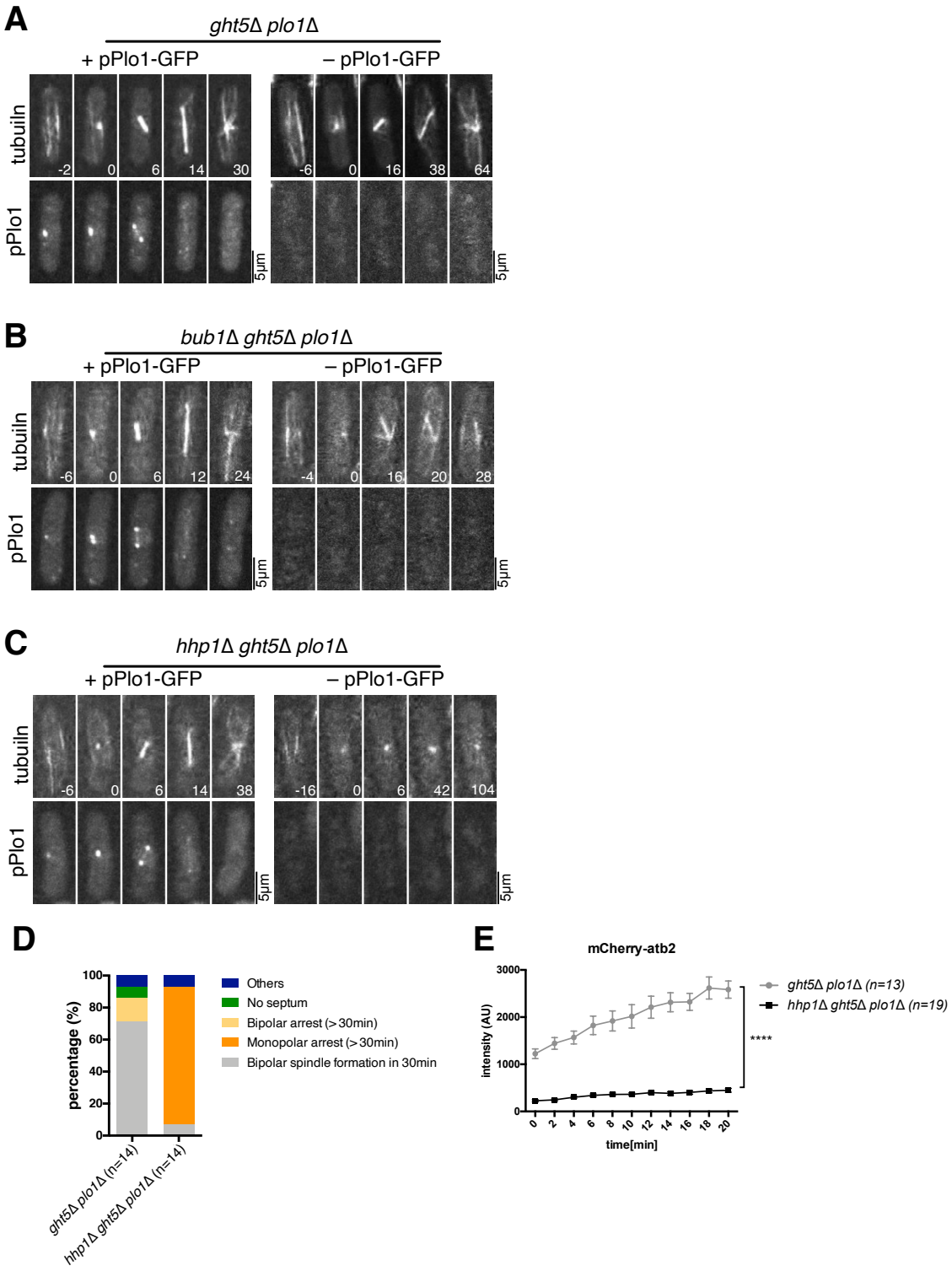

Figure 21. Hhp1^{CK1} becomes essential for spindle formation in the absence of Plo1

(A–C) Plasmid-loss experiment. The indicated double or triple disruptants transformed with Plo1-GFP plasmid were grown. Time-lapse imaging was performed and mitotic cells with or without Plo1-GFP signals were analyzed.

Time 0 (min) is set at the onset of spindle formation. (D) Frequency of mitotic phenotypes (in the absence of Plo1-GFP). (E) MT intensity decreased in the absence of Hhp1^{CK1}(****, $p < 0.0001$). Time 0 (min) is set at the onset of spindle formation.

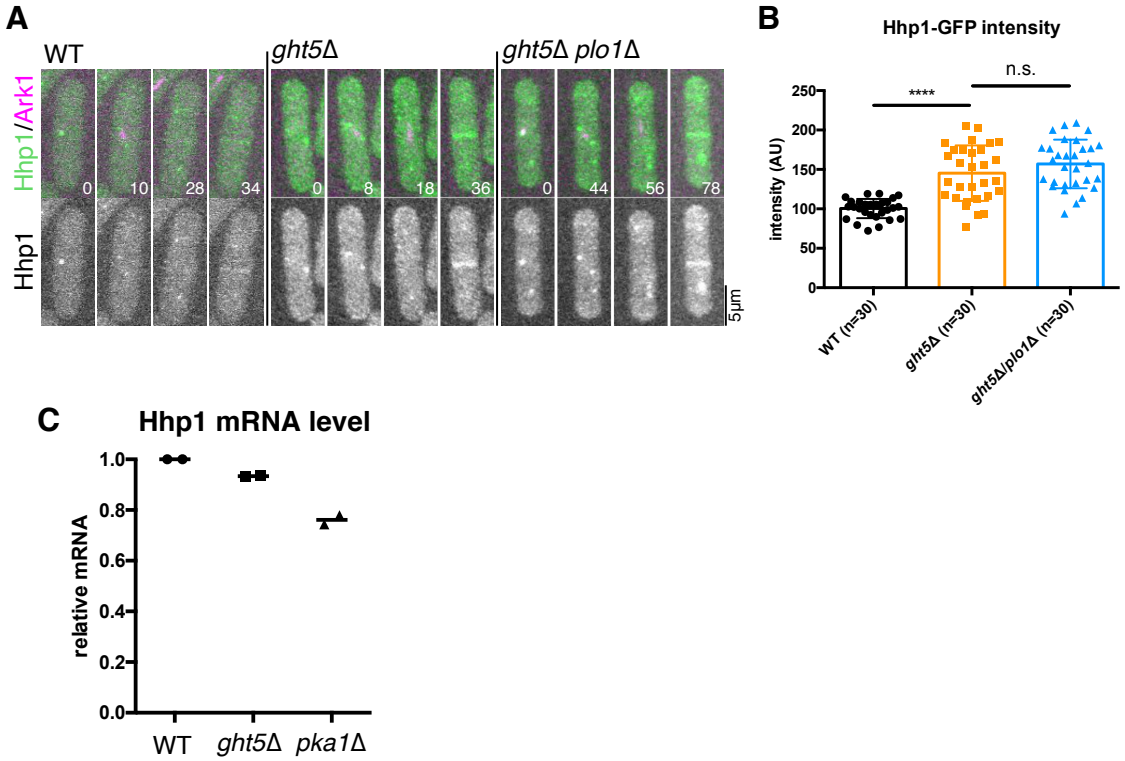

Figure 22. Amount of Hhp1^{CK1} protein is increased but mRNA levels of Hhp1 ^{CK1} do not change in the *ght5*Δ background

(A, B) The amount of Hhp1^{CK1} protein was increased in the *ght5*Δ background. Endogenous Hhp1^{CK1} was tagged with GFP in the indicated three backgrounds, and cellular GFP intensity (mean) was quantified (****, Tukey test p<0.0001. n.s, not significant). Error bars indicate SD. Time 0 (min) is set to the time just before SPBs separation (C) Relative *hhp1* mRNA levels in wild-type (WT), *ght5*Δ, and *pka1*Δ. Data from two independent experiments were plotted.

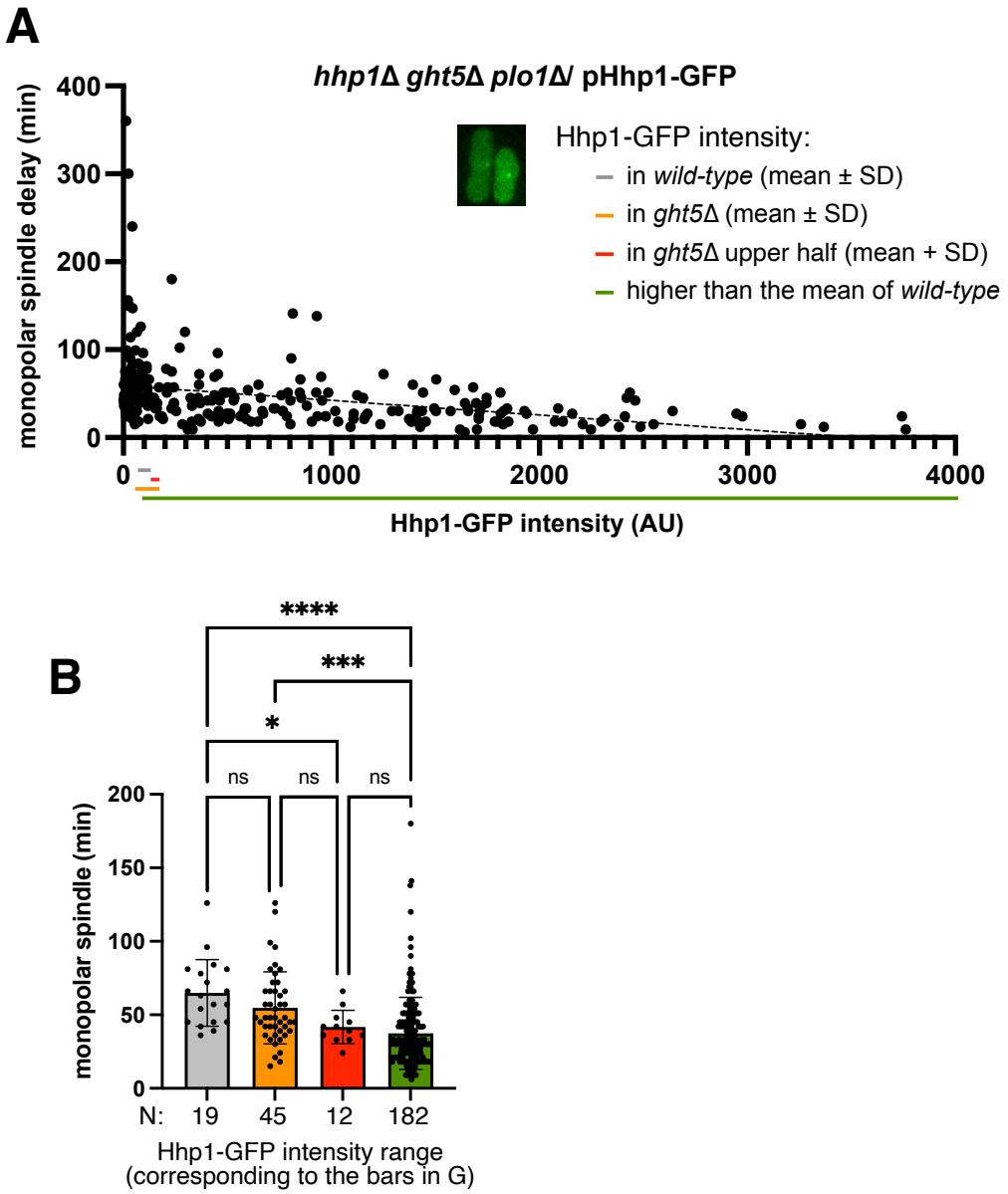

Figure 23. Hhp1^{CK1} is helpful for spindle formation in the absence of Plo1
(A) Plasmid-loss experiment using a *plo1*Δ *ght5*Δ *hhp1*Δ triple disruptant and multicopy Hhp1-GFP plasmid(*leu2*+). Time spent with monopolar spindles was plotted for each cell. GFP intensity (arbitrary unit) corresponds to the amount of Hhp1 in a cell. Mean intensities (± SD) of Hhp1-GFP signals in the wild-type background and *ght5*Δ background were indicated by grey and orange bars, respectively. In this analysis, the mean background intensity of the parental strain that had no GFP expression (80.3 AU, n = 30) was subtracted from the Hhp1-GFP intensity value. (B) Time required for monopolar-to-bipolar conversion. Three bars correspond to the samples with different GFP intensities described in (G). Error bars represent SD (*, p = 0.0458; ***, p =0.0001;****, p <0.0001), and ns stands for “not significant.”

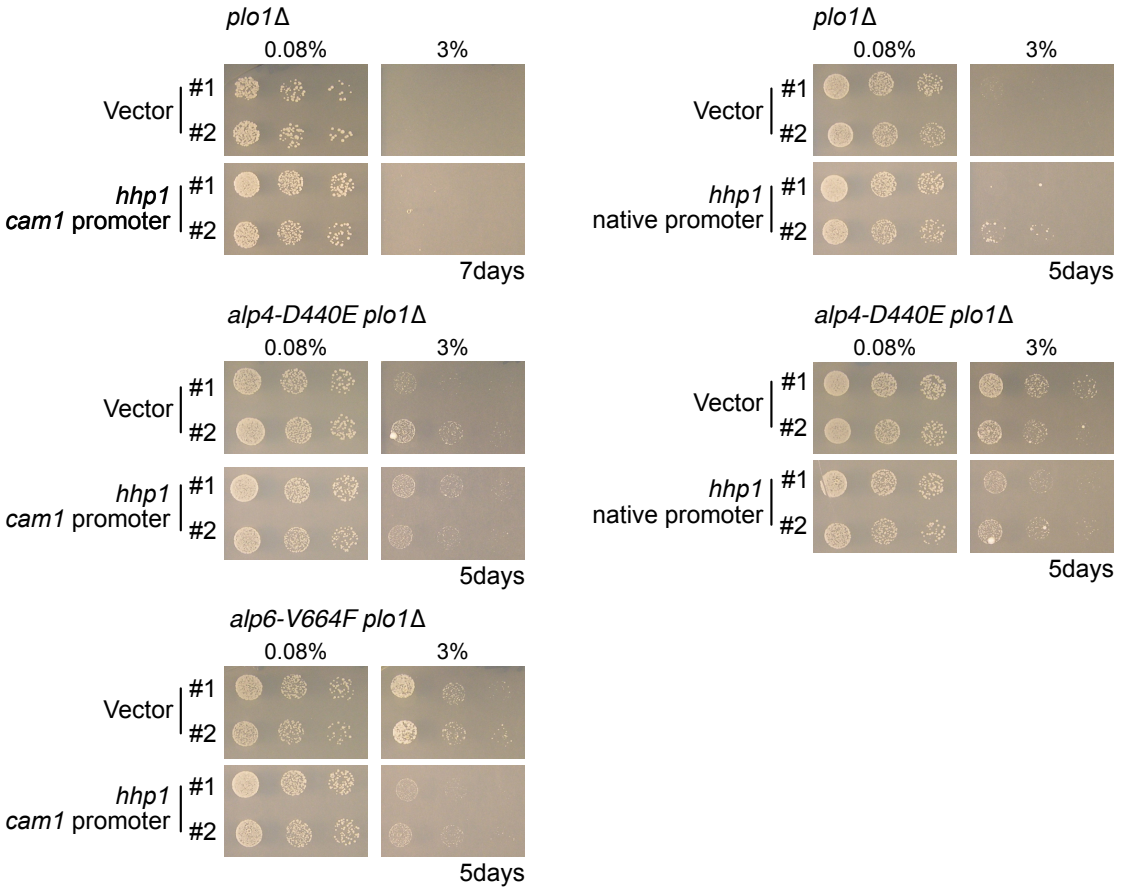

Figure 24. Hhp1^{CK1} overexpression alone does not increase the colony growth of *plo1*Δ.

(A) Investigation of the rescue ability by Hhp1 overexpression in the indicated strains. The calmodulin promoter (*cam1-pr*) (Matsuyama et al., 2008) and the native promoter of *hhp1*$^{+}$ gene were used. Hhp1 was expressed in the *plo1*Δ, *alp4-D440E plo1*Δ, and *alp6-V664F plo1*Δ strains. Cells (10,000, 5,000, and 1,000) were spotted and cultured in YE5S with G418 for 5 d at 32°C.

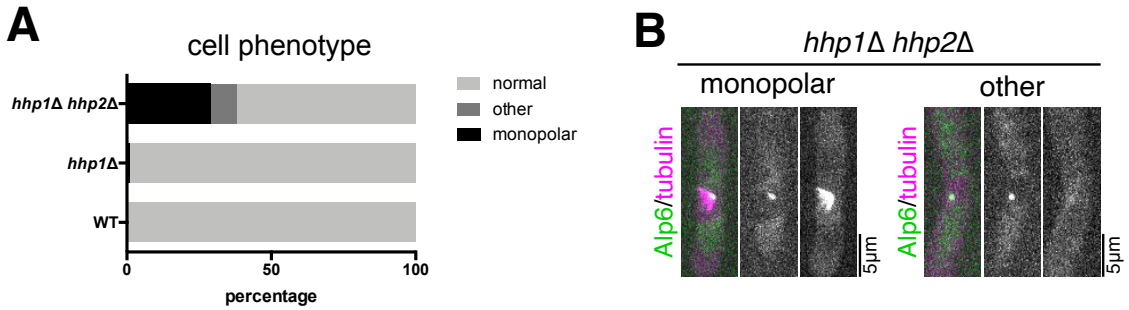

Figure 25 Loss of CK1 shows abnormal spindle phenotypes during mitosis
(A) A total of 29% of the *hhp1*Δ *hhp2*Δ cells (n = 79) and 1% of the *hhp1*Δ cells (n = 272) assembled monopolar spindles, whereas this never occurred in control cells (n = 336). (B) Monopolar spindle and a lack of spindle MTs were observed in the double disruptant (right). Time 0 (min) was set at the onset of spindle formation.

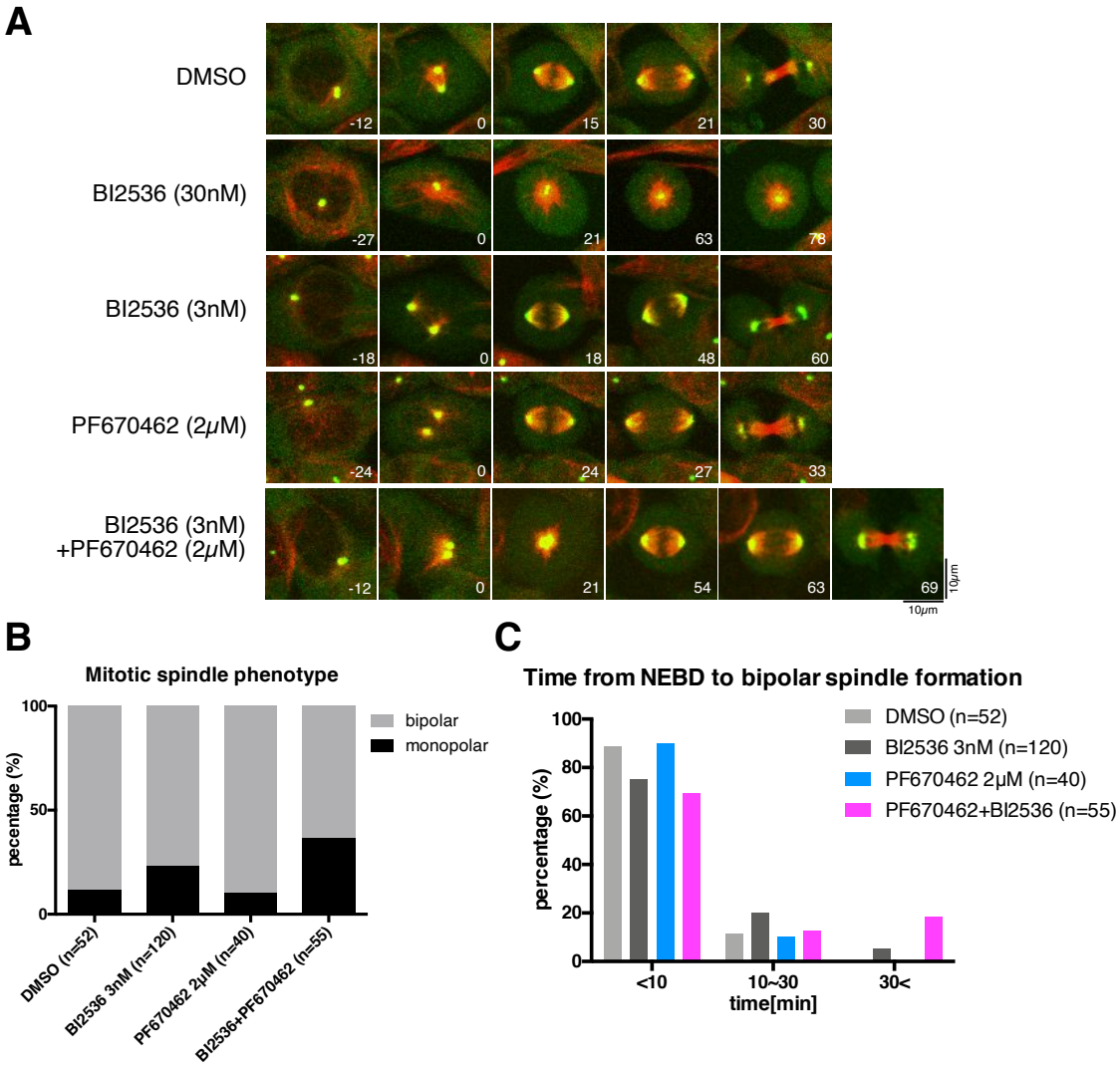

Figure 26. Synthetic monopolar spindle phenotype by partial inhibition of Polo-like kinase (Plk)1 and casein kinase I (CK1)δ in human colon cancer cells

(A) Mitosis of the HCT116 cell line in the presence of Plk1 and/or CK1 inhibitors (BI2536 for Plk1, PF670462 for CK1). Green, γ-tubulin-mClover (endogenously tagged); Red, Sir-tubulin. (B) Frequency of monopolar spindles (monopolar state for ≥10 min). (C) Duration of nuclear envelope breakdown (NEBD)-to-bipolar spindle formation. Time 0 (min) is set at the onset of spindle formation.

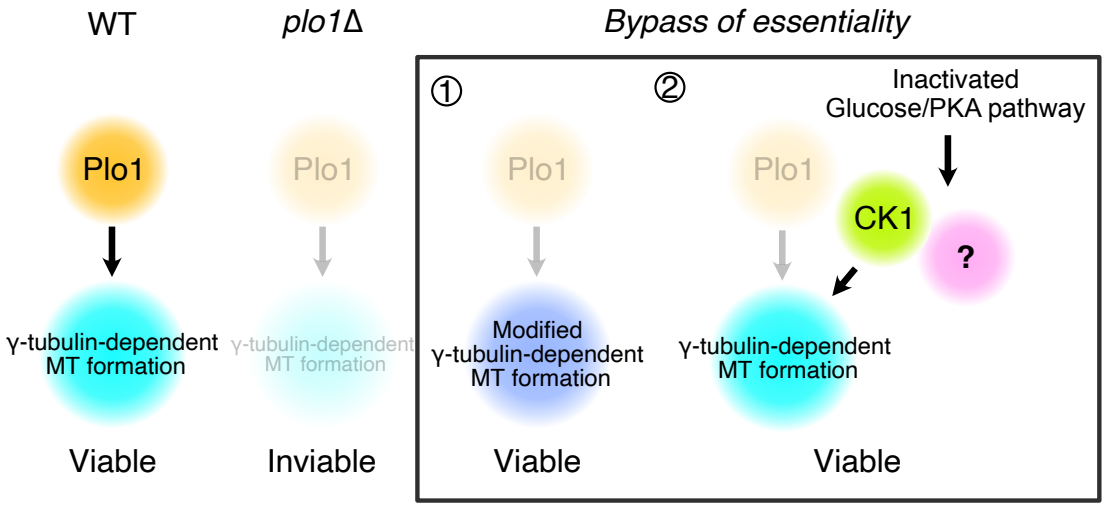

Figure 27. How Plo1 essentiality is bypassed
An increase in spindle microtubules (MTs) is the key to bypassing Plo1. This can be achieved by mutations in MT-associated proteins or nucleators (1) or global change in glucose metabolism (2), which involves casein kinase I and other unknown factors.

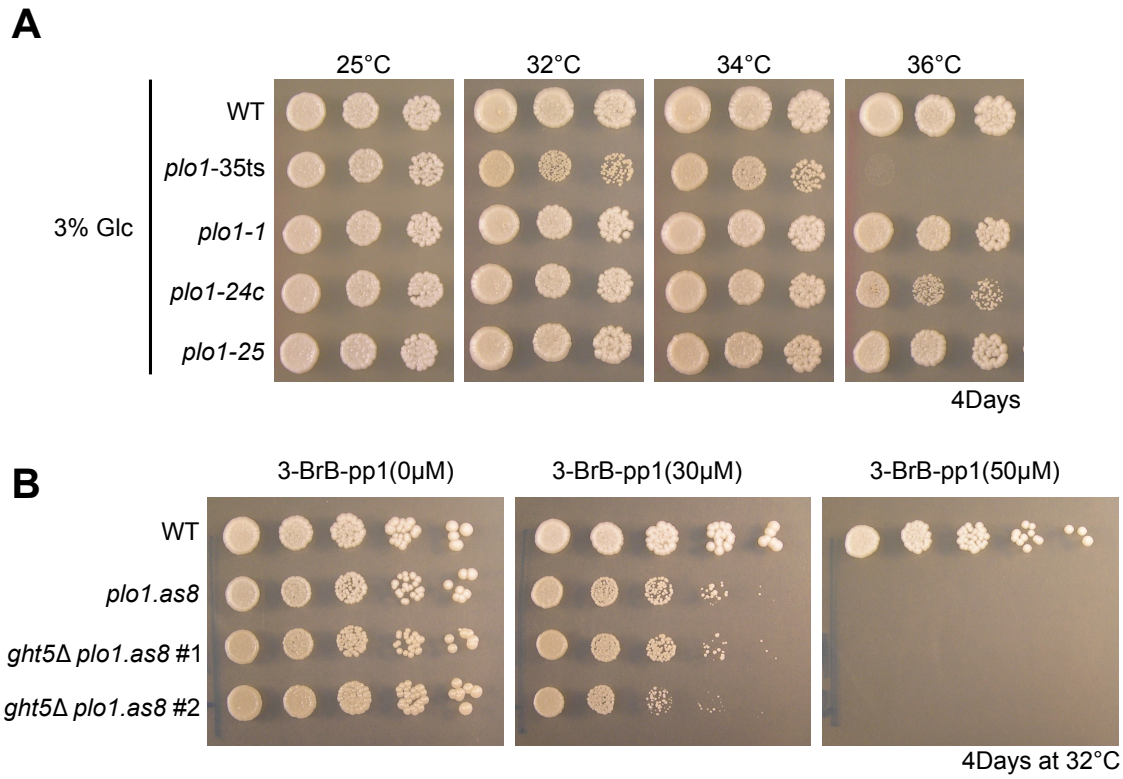

Figure 28. Viability of partial Plo1 mutants in non-permission condition
(A) *plo1-ts* mutants (5,000, 1,000, and 200) were spotted on normal YE5S plates and incubated for 4 days at various temperatures (25, 32, 34, and 36ºC). Except for the *plo1*-35 ts line, *plo1-ts* mutants were viable at 36ºC.
(B) a *plo1*.as8 mutant (5,000, 1,000, and 200) were spotted onto normal YE5S plates and incubated for 4 days at various 3-BrB-pp1 concentration (0, 30 and 50μM). EtOH included in 0uM 3-BrB-pp1 plate.

7. Tables

Table 1. List of strains

Strain name	Genotype	Note		
972	Wild-type (h-)	haploid		
975	Wild-type (h+)	haploid		
1D	h+ leu1 his2 ura4-D18 ade6-216	haploid		
5A	h- leu1 ura4-D18 ade6-210	haploid		
GG0028	h- ade6-210 leu1 ura4-D18 rpl42.sP56Q	haploid		
GG0029	1D/GG0028	diploid		
GG0092	plo1-delta in GG0029	diploid, ura4+, kanR		
GG0161	h+ plo1-delta::urakan	haploid, ura4+, kanR		
GG0756	plo1-delta::kan ght5-delta::hyg leu1 his2 ura4-D18 ade6 (rpl42.sP56Q)	haploid, kanR, hygR		
GG0757	plo1-delta::kan git1-delta::hyg leu1 his2 ura4-D18 ade6 (rpl42.sP56Q)	haploid, kanR, hygR		
GG0758	plo1-delta::kan pka1-delta::hyg leu1 his2 ura4-D18 ade6 (rpl42.sP56Q)	haploid, kanR, hygR		
GG0783	alp4-D440E-hyg plo1-delta::kan leu1 his2 ura4-D18 ade6 (rpl42.sP56Q)	haploid, kanR, hygR		
GG0784	alp6-V664F-hyg plo1-delta::kan leu1 his2 ura4-D18 ade6 (rpl42.sP56Q)	haploid, kanR, hygR		
GG0962	asp1-D507G-hyg plo1-delta::kan leu1-32 ura4-D18 ade6 (rpl42.sP56Q)	haploid, kanR, hygR		
GG1018	git1-delta::nat alp4-D440E-hyg plo1-delta::kan ade6 leu1 ura4 (rpl42.sP56Q)	haploid, kanR, hygR, natR		
GG1019	git1-delta::nat alp6-V664F-hyg plo1-delta::kan ade6 leu1 ura4 (rpl42.sP56Q)	haploid, kanR, hygR, natR		
GG0899	asp1-D507G-nat plo1-delta::kan git1-delta::hyg leu1-32 ura4-D18 ade6 (rpl42.sP56Q)	haploid, kanR, hygR, natR		
GG0148	h+ ade6-M216 leu1 Z::Padh15-mCherry-atb2+<<natr	haploid, natR	FY24870	PQ333
GG0605	plo1-delta::kan/+ ura4 leu1 ade6-210/216 sad1-GFP:LEU2 Z::Padh15-mCherry-atb2+<<nat	diploid leu2+ kanR, natR		
GG0685	h+ ade6 leu1 alp6-GFP-hyg Z::Padh15-mCherry-atb2+<<nat	haploid, natR, hygR		
GG0686	h- ade6 leu1 alp6-GFP-hyg Z::Padh15-mCherry-atb2+<<nat	haploid, natR, hygR		
GG0693	GG0685XGG0686 Diploid selection	diploid, natR, hygR		
GG0697	plo1-delta::bsd/+ in GG0693	diploid, bsdR, natR, hygR		
GG0754	cut7-delta::urakan/+ in GG0693	diploid, kanR, natR, hygR		
GG0755	cdc31-delta::kan/+ in GG0693	diploid, kanR, natR, hygR		
GG0761	ght5-delta::kan plo1-delta::bsd ade6 leu1 alp6-GFP-hyg Z::Padh15-mCherry-atb2+<<nat	haploid, bsdR, kanR, natR, hygR		
GG0762	alp4-D440E-kan plo1-delta::bsd ade6 leu1 alp6-GFP-hyg Z::Padh15-mCherry-atb2+<<nat	haploid, bsdR, kanR, natR, hygR		
GG0832	hhp1-delta::nat/+ plo1-delta::kan/+ ght5::hyg/+ leu1 his2 ura4-D18 ade6 rpl42.sP56Q/+	diploid, kanR, natR, hygR		
GG0942	hhp1-delta::bsd/+ plo1-delta::kan/+ git1-delta::hyg/+ leu1 his2 ura4-D18 ade6 rpl42.sP56Q/+	diploid, kanR, bsdR, hygR		
GG0943	hhp1-delta::bsd/+ plo1-delta::kan/+ pka1-delta::hyg/+ leu1 his2 ura4-D18 ade6 rpl42.sP56Q/+	diploid, kanR, bsdR, hygR		
GG0175	h- mid1-GFP::ura4+ ura4-D18 leu1-32 ade6-210	haploid, ura4+	FY32206	JB30
GG1008	h+ mid1-GFP::ura4+ Z::Padh15-mCherry-atb2+<<nat leu1-32 ade6 (ura4)	haploid, ura4+, natR		
GG1026	ght5-delta::hyg mid1-GFP::ura4 Z::Padh15-mCherry-atb2+<<nat	haploid, ura4+, natR, hygR		
GG1010	plo1-delta::kan ght5-delta::hyg mid1-GFP::ura4 Z::Padh15-mCherry-atb2+<<nat leu1-32 ade6 (ura4)	haploid, ura4+, natR, hygR, kanR		
GG1022	cdc7-GFP-nat Z::Padh15-mCherry-atb2+<<nat	haploid, natR		
GG1023	plo1-delta::kan ght5-delta::hyg cdc7-GFP-nat Z::Padh15-mCherry-atb2+<<nat	haploid, natR, kanR, hygR		
GG0174	h+ cyr1-delta::LEU2 ura4-D18 (leu1)	haploid, leu2+	FY32370	JB522
GG0191	cyr1-delta::LEU2 plo1::urakan leu1-32 ura4-D18 (ade6)	haploid, leu2+, ura4+, kanR		
GG0189	h+ pka1-delta::nat plo1-delta::urakan leu1-32, ura4-D18, ade6 (his2)	haploid, natR, kanR		
GG0172	h- rec6-delta::hyg ura4--aim ura4-D18	haploid, hygR	FY18836	KLY94
GG0694	h- leu1-32 cut7-GFP::LEU2	haploid, leu2+	FY20765	MY6803
GG0699	h- leu1 ade6-M216 cut7-GFP::LEU2 Z::Padh15-mCherry-atb2+<<nat	haploid, leu2+, natR		
GG0701	h+ leu1 ade6-M210 cut7-GFP::LEU2 Z::Padh15-mCherry-atb2+<<nat	haploid, leu2+, natR		
GG0709	GG0699XGG0701 Diploid selection	diploid, leu2+ natR		
GG0718	plo1-delta::bsd/+ in GG0709	diploid, leu2+ natR, bsdR		
GG1034	pPlo1-GFP-ura4 plo1-delta::kan ght5-delta::hyg hhp1-delta::nat Z::Padh15-mCherry-atb2+<<nat	haploid ura4+ kanR, hygR, natR		
GG1035	pPlo1-GFP-ura4 plo1-delta::kan ght5-delta::hyg Z::Padh15-mCherry-atb2+<<nat	haploid ura4+ kanR, hygR, natR		
GG1036	pPlo1-GFP-ura4 plo1-delta::kan ght5-delta::hyg bub1-delta::nat Z::Padh15-mCherry-atb2+<<nat	haploid ura4+ kanR, hygR, natR		
GG0217	h+ GG0161 #3 P20 experimental evolution (clone)	haploid, kanR		
GG0249	h+ GG0217 #3 p20 experimental evolution(clone)	haploid, kanR		
GG0440	h+ hyg-plo1 in GG0217	haploid, hygR		
GG0273	h+ hyg-plo1 in GG0249	haploid, hygR		
GG1062	h- dmf1-delta::ura4 ade6-216 leu1-32 ura4-D18	haploid, ura4+	FY19056	JB41
GG0528	h+ alp6-V664F-nat	haploid, natR		
GG0577	h- alp4-D440E-nat	haploid, natR		
GG0897	asp1-D507G-nat leu1-32 ura4-D18 ade6	haploid, natR		
GG0946	h+ hhp1-delta::hyg alp6-GFP-LEU2 ade6-M216 leu1 Z::Padh15-mCherry-atb2+<<nat	haploid, leu2+, natR, hygR		
GG1066	hhp2-delta::bsd in GG0946	haploid, bsdR		
GG0176	h- pcp1-GFP-kan cut12-CFP-nat leu1 ura4	haploid, kanR, natR	FY17669	MT675
GG1047	pcp1-GFP-kan Z::Padh15-mCherry-atb2+<<nat ade6-M216 leu1	haploid, kanR, natR		
GG1069	GG1047X5A Diploid selection	diploid, kanR, natR		
GG1082	plo1-delta::bsd/+ in GG1069	diploid, bsdR, kanR, natR		
GG1092	pcp1-GFP-kan cut12-1 Z::Padh15-mCherry-atb2+<<nat	haploid, kanR, natR, ts		
GG1060	h- int::pREP3X-SV40NLS-GFP-lacZ leu1-32 ura4-D18 ade6-m216	haploid, lacZ	FY21444	ss482
GG1065	ade6-M210 leu1 Z::Padh15-mCherry-atb2+<<nat (ura4)	haploid, hygR		
GG1070	GG1060XGG1065 Diploid selection	diploid, hygR		
GG1083	plo1-delta::bsd/+ in GG1070	diploid, bsdR, hygR		
GG1086	cut12-1 int::pREP3X-SV40NLS-GFP-lacZ Z::Padh15-mCherry-atb2+<<nat	haploid, natR, ts, lacZ		
GG1080	ght5-delta::kan plo1-delta::bsd int::pREP3X-SV40NLS-GFP-lacZ Z::Padh15-mCherry-atb2+<<nat	haploid, bsdR, kanR, natR, lacZ		
GG1081	Alp4-D440E-kan plo1-delta::bsd int::pREP3X-SV40NLS-GFP-lacZ Z::Padh15-mCherry-atb2+<<nat	haploid, bsdR, kanR, natR, lacZ		
GG1061	h- plo1+::GFP-HA-kan leu1-32 ura4-D18 lys1-131	haploid, kanR	FY15526	HR1030
GG1076	plo1+::GFP-HA-kan Z::Padh15-mCherry-atb2+<<nat leu1-32 (ura4-D18 lys1-131 ade6)	haploid, kanR, natR		
GG0997	ght5-delta::hyg leu1-32 ura4-D18 ade6 (his2)	haploid, hygR		
GG0999	pka1-delta::hyg leu1-32 ura4-D18 ade6 (his2)	haploid, hygR		
GG0850	hhp1-GFP-nat ark1-mCherry-hyg	haploid, hygR, natR		
GG0845	ght5-delta::kan hhp1-GFP-nat ark1-mCherry-hyg #2,3,4,5	haploid, kanR, hygR, natR		
GG1101	pHhp1-GFP-LEU2 plo1-delta::kan ght5-delta::hyg hhp1-delta::nat Z::Padh15-mCherry-atb2+<<hyg	haploid, leu2+, kanR, hygR, natR		

Table 2. List of plasmids

Plasmid number	Insert	Vector
pGG994	cut7-delta::ura4kan	pFA6a-ura4-kanMX6
pGG1012	plo1-delta::urakan	pFA6a-ura4-kanMX6
pGG1160	alp6-V664F	pFA6a-hyg
pGG1161	alp4-D440E	pFA6a-hyg
pGG1202	hhp1	pFA6a-natMX6
pGG1205	cam1 promoter	pFA6a-natMX6
pGG1206	cam1-promoter-hhp1	pFA6a-natMX6
pGG1193	asp1D507G	pFA6a-hyg
pGG1220	plo1-GFP	pREP2
pGG1223	hhp1-GFP	pREP1

Table 3. List of primers

	Oligoname	Sequence
Plo1 deletion	903-plo1-5UTR-Fw	ATAGAACGCGGCCGCGAGAAAGAAAGAACAGTTGAGC
	904-plo1-5UTR-Rv	TAAACGTGAGTCGACGCCATTTGGTATTTGTTTCTAAC
	905-plo1-3UTR-Fw	TGGTCGCTATACTGCCGTTAATCTATACTTGGGCGTTA
	906-plo1-3UTR-Rv	CGAGCTCGTTTAAACGCTATTAACATAGCATAGCGTAGG
Plo1 deletion confirmation	921-plo1urakan-soto-Fw	GATACACAGAGACGAGTTTGG
	922-plo1urakan-soto-Rv	CTACGCAAAGCTTCATATTCG
Ght5 deletion	3483-ght5-5UTR-fw	CAAGGTATGGGCAAGATG
	3484-ght5-5UTR-rv	TAACCCGGGGATCCGGCTTTCAATGACAAGACAAAAG
	3485-ght5-3UTR-fw	TGGTCGCTATACTGCTTGTCGTGGTTCGTTGATTC
	3486-ght5-3UTR-rv	ATTCCGTTCCTCTAATCACC
Ght5 deletion confirmation	3487-ght5-soto-fw	CCCTACTTCATACACTTAACC
	3488-ght5-soto-rv	CACAAGCTGCAATAACATATC
Git1 deletion	4521-git1-5UTR-fw	TAAATGATCAGCGCCATTTTC
	4522-git1-5UTR-rv	TAACCCGGGGATCCGCGATTTGCTGAGTAGAGAGTG
	4523-git1-3UTR-fw	TGGTCGCTATACTGCACTACGGTAATGATGGAGAC
	4524-git1-3UTR-rv	ACATATGGCCCACGTATATC
Git1 deletion confirmation	4480-git1-soto2-fw	TGCAGTTTAGGCAAGGTATG
	4481-git1-soto2-rv	CAAGCACAAAGAAGTCAAC
Pka1 deletion	2058-pka1-5UTR-fw	ATAGAACGCGGCCGCGAATAGCTCGTTTCTCGAAAG
	2059-pka1-5UTR-rv	taacccggggatccGATTCACTAATCGTTCGTCAAAC
	2060-pka1-3UTR-fw	TGGTCGCTATACTGCCATTGTACTATTGCCTTAAAGC
	2061-pka1-3UTR-rv	CGAGCTCGTTTAAACGTTAACTGTTTGGCACAAATTTC
Pka1 deletion confirmation	2062-pka1-soto-fw	CAAAACACAAATTGAAGCTTGC
	2063-pka1-soto-rv	GTCTTTTTATCTATCGCCGATG
Hhp1 deletion	7702-hhp1-5UTR-fw	ATTCTATTCGCTCAGTCGTC
	7704-hhp1-5UTR-rv	TAACCCGGGGATCCGAACGCTTTTAAGGCTAAAGG
	7613-hhp1-3UTR-fw	TGGTCGCTATACTGCCTTCTCATCTGGAGTCTTCC
	7614-hhp1-3UTR-rv	GCTTCAATAAAACAGTCAAGC
Hhp1 deletion confirmation	7703-hhp1-soto-fw	TCCCCTTTCTTTTATCCTGC
	7592-hhp1-soto-rv	ACATCGAAAGACACTTCATG
Bub1 deletion	7667-bub1-5UTR-fw	ATCGCAAAATTCAGGAAGTG
	7668-bub1-5UTR-rv	TAACCCGGGGATCCGCATAGTGATACGCACATTGA
	7669-bub1-3UTR-fw	TGGTCGCTATACTGCCCTAGAGGGAAGTTTCCATC
	7670-bub1-3UTR-rv	ATGAAGGGTTCTGCTATCAC
Bub1 deletion confirmation	7666-bub1-soto-fw	CTTTTTCAACACTTTCCTGG
	7671-bub1-soto-rv	TGTTATTGTCAACCCCAAGG
Cdc31 deletion	7554-cdc31-5UTR-fw	GTGAAGCCTTGCTATTCATG
	7555-cdc31-5UTR-rv	TAACCCGGGGATCCGTGTGGTGGTAAACAGAACG
	7556-cdc31-3UTR-fw	TGGTCGCTATACTGCGATGGATGAAGCATAATGGAG
	7557-cdc31-3UTR-rv	GTATGACTGCCCAACTAGAAG
Cdc31 deletion confirmation	7553-cdc31-soto-fw	GTTTCGGGTGATAGCATTTG
	7558-cdc31-soto-rv	AGAGAAAGGAGGGACAAATAC
Hhp2 deletion	7779-hhp2-5UTR-fw	TTGAAGTGATTCTCTTTGAGG
	7780-hhp2-5UTR-rv	TAACCCGGGGATCCGAATTCACAGAGATGACTGTGG
	7781-hhp2-3UTR-fw	TGGTCGCTATACTGCAATTCCAAACCATCTGTTGAC
	7782-hhp2-3UTR-rv	TGTAAAACTTGATGATCCAGC
Hhp2 deletion confirmation	7778-hhp2-soto-fw	CTCTAGAACTGAGGCTTTTAC
	7783-hhp2-soto-rv	GGTTAAAATACCACAGAAAGC
Alp6-GFP	4512-alp6-SEQ-fw	CAGACACAATTTGACTGCTTC
	7514-alp6-gfp-infusion-rv	TAACCCGGGGATCCGTTGACTGGTAACATCCTTATCA
	7515-alp6-gfp-infusion-fw	TGGTCGCTATACTGCATGAGGTTCATGCATGATTAT
	3512-alp6-B-soto-rv	AGCAAATGACAGCTTCAATC
Alp6-GFP confirmation	4539-alp6-amplify-fw	AAACTTCGCACGTTATGG
	1452-alp6-soto-rv	AATACTCCGAGTTGACAAATC
Cdc7-GFP	3207-cdc7-GFP-natR-fw	CCATCAATGAGCACAAATCCCCCATTTCGAAACCGCATATGCCTCCACCTAGATGGCAACCAAAGCAGCCATTAACGCAGCGGATCCCCGGGTTAATTAA
	3208-cdc7-GFP-natR-rv	TATTAATCATTAAGCCATAAATACAGAAATATCATAAACAAGTAATATAGTCGTGCACTGGGAAATGCGTTTAATAGTGTCAGTATAGCGACCAGCATTC
Cdc7-GFP confirmation	3209-cdc7-soto-fw	TTAACTCATAAGGGGACCAAG
	3210-cdc7-soto-rv	ATAGTCTTCATTGCGGTACTC
Hhp1-GFP	7590-hhp1-ORF#1	TGGAGAGAAAAAGCGAGTG
	7615-hhp1-GFP-A-rv	TAACCCGGGGATCCGATTAGGTCTGTTGATATATTGAG
	7592-hhp1-soto-rv	ACATCGAAAGACACTTCATG
	7613-hhp1-3UTR-fw	TGGTCGCTATACTGCCTTCTCATCTGGAGTCTTCC
Hhp1-GFP confirmation	7589-hhp1-soto-fw	ACTTGCTCTACTTTTTCGAAC
	7592-hhp1-soto-rv	ACATCGAAAGACACTTCATG
Hhp1 (RT-PCR)	7784–hhp1_RT_PCR_fw1	GACAAACCTGATTACGCCTACCTT
	7785–hhp1_RT_PCR_Rv1	GTTGTTCGTCTTGTTGAGTCTTTCTC
Act1 (RT-PCR)	7788–act1_RT_PCR_fw	CTTTCTACAACGAGCTTCGTGTTG
	7789–act1_RT_PCR_rv	GAGTCATCTTCTCACGGTTGGAT

8. References

Al-Bassam, J., Kim, H., Brouhard, G., van Oijen, A., Harrison, S. C., & Ch ang, F. (2010). CLASP promotes microtubule rescue by recruiting tu bulin dimers to the microtubule. *Dev Cell*, *19*(2), 245–258. https://doi. org/10.1016/j.devcel.2010.07.016

Almonacid, M., Celton-Morizur, S., Jakubowski, J. L., Dingli, F., Loew, D., Mayeux, A., Chen, J.-S., Gould, K. L., Clifford, D. M., & Paoletti, A. (2011). Temporal Control of Contractile Ring Assembly by Plo1 Reg ulation of Myosin II Recruitment by Mid1/Anillin. *Current Biology*, *21* (6), 473–479. https://doi.org/10.1016/j.cub.2011.02.003

Aquino Perez, C., Burocziova, M., Jenikova, G., & Macurek, L. (2021). CK 1-mediated phosphorylation of FAM110A promotes its interaction with mitotic spindle and controls chromosomal alignment. *EMBO Rep*, *2 2*(7), e51847. https://doi.org/10.15252/embr.202051847

Archambault, V., & Glover, D. M. (2009). Polo-like kinases: Conservation a nd divergence in their functions and regulation. *Nat Rev Mol Cell Bi ol*, *10*(4), 265–275. https://doi.org/10.1038/nrm2653

Arnaud, L., Pines, J., & Nigg, E. A. (1998). GFP tagging reveals human P olo-like kinase 1 at the kinetochore/centromere region of mitotic chro mosomes. *Chromosoma*, *107*(6–7), 424–429. https://doi.org/10.1007/s 004120050326

Ashraf, S., Tay, Y. D., Kelly, D. A., & Sawin, K. E. (2021). Microtubule-ind ependent movement of the fission yeast nucleus. *J Cell Sci*, *134*(6). https://doi.org/10.1242/jcs.253021

Ashworth, A., Lord, C. J., & Reis-Filho, J. S. (2011). Genetic interactions i n cancer progression and treatment. *Cell*, *145*(1), 30–38. https://doi.o rg/10.1016/j.cell.2011.03.020

Bahler, J., Steever, A. B., Wheatley, S., Wang, Y., Pringle, J. R., Gould, K. L., & McCollum, D. (1998). Role of polo kinase and Mid1p in det ermining the site of cell division in fission yeast. *J Cell Biol*, *143*(6), 1603–1616. https://doi.org/10.1083/jcb.143.6.1603

Behrend, L., Stöter, M., Kurth, M., Rutter, G., Heukeshoven, J., Deppert, W., & Knippschild, U. (2000). *Interaction of casein kinase 1 delta (C K1d) with post- Golgi structures, microtubules and the spindle appar atus*. 12.

Bernard, P., Hardwick, K., & Javerzat, J. P. (1998). Fission yeast bub1 is a mitotic centromere protein essential for the spindle checkpoint and the preservation of correct ploidy through mitosis. *J Cell Biol*, *143* (7), 1775–1787. https://doi.org/10.1083/jcb.143.7.1775

Bestul, A. J., Yu, Z., Unruh, J. R., & Jaspersen, S. L. (2017). Molecular model of fission yeast centrosome assembly determined by superres olution imaging. *Journal of Cell Biology*, *216*(8), 2409–2424. https://d

oi.org/10.1083/jcb.201701041
Bestul, A. J., Yu, Z., Unruh, J. R., & Jaspersen, S. L. (2021). Redistributio n of centrosomal proteins by centromeres and Polo kinase controls partial nuclear envelope breakdown in fission yeast. *Molecular Biolog y of the Cell*, *32*(16), 1487–1500. https://doi.org/10.1091/mbc.E21-05-0239
Bouhlel, I. B., Ohta, M., Mayeux, A., Bordes, N., Dingli, F., Boulanger, J., Velve Casquillas, G., Loew, D., Tran, P. T., Sato, M., & Paoletti, A. (2015). Cell cycle control of spindle pole body duplication and splitti ng by Sfi1 and Cdc31 in fission yeast. *Journal of Cell Science*, *128* (8), 1481–1493. https://doi.org/10.1242/jcs.159657
Bridge, A. J., Morphew, M., Bartlett, R., & Hagan, I. M. (1998). The fissio n yeast SPB component Cut12 links bipolar spindle formation to mit otic control. *Genes & Development*, *12*(7), 927–942. https://doi.org/1 0.1101/gad.12.7.927
Brouhard, G. J., & Rice, L. M. (2018). Microtubule dynamics: An interplay of biochemistry and mechanics. *Nature Reviews Molecular Cell Biolo gy*, *19*(7), 451–463. https://doi.org/10.1038/s41580-018-0009-y
Byrne, S. M., & Hoffman, C. S. (1993). Six git genes encode a glucose-in duced adenylate cyclase activation pathway in the fission yeast Schi zosaccharomyces pombe. *J Cell Sci*, *105 (Pt 4)*, 1095–1100.
Casenghi, M., Meraldi, P., Weinhart, U., Duncan, P. I., Körner, R., & Nigg, E. A. (2003). Polo-like Kinase 1 Regulates Nlp, a Centrosome Prot ein Involved in Microtubule Nucleation. *Developmental Cell*, *5*(1), 113 –125. https://doi.org/10.1016/S1534-5807(03)00193-X
Conduit, P. T., Wainman, A., & Raff, J. W. (2015). Centrosome function a nd assembly in animal cells. *Nat Rev Mol Cell Biol*, *16*(10), 611–62 4. https://doi.org/10.1038/nrm4062
Cunningham, C. E., MacAuley, M. J., Vizeacoumar, F. S., Abuhussein, O., Freywald, A., & Vizeacoumar, F. J. (2020). The CINs of Polo-Like K inase 1 in Cancer. *Cancers (Basel)*, *12*(10). https://doi.org/10.3390/ca ncers12102953
Dhillon, N., & Hoekstra, M. F. (1994). Characterization of two protein kinas es from Schizosaccharomyces pombe involved in the regulation of D NA repair. *EMBO J*, *13*(12), 2777–2788.
Ding, R., West, R. R., Morphew, D. M., Oakley, B. R., & McIntosh, J. R. (1997). The spindle pole body of Schizosaccharomyces pombe enter s and leaves the nuclear envelope as the cell cycle proceeds. *Mole cular Biology of the Cell*, *8*(8), 1461–1479. https://doi.org/10.1091/mb c.8.8.1461
Elmore, Z. C., Guillen, R. X., & Gould, K. L. (2018). The kinase domain o f CK1 enzymes contains the localization cue essential for compartm entalized signaling at the spindle pole. *Molecular Biology of the Cell*, *29*(13), 1664–1674. https://doi.org/10.1091/mbc.E18-02-0129
Elowe, S., Hümmer, S., Uldschmid, A., Li, X., & Nigg, E. A. (2007). Tensi

on-sensitive Plk1 phosphorylation on BubR1 regulates the stability of kinetochore microtubule interactions. *Genes & Development*, *21*(17), 2205–2219. https://doi.org/10.1101/gad.436007

Fantes, P. (1979). Epistatic gene interactions in the control of division in fi ssion yeast. *Nature*, *279*(5712), 428–430. https://doi.org/10.1038/2794 28a0

Ferenz, N. P., Gable, A., & Wadsworth, P. (2010). Mitotic functions of kine sin-5. *Seminars in Cell & Developmental Biology*, *21*(3), 255–259. ht tps://doi.org/10.1016/j.semcdb.2010.01.019

Fernández-Álvarez, A., Bez, C., O'Toole, E. T., Morphew, M., & Cooper, J. P. (2016). Mitotic Nuclear Envelope Breakdown and Spindle Nuclea tion Are Controlled by Interphase Contacts between Centromeres an d the Nuclear Envelope. *Developmental Cell*, *39*(5), 544–559. https:// doi.org/10.1016/j.devcel.2016.10.021

Flory, M. R., Morphew, M., Joseph, J. D., Means, A. R., & Davis, T. N. (2002a). Pcp1p, an Spc110p-related calmodulin target at the centros ome of the fission yeast Schizosaccharomyces pombe. *Cell Growth & Differentiation: The Molecular Biology Journal of the American Ass ociation for Cancer Research*, *13*(2), 47–58.

Flory, M. R., Morphew, M., Joseph, J. D., Means, A. R., & Davis, T. N. (2002b). Pcp1p, an Spc110p-related calmodulin target at the centros ome of the fission yeast Schizosaccharomyces pombe. *Cell Growth & Differentiation: The Molecular Biology Journal of the American Ass ociation for Cancer Research*, *13*(2), 47–58.

Fong, C. S., Sato, M., & Toda, T. (2010). Fission yeast Pcp1 links polo ki nase-mediated mitotic entry to γ-tubulin-dependent spindle formation. *The EMBO Journal*, *29*(1), 120–130. https://doi.org/10.1038/emboj.200 9.331

Fu, C., Ward, J. J., Loiodice, I., Velve-Casquillas, G., Nedelec, F. J., & Tr an, P. T. (2009). Phospho-Regulated Interaction between Kinesin-6 Klp9p and Microtubule Bundler Ase1p Promotes Spindle Elongation. *Developmental Cell*, *17*(2), 257–267. https://doi.org/10.1016/j.devcel.2 009.06.012

Gourguechon, S., Holt, L. J., & Cande, W. Z. (2013). The Giardia cell cycl e progresses independently of the anaphase-promoting complex. *Jou rnal of Cell Science*, *126*(Pt 10), 2246–2255. https://doi.org/10.1242/j cs.121632

Grallert, A., Patel, A., Tallada, V. A., Chan, K. Y., Bagley, S., Krapp, A., Simanis, V., & Hagan, I. M. (2013). Centrosomal MPF triggers the mitotic and morphogenetic switches of fission yeast. *Nature Cell Biol ogy*, *15*(1), 88–95. https://doi.org/10.1038/ncb2633

Grant, P. A., Winston, F., & Berger, S. L. (2021). The biochemical and ge netic discovery of the SAGA complex. *Biochim Biophys Acta Gene Regul Mech*, *1864*(2), 194669. https://doi.org/10.1016/j.bbagrm.2020.1 94669

Greer, Y. E., & Rubin, J. S. (2011). Casein kinase 1 delta functions at the centrosome to mediate Wnt-3a-dependent neurite outgrowth. *J Cell Biol*, *192*(6), 993–1004. https://doi.org/10.1083/jcb.201011111

Greer, Y. E., Westlake, C. J., Gao, B., Bharti, K., Shiba, Y., Xavier, C. P., Pazour, G. J., Yang, Y., & Rubin, J. S. (2014). Casein kinase 1delta functions at the centrosome and Golgi to promote ciliogenesis. *Mol Biol Cell*, *25*(10), 1629–1640. https://doi.org/10.1091/mbc.E13-10-0598

Habedanck, R., Stierhof, Y.-D., Wilkinson, C. J., & Nigg, E. A. (2005). The Polo kinase Plk4 functions in centriole duplication. *Nature Cell Biology*, *7*(11), 1140–1146. https://doi.org/10.1038/ncb1320

Hagan, I., & Yanagida, M. (1990). Novel potential mitotic motor protein encoded by the fission yeast cut7+ gene. *Nature*, *347*(6293), 563–566. https://doi.org/10.1038/347563a0

Hagan, I., & Yanagida, M. (1992). Kinesin-related cut7 protein associates with mitotic and meiotic spindles in fission yeast. *Nature*, *356*(6364), 74–76. https://doi.org/10.1038/356074a0

Hagan, I., & Yanagida, M. (1995). The product of the spindle formation gene sad1+ associates with the fission yeast spindle pole body and is essential for viability. *Journal of Cell Biology*, *129*(4), 1033–1047. https://doi.org/10.1083/jcb.129.4.1033

Hara, M., Ariyoshi, M., Okumura, E., Hori, T., & Fukagawa, T. (2018). Multiple phosphorylations control recruitment of the KMN network onto kinetochores. *Nature Cell Biology*, *20*(12), 1378–1388. https://doi.org/10.1038/s41556-018-0230-0

Hartwell, L. H., Mortimer, R. K., Culotti, J., & Culotti, M. (1973). Genetic Control of the Cell Division Cycle in Yeast: V. Genetic Analysis of cdc Mutants. *Genetics*, *74*(2), 267–286. https://doi.org/10.1093/genetics/74.2.267

Hasegawa, H., Hyodo, T., Asano, E., Ito, S., Maeda, M., Kuribayashi, H., Natsume, A., Wakabayashi, T., Hamaguchi, M., & Senga, T. (2013). The role of PLK1-phosphorylated SVIL in myosin II activation and cytokinetic furrowing. *Journal of Cell Science*, *126*(16), 3627–3637. https://doi.org/10.1242/jcs.124818

Hayles, J., & Nurse, P. (2018). Introduction to Fission Yeast as a Model System. *Cold Spring Harbor Protocols*, *2018*(5), pdb.top079749. https://doi.org/10.1101/pdb.top079749

Hoffman, C. S., Wood, V., & Fantes, P. A. (2015). An Ancient Yeast for Young Geneticists: A Primer on the Schizosaccharomyces pombe Model System. *Genetics*, *201*(2), 403–423. https://doi.org/10.1534/genetics.115.181503

Hou, H., Zhou, Z., Wang, Y., Wang, J., Kallgren, S. P., Kurchuk, T., Miller, E. A., Chang, F., & Jia, S. (2012). Csi1 links centromeres to the nuclear envelope for centromere clustering. *Journal of Cell Biology*, *199*(5), 735–744. https://doi.org/10.1083/jcb.201208001

Johnson, A. E., Chen, J. S., & Gould, K. L. (2013). CK1 is required for a mitotic checkpoint that delays cytokinesis. *Curr Biol*, *23*(19), 1920–1926. https://doi.org/10.1016/j.cub.2013.07.077

Kelkar, M., & Martin, S. G. (2015). PKA antagonizes CLASP-dependent microtubule stabilization to re-localize Pom1 and buffer cell size upon glucose limitation. *Nat Commun*, *6*, 8445. https://doi.org/10.1038/ncomms9445

Klip, A., Tsakiridis, T., Marette, A., & Ortiz, P. A. (1994). Regulation of expression of glucose transporters by glucose: A review of studies in vivo and in cell cultures. *FASEB J*, *8*(1), 43–53. https://doi.org/10.1096/fasebj.8.1.8299889

Knippschild, U., Gocht, A., Wolff, S., Huber, N., Löhler, J., & Stöter, M. (2005). The casein kinase 1 family: Participation in multiple cellular processes in eukaryotes. *Cellular Signalling*, *17*(6), 675–689. https://doi.org/10.1016/j.cellsig.2004.12.011

Knippschild, U., Krüger, M., Richter, J., Xu, P., García-Reyes, B., Peifer, C., Halekotte, J., Bakulev, V., & Bischof, J. (2014). The CK1 Family: Contribution to Cellular Stress Response and Its Role in Carcinogenesis. *Frontiers in Oncology*, *4*. https://www.frontiersin.org/article/10.3389/fonc.2014.00096

Laan, L., Koschwanez, J. H., & Murray, A. W. (2015). Evolutionary adaptation after crippling cell polarization follows reproducible trajectories. *Elife*, *4*. https://doi.org/10.7554/eLife.09638

LaBar, T., Phoebe Hsieh, Y.-Y., Fumasoni, M., & Murray, A. W. (2020). Evolutionary Repair Experiments as a Window to the Molecular Diversity of Life. *Current Biology*, *30*(10), R565–R574. https://doi.org/10.1016/j.cub.2020.03.046

Lane, H. A., & Nigg, E. A. (1996). Antibody microinjection reveals an essential role for human polo-like kinase 1 (Plk1) in the functional maturation of mitotic centrosomes. *Journal of Cell Biology*, *135*(6), 1701–1713. https://doi.org/10.1083/jcb.135.6.1701

Lee, I.-J., Wang, N., Hu, W., Schott, K., Bähler, J., Giddings, T. H., Pringle, J. R., Du, L.-L., & Wu, J.-Q. (2014). Regulation of spindle pole body assembly and cytokinesis by the centrin-binding protein Sfi1 in fission yeast. *Molecular Biology of the Cell*, *25*(18), 2735–2749. https://doi.org/10.1091/mbc.E13-11-0699

Lenart, P., Petronczki, M., Steegmaier, M., Di Fiore, B., Lipp, J. J., Hoffmann, M., Rettig, W. J., Kraut, N., & Peters, J. M. (2007). The small-molecule inhibitor BI 2536 reveals novel insights into mitotic roles of polo-like kinase 1. *Curr Biol*, *17*(4), 304–315. https://doi.org/10.1016/j.cub.2006.12.046

Leong, S. Y., Edzuka, T., Goshima, G., & Yamada, M. (2020). Kinesin-13 and Kinesin-8 Function during Cell Growth and Division in the Moss Physcomitrella patens. *Plant Cell*, *32*(3), 683–702. https://doi.org/10.1105/tpc.19.00521

Li, G., Yin, H., & Kuret, J. (2004). Casein Kinase 1 Delta Phosphorylates Tau and Disrupts Its Binding to Microtubules *. *Journal of Biological Chemistry*, *279*(16), 15938–15945. https://doi.org/10.1074/jbc.M314116200

Li, J., Wang, H. T., Wang, W. T., Zhang, X. R., Suo, F., Ren, J. Y., Bi, Y., Xue, Y. X., Hu, W., Dong, M. Q., & Du, L. L. (2019). Systematic analysis reveals the prevalence and principles of bypassable gene essentiality. *Nat Commun*, *10*(1), 1002. https://doi.org/10.1038/s41467-019-08928-1

Lin, X., Xiao, Z., Chen, T., Liang, S. H., & Guo, H. (2020). Glucose Metabolism on Tumor Plasticity, Diagnosis, and Treatment. *Frontiers in Oncology*, *10*. https://www.frontiersin.org/article/10.3389/fonc.2020.00317

Liu, C., Li, Y., Semenov, M., Han, C., Baeg, G. H., Tan, Y., Zhang, Z., Lin, X., & He, X. (2002). Control of beta-catenin phosphorylation/degradation by a dual-kinase mechanism. *Cell*, *108*(6), 837–847. https://doi.org/10.1016/s0092-8674(02)00685-2

Liu, D., Davydenko, O., & Lampson, M. A. (2012). Polo-like kinase-1 regulates kinetochore–microtubule dynamics and spindle checkpoint silencing. *Journal of Cell Biology*, *198*(4), 491–499. https://doi.org/10.1083/jcb.201205090

Liu, G., Yong, M. Y., Yurieva, M., Srinivasan, K. G., Liu, J., Lim, J. S., Poidinger, M., Wright, G. D., Zolezzi, F., Choi, H., Pavelka, N., & Rancati, G. (2015). Gene Essentiality Is a Quantitative Property Linked to Cellular Evolvability. *Cell*, *163*(6), 1388–1399. https://doi.org/10.1016/j.cell.2015.10.069

Liu, P., Wurtz, M., Zupa, E., Pfeffer, S., & Schiebel, E. (2021). Microtubule nucleation: The waltz between gamma-tubulin ring complex and associated proteins. *Curr Opin Cell Biol*, *68*, 124–131. https://doi.org/10.1016/j.ceb.2020.10.004

Liu, X., Zhou, T., Kuriyama, R., & Erikson, R. L. (2004). Molecular interactions of Polo-like-kinase 1 with the mitotic kinesin-like protein CHO1/MKLP-1. *Journal of Cell Science*, *117*(Pt 15), 3233–3246. https://doi.org/10.1242/jcs.01173

Loïodice, I., Staub, J., Setty, T. G., Nguyen, N.-P. T., Paoletti, A., & Tran, P. T. (2005). Ase1p organizes antiparallel microtubule arrays during interphase and mitosis in fission yeast. *Molecular Biology of the Cell*, *16*(4), 1756–1768. https://doi.org/10.1091/mbc.e04-10-0899

Maeda, T., Watanabe, Y., Kunitomo, H., & Yamamoto, M. (1994). Cloning of the pka1 gene encoding the catalytic subunit of the cAMP-dependent protein kinase in Schizosaccharomyces pombe. *J Biol Chem*, *269*(13), 9632–9637.

Malvezzi, F., Litos, G., Schleiffer, A., Heuck, A., Mechtler, K., Clausen, T., & Westermann, S. (2013). A structural basis for kinetochore recruitment of the Ndc80 complex via two distinct centromere receptors. *EMBO J*, *32*(3), 409–423. https://doi.org/10.1038/emboj.2012.356

Matsuyama, A., Shirai, A., & Yoshida, M. (2008). A series of promoters for constitutive expression of heterologous genes in fission yeast. *Yeast*, *25*(5), 371–376. https://doi.org/10.1002/yea.1593

McCully, E. K., & Robinow, C. F. (1971). Mitosis in the Fission Yeast Schizosaccharomyces Pombe: A Comparative Study with Light and Electron Microscopy. *Journal of Cell Science*, *9*(2), 475–507. https://doi.org/10.1242/jcs.9.2.475

McKinley, K. L., & Cheeseman, I. M. (2017). Large-Scale Analysis of CRISPR/Cas9 Cell-Cycle Knockouts Reveals the Diversity of p53-Dependent Responses to Cell-Cycle Defects. *Dev Cell*, *40*(4), 405-420 e2. https://doi.org/10.1016/j.devcel.2017.01.012

Meng, Q. J., Maywood, E. S., Bechtold, D. A., Lu, W. Q., Li, J., Gibbs, J. E., Dupre, S. M., Chesham, J. E., Rajamohan, F., Knafels, J., Sneed, B., Zawadzke, L. E., Ohren, J. F., Walton, K. M., Wager, T. T., Hastings, M. H., & Loudon, A. S. (2010). Entrainment of disrupted circadian behavior through inhibition of casein kinase 1 (CK1) enzymes. *Proc Natl Acad Sci U S A*, *107*(34), 15240–15245. https://doi.org/10.1073/pnas.1005101107

Moreno, S., Klar, A., & Nurse, P. (1991). Molecular genetic analysis of fission yeast Schizosaccharomyces pombe. *Methods Enzymol*, *194*, 795–823. https://doi.org/10.1016/0076-6879(91)94059-l

Moritz, M., Braunfeld, M. B., Guénebaut, V., Heuser, J., & Agard, D. A. (2000). Structure of the γ-tubulin ring complex: A template for microtubule nucleation. *Nature Cell Biology*, *2*(6), 365–370. https://doi.org/10.1038/35014058

Mulvihill, D. P., Petersen, J., Ohkura, H., Glover, D. M., & Hagan, I. M. (1999). Plo1 kinase recruitment to the spindle pole body and its role in cell division in Schizosaccharomyces pombe. *Molecular Biology of the Cell*, *10*(8), 2771–2785. https://doi.org/10.1091/mbc.10.8.2771

Nasmyth, K., NURSE, P., & FRASER, R. S. S. (1979). The Effect of Cell Mass on the Cell Cycle Timing and Duration of S-Phase in Fission Yeast. *Journal of Cell Science*, *39*(1), 215–233. https://doi.org/10.1242/jcs.39.1.215

Neef, R., Preisinger, C., Sutcliffe, J., Kopajtich, R., Nigg, E. A., Mayer, T. U., & Barr, F. A. (2003). Phosphorylation of mitotic kinesin-like protein 2 by polo-like kinase 1 is required for cytokinesis. *Journal of Cell Biology*, *162*(5), 863–876. https://doi.org/10.1083/jcb.200306009

Neumann, B., Walter, T., Heriche, J. K., Bulkescher, J., Erfle, H., Conrad, C., Rogers, P., Poser, I., Held, M., Liebel, U., Cetin, C., Sieckmann, F., Pau, G., Kabbe, R., Wunsche, A., Satagopam, V., Schmitz, M. H., Chapuis, C., Gerlich, D. W., … Ellenberg, J. (2010). Phenotypic profiling of the human genome by time-lapse microscopy reveals cell division genes. *Nature*, *464*(7289), 721–727. https://doi.org/10.1038/nature08869

Nigg, E. A. (2001). Mitotic kinases as regulators of cell division and its ch

eckpoints. *Nature Reviews Molecular Cell Biology*, *2*(1), 21–32. https://doi.org/10.1038/35048096

Nishimura, A., Yamamoto, K., Oyama, M., Kozuka-Hata, H., Saito, H., & Tatebayashi, K. (2016). Scaffold Protein Ahk1, Which Associates with Hkr1, Sho1, Ste11, and Pbs2, Inhibits Cross Talk Signaling from the Hkr1 Osmosensor to the Kss1 Mitogen-Activated Protein Kinase. *Molecular and Cellular Biology*, *36*(7), 1109–1123. https://doi.org/10.1128/MCB.01017-15

Nurse, P. (1975). Genetic control of cell size at cell division in yeast. *Nature*, *256*(5518), 547–551. https://doi.org/10.1038/256547a0

Ohkura, H., Hagan, I. M., & Glover, D. M. (1995). The conserved Schizosaccharomyces pombe kinase plo1, required to form a bipolar spindle, the actin ring, and septum, can drive septum formation in G1 and G2 cells. *Genes Dev*, *9*(9), 1059–1073. https://doi.org/10.1101/gad.9.9.1059

Okamura, E., Sakamoto, T., Sasaki, T., & Matsunaga, S. (2017). A Plant Ancestral Polo-Like Kinase Sheds Light on the Mystery of the Evolutionary Disappearance of Polo-Like Kinases in the Plant Kingdom. *Cytologia*, *82*(3), 261–266. https://doi.org/10.1508/cytologia.82.261

Olmsted, Z. T., Colliver, A. G., Riehlman, T. D., & Paluh, J. L. (2014). Kinesin-14 and kinesin-5 antagonistically regulate microtubule nucleation by gamma-TuRC in yeast and human cells. *Nat Commun*, *5*, 5339. https://doi.org/10.1038/ncomms6339

Olmsted, Z. T., Riehlman, T. D., Branca, C. N., Colliver, A. G., Cruz, L. O., & Paluh, J. L. (2013). Kinesin-14 Pkl1 targets γ-tubulin for release from the γ-tubulin ring complex (γ-TuRC) . *Cell Cycle (Georgetown, Tex.)*, *12*(5), 842–848. https://doi.org/10.4161/cc.23822

Otto, T., & Sicinski, P. (2017). Cell cycle proteins as promising targets in cancer therapy. *Nat Rev Cancer*, *17*(2), 93–115. https://doi.org/10.1038/nrc.2016.138

Paoletti, A., Bordes, N., Haddad, R., Schwartz, C. L., Chang, F., & Bornens, M. (2003). Fission yeast cdc31p is a component of the half-bridge and controls SPB duplication. *Mol Biol Cell*, *14*(7), 2793–2808. https://doi.org/10.1091/mbc.e02-10-0661

Peng, Y., Moritz, M., Han, X., Giddings, T. H., Lyon, A., Kollman, J., Winey, M., Yates, J., Agard, D. A., Drubin, D. G., & Barnes, G. (2015). Interaction of CK1delta with gammaTuSC ensures proper microtubule assembly and spindle positioning. *Mol Biol Cell*, *26*(13), 2505–2518. https://doi.org/10.1091/mbc.E14-12-1627

Petersen, J., & Hagan, I. M. (2005). Polo kinase links the stress pathway to cell cycle control and tip growth in fission yeast. *Nature*, *435*(7041), 507–512. https://doi.org/10.1038/nature03590

Petersen, J., & Nurse, P. (2007). TOR signalling regulates mitotic commitment through the stress MAP kinase pathway and the Polo and Cdc2 kinases. *Nature Cell Biology*, *9*(11), 1263–1272. https://doi.org/10.10

38/ncb1646

Petronczki, M., Lénárt, P., & Peters, J.-M. (2008). Polo on the Rise-from Mitotic Entry to Cytokinesis with Plk1. *Developmental Cell*, *14*(5), 646–659. https://doi.org/10.1016/j.devcel.2008.04.014

Phadnis, N., Cipak, L., Polakova, S., Hyppa, R. W., Cipakova, I., Anrather, D., Karvaiova, L., Mechtler, K., Smith, G. R., & Gregan, J. (2015). Casein Kinase 1 and Phosphorylation of Cohesin Subunit Rec11 (SA3) Promote Meiotic Recombination through Linear Element Formation. *PLoS Genet*, *11*(5), e1005225. https://doi.org/10.1371/journal.pgen.1005225

Pohlmann, J., Risse, C., Seidel, C., Pohlmann, T., Jakopec, V., Walla, E., Ramrath, P., Takeshita, N., Baumann, S., Feldbrugge, M., Fischer, R., & Fleig, U. (2014). The Vip1 inositol polyphosphate kinase family regulates polarized growth and modulates the microtubule cytoskeleton in fungi. *PLoS Genet*, *10*(9), e1004586. https://doi.org/10.1371/journal.pgen.1004586

PomBase—The Schizosaccharomyces pombe genome database. (n.d.). Retrieved June 3, 2022, from https://www.pombase.org/

Rancati, G., Moffat, J., Typas, A., & Pavelka, N. (2018). Emerging and evolving concepts in gene essentiality. *Nat Rev Genet*, *19*(1), 34–49. https://doi.org/10.1038/nrg.2017.74

Reinfeld, B. I., Madden, M. Z., Wolf, M. M., Chytil, A., Bader, J. E., Patterson, A. R., Sugiura, A., Cohen, A. S., Ali, A., Do, B. T., Muir, A., Lewis, C. A., Hongo, R. A., Young, K. L., Brown, R. E., Todd, V. M., Huffstater, T., Abraham, A., O'Neil, R. T., … Rathmell, W. K. (2021). Cell-programmed nutrient partitioning in the tumour microenvironment. *Nature*, *593*(7858), 282–288. https://doi.org/10.1038/s41586-021-03442-1

Rincon, S. A., Lamson, A., Blackwell, R., Syrovatkina, V., Fraisier, V., Paoletti, A., Betterton, M. D., & Tran, P. T. (2017). Kinesin-5-independent mitotic spindle assembly requires the antiparallel microtubule crosslinker Ase1 in fission yeast. *Nature Communications*, *8*(1), 15286. https://doi.org/10.1038/ncomms15286

Ringel, A. E., Cieniewicz, A. M., Taverna, S. D., & Wolberger, C. (2015). Nucleosome competition reveals processive acetylation by the SAGA HAT module. *Proc Natl Acad Sci U S A*, *112*(40), E5461-70. https://doi.org/10.1073/pnas.1508449112

Roth, A., Gihring, A., Bischof, J., Pan, L., Oswald, F., & Knippschild, U. (2022). CK1 Is a Druggable Regulator of Microtubule Dynamics and Microtubule-Associated Processes. *Cancers*, *14*(5), 1345. https://doi.org/10.3390/cancers14051345

Rumpf, C., Cipak, L., Dudas, A., Benko, Z., Pozgajova, M., Riedel, C. G., Ammerer, G., Mechtler, K., & Gregan, J. (2010). Casein kinase 1 is required for efficient removal of Rec8 during meiosis I. *Cell Cycle*, *9*(13), 2657–2662. https://doi.org/10.4161/cc.9.13.12146

Rüthnick, D., & Schiebel, E. (2016). Duplication of the Yeast Spindle Pole Body Once per Cell Cycle. *Molecular and Cellular Biology*, *36*(9), 1324–1331. https://doi.org/10.1128/MCB.00048-16

Ryan, C. J., Krogan, N. J., Cunningham, P., & Cagney, G. (2013). All or nothing: Protein complexes flip essentiality between distantly related eukaryotes. *Genome Biol Evol*, *5*(6), 1049–1059. https://doi.org/10.1093/gbe/evt074

Saha, S., Unruh, J. R., & Jaspersen, S. L. (2021). Distribution of γ-tubulin ring complex at the Schizosaccharomyces pombe spindle pole. *Micro Publication Biology*, *2021*, 10.17912/micropub.biology.000464. https://doi.org/10.17912/micropub.biology.000464

Saitoh, S., Mori, A., Uehara, L., Masuda, F., Soejima, S., & Yanagida, M. (2015). Mechanisms of expression and translocation of major fission yeast glucose transporters regulated by CaMKK/phosphatases, nuclear shuttling, and TOR. *Mol Biol Cell*, *26*(2), 373–386. https://doi.org/10.1091/mbc.E14-11-1503

Saitoh, S., & Yanagida, M. (2014). Does a shift to limited glucose activate checkpoint control in fission yeast? *FEBS Lett*, *588*(15), 2373–2378. https://doi.org/10.1016/j.febslet.2014.04.047

Saxton, R. A., & Sabatini, D. M. (2017). MTOR Signaling in Growth, Metabolism, and Disease. *Cell*, *168*(6), 960–976. https://doi.org/10.1016/j.cell.2017.02.004

Scholey, J. M., Brust-Mascher, I., & Mogilner, A. (2003). Cell division. *Nature*, *422*(6933), 746–752. https://doi.org/10.1038/nature01599

Shashkova, S., Welkenhuysen, N., & Hohmann, S. (2015). Molecular communication: Crosstalk between the Snf1 and other signaling pathways. *FEMS Yeast Res*, *15*(4), fov026. https://doi.org/10.1093/femsyr/fov026

Silk, A. D., Zasadil, L. M., Holland, A. J., Vitre, B., Cleveland, D. W., & Weaver, B. A. (2013). Chromosome missegregation rate predicts whether aneuploidy will promote or suppress tumors. *Proceedings of the National Academy of Sciences*, *110*(44), E4134–E4141. https://doi.org/10.1073/pnas.1317042110

Sonnichsen, B., Koski, L. B., Walsh, A., Marschall, P., Neumann, B., Brehm, M., Alleaume, A. M., Artelt, J., Bettencourt, P., Cassin, E., Hewitson, M., Holz, C., Khan, M., Lazik, S., Martin, C., Nitzsche, B., Ruer, M., Stamford, J., Winzi, M., … Echeverri, C. J. (2005). Full-genome RNAi profiling of early embryogenesis in Caenorhabditis elegans. *Nature*, *434*(7032), 462–469. https://doi.org/nature03353 [pii] 10.1038/nature03353

Steidle, E. A., Chong, L. S., Wu, M., Crooke, E., Fiedler, D., Resnick, A. C., & Rolfes, R. J. (2016). A Novel Inositol Pyrophosphate Phosphatase in Saccharomyces cerevisiae: Siw14 PROTEIN SELECTIVELY CLEAVES THE β-PHOSPHATE FROM 5-DIPHOSPHOINOSITOL PENTAKISPHOSPHATE (5PP-IP5) *. *Journal of Biological Chemistry*, *29*

1(13), 6772–6783. https://doi.org/10.1074/jbc.M116.714907
Sunkel, C. E., & Glover, D. M. (1988). Polo, a mitotic mutant of Drosophil a displaying abnormal spindle poles. *Journal of Cell Science*, *89 (P t 1)*, 25–38. https://doi.org/10.1242/jcs.89.1.25
Syrovatkina, V., & Tran, P. T. (2015). Loss of kinesin-14 results in aneupl oidy via kinesin-5-dependent microtubule protrusions leading to chro mosome cut. *Nat Commun*, *6*, 7322. https://doi.org/10.1038/ncomms8 322
Takeda, A., Saitoh, S., Ohkura, H., Sawin, K. E., & Goshima, G. (2019). I dentification of 15 New Bypassable Essential Genes of Fission Yeas t. *Cell Struct Funct*, *44*(2), 113–119. https://doi.org/10.1247/csf.19025
Tallada, V. A., Tanaka, K., Yanagida, M., & Hagan, I. M. (2009). The S. p ombe mitotic regulator Cut12 promotes spindle pole body activation and integration into the nuclear envelope. *Journal of Cell Biology*, *1 85*(5), 875–888. https://doi.org/10.1083/jcb.200812108
Tanaka, K., Petersen, J., MacIver, F., Mulvihill, D. P., Glover, D. M., & Ha gan, I. M. (2001). The role of Plo1 kinase in mitotic commitment an d septation in Schizosaccharomyces pombe. *EMBO J*, *20*(6), 1259–1 270. https://doi.org/10.1093/emboj/20.6.1259
Tanenbaum, M. E., & Medema, R. H. (2010). Mechanisms of Centrosome Separation and Bipolar Spindle Assembly. *Developmental Cell*, *19*(6), 797–806. https://doi.org/10.1016/j.devcel.2010.11.011
Thompson, S. L., & Compton, D. A. (2011). Chromosome missegregation i n human cells arises through specific types of kinetochore–microtubu le attachment errors. *Proceedings of the National Academy of Scien ces*, *108*(44), 17974–17978. https://doi.org/10.1073/pnas.1109720108
Tsuchiya, K., & Goshima, G. (2021). Microtubule-associated proteins promo te microtubule generation in the absence of γ-tubulin in human colo n cancer cells. *Journal of Cell Biology*, *220*(12), e202104114. https:// doi.org/10.1083/jcb.202104114
Uzawa, S., Li, F., Jin, Y., McDonald, K. L., Braunfeld, M. B., Agard, D. A., & Cande, W. Z. (2004). Spindle pole body duplication in fission ye ast occurs at the G1/S boundary but maturation is blocked until exit from S by an event downstream of cdc10+. *Molecular Biology of th e Cell*, *15*(12), 5219–5230. https://doi.org/10.1091/mbc.e04-03-0255
Vale, R. D. (2003). The molecular motor toolbox for intracellular transport. *Cell*, *112*(4), 467–480.
van Leeuwen, J., Pons, C., Tan, G., Wang, J. Z., Hou, J., Weile, J., Geb bia, M., Liang, W., Shuteriqi, E., Li, Z., Lopes, M., Usaj, M., Dos S antos Lopes, A., van Lieshout, N., Myers, C. L., Roth, F. P., Aloy, P., Andrews, B. J., & Boone, C. (2020). Systematic analysis of bypa ss suppression of essential genes. *Mol Syst Biol*, *16*(9), e9828. http s://doi.org/10.15252/msb.20209828
Vardy, L., & Toda, T. (2000). The fission yeast gamma-tubulin complex is required in G(1) phase and is a component of the spindle assembly

checkpoint. *EMBO J*, *19*(22), 6098–6111. https://doi.org/10.1093/emboj/19.22.6098

Vasquez-Limeta, A., & Loncarek, J. (2021). Human centrosome organization and function in interphase and mitosis. *Seminars in Cell & Developmental Biology*, *117*, 30–41. https://doi.org/10.1016/j.semcdb.2021.03.020

Wachowicz, P., Chasapi, A., Krapp, A., Cano Del Rosario, E., Schmitter, D., Sage, D., Unser, M., Xenarios, I., Rougemont, J., & Simanis, V. (2015). Analysis of S. pombe SIN protein association to the SPB reveals two genetically separable states of the SIN. *J Cell Sci*, *128*(4), 741–754. https://doi.org/10.1242/jcs.160150

Walde, S., & King, M. C. (2014). The KASH protein Kms2 coordinates mitotic remodeling of the spindle pole body. *J Cell Sci*, *127*(Pt 16), 3625–3640. https://doi.org/10.1242/jcs.154997

West, R. R., Vaisberg, E. V., Ding, R., Nurse, P., & McIntosh, J. R. (1998). cut11(+): A gene required for cell cycle-dependent spindle pole body anchoring in the nuclear envelope and bipolar spindle formation in Schizosaccharomyces pombe. *Molecular Biology of the Cell*, *9*(10), 2839–2855. https://doi.org/10.1091/mbc.9.10.2839

Wolff, S., Xiao, Z., Wittau, M., Süssner, N., Stöter, M., & Knippschild, U. (2005). Interaction of casein kinase 1 delta (CK1δ) with the light chain LC2 of microtubule associated protein 1A (MAP1A). *Biochimica et Biophysica Acta (BBA) - Molecular Cell Research*, *1745*(2), 196–206. https://doi.org/10.1016/j.bbamcr.2005.05.004

Wood, V., Gwilliam, R., Rajandream, M.-A., Lyne, M., Lyne, R., Stewart, A., Sgouros, J., Peat, N., Hayles, J., Baker, S., Basham, D., Bowman, S., Brooks, K., Brown, D., Brown, S., Chillingworth, T., Churcher, C., Collins, M., Connor, R., … Nurse, P. (2002). The genome sequence of Schizosaccharomyces pombe. *Nature*, *415*(6874), 871–880. https://doi.org/10.1038/nature724

Yamada, M., & Goshima, G. (2017). Mitotic Spindle Assembly in Land Plants: Molecules and Mechanisms. *Biology (Basel)*, *6*(1). https://doi.org/10.3390/biology6010006

York, S. J., Armbruster, B. N., Greenwell, P., Petes, T. D., & York, J. D. (2005). Inositol Diphosphate Signaling Regulates Telomere Length *. *Journal of Biological Chemistry*, *280*(6), 4264–4269. https://doi.org/10.1074/jbc.M412070200

Yukawa, M., Ikebe, C., & Toda, T. (2015). The Msd1-Wdr8-Pkl1 complex anchors microtubule minus ends to fission yeast spindle pole bodies. *J Cell Biol*, *209*(4), 549–562. https://doi.org/10.1083/jcb.201412111

Yukawa, M., Yamada, Y., Yamauchi, T., & Toda, T. (2018). Two spatially distinct kinesin-14 proteins, Pkl1 and Klp2, generate collaborative inward forces against kinesin-5 Cut7 in S. pombe. *Journal of Cell Science*, *131*(1), jcs210740. https://doi.org/10.1242/jcs.210740

9. Acknowledgments

I express my gratitude to Prof. Gohta Goshima. He guided me extensively on my research ideas, data analysis, or even experimental methods. He often consulted with me about my career path and personal problems, which enabled me to finish graduate school well. Also, he supported me with a comfortable experimental environment, which allowed me to concentrate on my research.

I would like to thank Dr. Moé Yamada. She gave me a lot of advice on how to prepare presentation for conferences, how to analyze data, and how to conduct experiments. She also taught me about life in Japan and made my stay in Japan enjoyable.

I thank Mr. Aoi Takeda. He did experimental evolution for this project and kindly shared several culture media and strains.

I thank Dr. Tomoya Edzuka and Ms. Elsa Amelia Tungadi for their technical suggestions and for teaching me how to analyze the data.

I thank all Goshima lab members, Dr. Tomomi Kiyomitsu, Dr. Peishan Yi, Dr. Elena Kozgunova, Dr. Kenta Tsuchiya, Ms. Shu Yao Leong, Ms. Mari Yoshida, Ms. Mao Fujiwara, Ms. Marie Nishikawa, Ms. Noiri Oguri and Ms. Maya Hakozaki for suggesting brilliant ideas for developing this project. And I always thank Ms. Rie Inaba, Ms. Kyoko Zenbutsu, Ms. Miki Ueda, and Ms. Koketsu Chiemi for supplying materials, lab maintenance, and giving off positive energy to the lab.

I thank Prof. Shigeaki Saitoh (Kurume University), Prof. Kojiro Takeda (Konan University), Prof. Masamitsu Sato (Waseda University), Prof. Iain Hagan (University of Manchester), Dr. Ye Dee Tay (University of Edinburgh), and National Bio-Resource Project (NBRP) of the MEXT, Japan, for yeast strains and plasmids.

I thank Dr. Kazuma Uesaka for his help with sequence analysis, Prof. Ken Sawin, Prof. Hiro Ohkura, and Dr. Ye Dee Tay for valuable discussions and protocols, and Prof. Shigeaki Saitoh for his comments on the manuscript.

Lastly, I would like to express my deepest gratitude to my family and friends for their support.